Frequency-dependent heat capacity

experimental work to improve and understand planar heater experiments using the 3[omega] detection technique

Behrens, Claus Flensted

Publication date:
2004

Frequency–dependent heat capacity

- Experimental work to improve and understand planar heater experiments using the 3ω detection technique

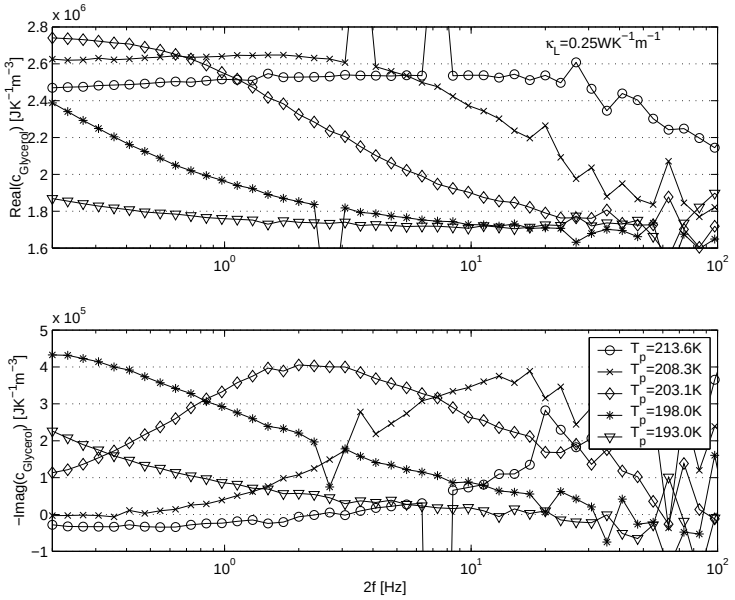

Ph.D. thesis by Claus Flensted Behrens
Supervisor: Tage Christensen

Department of Mathematics and Physics (IMFUFA),
Roskilde University, DK–4000 Roskilde, Denmark.

Second edition.

Abstract

In English:

The frequency–dependent heat capacity of super-cooled glycerol near the glass transition is measured using the 3ω detection technique. An electrical conducting thin film with a temperature–dependent electrical resistance is deposited on a substrate. The thin film is used simultaneously as a heater and as a thermometer.

The aim of the work is to improve and understand this planar heater experiment. I find:

- Carbon has advantages as heater material over the traditionally used metal (nickel) heaters.
- The thermal coupling to the surrounding temperature bath should not be made through the liquid but through the substrate.
- Edge effects, as a result of the finite size of the heater, play an important role. The traditionally way of dealing with these effects are not entirely correct.
- The Cole–Davidson function with $\beta_{CD} = 0.62 \pm 0.02$ fits the measured data for glycerol.

(This thesis can be downloaded at: http://dirac.ruc.dk/ ˜cfb/)

In Danish:

Den frekvensafhængige varmefylde af underafkølet glycerol nær glasovergangen er målt vha. 3ω måleteknikken. En tynd, elektrisk ledende film med en temperaturafhængig elektrisk modstand er deponeret på et substrat. Filmen benyttes samtidig som varmekilde og termometer.

Målet for dette arbejde er at forbedre og forstå dette plan–plade eksperimentet. Det konkluderes at:

- Det er en fordel at benytte en kulfilm som varmeplade fremfor de traditionelt benyttede metalfilm.

- Den termiske kobling til det omkringliggende temperaturbad bør være gennem substratet og ikke gennem væsken.
- Randeffekter, der skyldes den endelige udstrækning af varmepladen, spiller en vigtig rolle. Den traditionelle måde hvorpå der korrigeres for disse effekter er kun delvis korrekt.
- Cole–Davidson funktionen med $\beta_{CD} = 0.62 \pm 0.02$ stemmer overens med de målte data for glycerol.

(Denne afhandling kan hentes fra: http://dirac.ruc.dk/ ˜cfb/)

Contents

1 Preface

This treatise is based on the work that I have done during 3 years as a Ph.D. student at IMFUFA (the institute of physics), University of Roskilde, Denmark. The overall aim of the work has been to improve existing, or develop new, measuring techniques to be used in measuring frequency dependent specific heat capacity of highly viscous liquids, such as super–cooled liquids near the glass transition.

In this first chapter the objectives that were formulated at the onset of this work, will be presented, and the objectives that in fact have been reached, will be mentioned. At the end of the chapter there are a few practical notes to the reader.

1.1 Intended objectives

In principle the measurement of a heat capacity is very simple: supply a known amount of heat, and measure the resulting change in the temperature. For a highly viscous liquid this is complicated by relaxation phenomena. Thus, if heat is supplied in a oscillatory manner the relaxation phenomena will influenced the measured phase and amplitude of the resulting temperature change.

Such measurements can, for example, be made using a thin metal film on a glass substrate, as a heater, immersed into a liquid. If the electrical resistance of the thin film vary with temperature, it can simultaneously function as a thermometer. The temperature amplitude and phase shift can be detected using the "3ω detection technique" (which will be described in chapter 6). Results of such measurements have, since 1985, been reported in the literature.

One problem is that there can be raised doubts about what quantity is actually measured in this "stiff planar heater experiment". What is usually assumed is that it is the specific heat capacity at constant pressure c_p (multiplied by the thermal conductivity). But this is doubtful. In some cases, depending on the exact experimental conditions, it is instead a quantity that can be called the longitudinal heat capacity (c_l) [Christensen and Olsen, 1997][1]. This has to do with the thermo–

[1] $c_p = \frac{K_s}{K_T} c_V$, where K_s and K_T is the adiabatic and isothermal bulk modulus, respectively, and

visco–elastic property of the highly viscous liquid. When heat is supplied to the liquid the liquid expands, but at the glass liquid interface the liquid can not expand in the direction parallel with the glass surface, since it is clamped to the stiff glass substrate (assuming that the glass does not expand, or at least does not expand as much as the liquid), see figure 1.1.

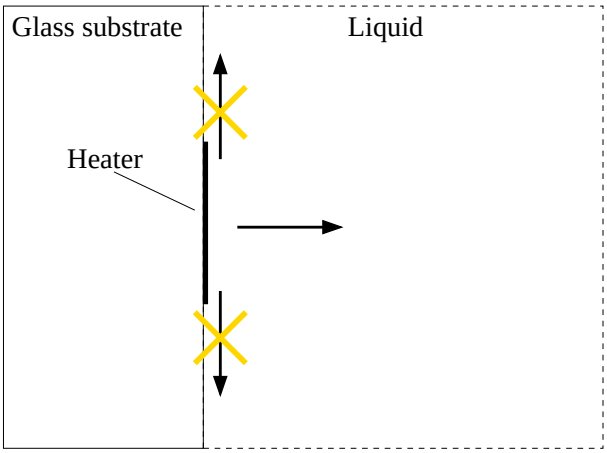

Figure 1.1 In the stiff planar heater experiment the liquid is clamped to the stiff glass substrate. It can expand freely perpendicular to the glass substrate surface (and heater), but not in the parallel direction, as indicated on the figure.

With time, of course, the liquid will flow, and the deformation due to the clamping will relax away. But the time–scale of this relaxation is the same, as is relevant for the heat capacity relaxation phenomena. Thus the heat capacity is not measured under constant pressure. This "problem" will be called the thermo–mechanical problem. Probably, the simplest way to model this is to assume that the liquid can expand freely in the direction perpendicular to the heater (and glass substrate), but not in the parallel direction [Christensen and Olsen, 1997, p. 275-276]. The measured heat capacity is in this case the longitudinal heat capacity, and it can be shown[2] that $c_V \leq c_l \leq c_p$, where c_V is the heat capacity at constant volume.

The thermo–mechanical problem might be overcome if the heater and substrate is flexible, that is, if it can expand with the liquid. With this in mind, three major preliminary objectives for the project was set from the beginning:

1. Make a setup, using the stiff planar heater and 3ω detection technique, and measure c_l.

c_V is the heat capacity at constant volume. $c_l = \frac{M_s}{M_T} c_V$, where $M_x = K_x + \frac{4}{3}G$ (for $x = s$ or $x = T$) is the longitudinal modulus and G is the shear modulus.

[2] It follows from the definition of c_p and c_l given in the previous footnote and that $K_T \leq K_s$.

2. Improve the setup, in order to get more accurate data than already available in the literature.

3. Develop a new, or partly new, technique that measures c_p, and compare the results with the measurements of c_l.

Basically the idea was to make the stiff planar heater experiment in a similar way as was already reported in the literature, and then try to improve the quality of the data, by somehow improving the design of the setup, and finally to try to make the planar heater experiment on a flexible substrate.

The aim of the work has not been to enlarge the frequency range of the measurements, of the frequency dependent heat capacity, but rather to try to measure more accurate data, with less scatter and systematic errors, even if that would mean narrowing the frequency range. As the accuracy of the data becomes larger it at the same time becomes even more important to be sure what physical quantity actually is measured in the experiments (i.e. is it c_p or some quantity e.g. c_l with a value close to c_p), and to understand the limits of the approximations and assumptions done.

1.2 Reached objectives

As time has passed, it has become clear that the preliminary objectives, described above, will not be reached within the limits of this work. Partly due to numerous experimental problems, the aim to make a setup and accurately measure c_l has only partly been reached. Some modifications of the traditional setup, that are important in order to measure a well defined quantity (c_l), have been developed. Further, the possibility of using carbon thin film heaters, which have several advantages compared to metal heaters, has been explored. The development of a setup to measure c_p has not even begun, and the thermo–mechanical problem will only be treated superficially in this report.

1.3 Notes to the reader

A few remarks on the notation used in this report:

When a ˜ is placed over a quantity, e.g. $\tilde{c}$, it means that it is a complex quantity. RE$\{\tilde{c}\}$, IM$\{\tilde{c}\}$ means the real and imaginary part of $\tilde{c}$, respectively.

To indicate the unit of a quantity square parentheses are used, e.g. if the unit of the diffusion constant (D) is millimeters squared per second it is written: $[D] = [mm^2 s^{-1}]$.

In this report c is used for the specific heat capacity deliberately not stating whether it is c_p, c_V, c_l or another heat capacity. This is done since it is not always easy to determine which heat capacity is in play (it depend on the exact experimental conditions). c is always the specific heat capacity per unit volume (not per unit mass).

Part I

Introduction

2 Project story

I started my Ph.D. project April 1^{st} 2000 and turned in the thesis on May 30^{th} 2003. During the first couple of months the ambitious goals of the project was formulated. Far from all of these goals have been reached. In this chapter, a brief informal tale of how this project originally started, how it developed, and how it ended, will be given. Though many details are left out this may help the reader to understand the context of the work, reported in the subsequent chapters, *but this chapter can be skipped, if only the final results of the work is found interesting*.

2.1 Framework and resources

From the beginning, most of the hardware was well established at the institute, including cryostate, frequency generator, and voltmeter for the 3ω detection. What was needed, was a measuring cell with the planar heater. For the production of the heaters, there was a electron beam evaporation chamber, which had not been used much.

Besides this, a lot of knowledge and creative thinking was available in the group consisting of Niels Boye Olsen, Jeppe C. Dyre, Thomas B. Schrøder, and my supervisor Tage E. Christensen. Later on Ph.D. student Niels L. Ellegaard joined the group. Every Thursday morning (except in June till August, and December, and January) the group meet to discuss the resent work by one or more of the people in the group, or to discuss articles and the like. Also, many students have attended these meetings. Among them Kristine Niss, Bo Jakobsen and Eva Uhre. At the well functioning institute electronic and mechanical workshop Torben Steen Rasmussen, Ebbe Hyldahl Larsen, Mogens Holte Jensen, David Brisson Andersen, Micheal Jensen, and Hans Wallin was ready to help me in any way possible. All these people have undoubtedly been the largest and most important resource, I have had access to. This work would have been impossible without them.

2.2 Heaters

After the electron beam evaporation chamber was set up[1] I started exploring how I could use it to fabricate the planar heaters. In the beginning the aim was to fabricate a nickel heater on a glass substrate and with gold electrodes, since this was the most widely used in the experiments reported in the literature. But I also experimented with other metals. I used a lot of time finding out how to adjust the different parameters of the chamber in order to get metal films of different thickness, and how the thickness affected the temperature coefficient (relative change of resistance with temperature) of the films. At my disposal was a simple interferometer, with which the thickness can be measured with a accuracy of around $\pm 15\%$. The problem with this method is that a light reflecting metal, such as silver, must be evaporated over the edge of the film, and thus in many cases the film can no longer be used for its purpose. For the heaters the gold electrodes served the purpose of this reflecting layer, and thus the heater film thickness could be determined in a non–destructive manner.

The deals that contain the source (the metal to be evaporated) in the chamber was originally made of some alloy. In some cases the deals melted, and a mixture of the deal alloy and source metal was evaporated. To overcome this problem the workshop fabricated deals in carbon. But also with the carbon deals, sometimes part of the deal material was mixed with the source metal. I experimented with different quality of carbon that can withstand different temperatures. I found that it does not matter so much what quality is used, it is more important that the deal is well filled with the source metal.

Since some of the carbon from the deals sometimes ended up on the substrate, I got the idea to fabricate carbon thin films. From the beginning this seemed promising. The carbon thin films have a larger resistance than the metal films, and they have a larger temperature coefficient (absolute value), both of which is advantageous. Much time have been spent on optimizing the carbon thin films. During this process some changes have been made inside the chamber, including the design of masks, and mask and substrate holder.

Along with this work, I tried to find out how to connect wires to the gold electrodes. I soon found out that soldering with ordinary solder was impossible, and I was not satisfied with the quality and durability of silver epoxy. After studying the literature I found that indium based solders can be used. It was not easy to find somewhere to bye this, but finally, with the help of Keld Kortsen from the

[1] Here, I will not describe how the chamber works or is designed. It will be done in chapter 13 (starting on page 87). For figures illustrating the chamber see figure 13.1, 13.2, 13.3, 13.4, and 13.5.

company Ketec A/S, I got the solder, and it works very well.

When I first started out, I had never guessed that I would use so much time on fabricating the thin films, but I have used much time on making somewhere between 300 and 400 carbon and metal depositions during these three years, opening and closing the chamber each time, not to mention the time spent testing the films afterwards.

2.3 Cell design

To begin with I measured the temperature coefficient of the heaters by placing them on a hot plate, and using a simple digital thermometer and a ohm-meter to measure pairs of temperature and resistance. The precision of the measured temperature coefficient was probably around 20%.

Later on I used a complete computer controlled setup including a cryostate and digital voltmeter (this will be described in chapter 15). The glass substrate was fixed at two edges by a PEEK (poly–ether–ether–ketone) holder (see figure 2.1).

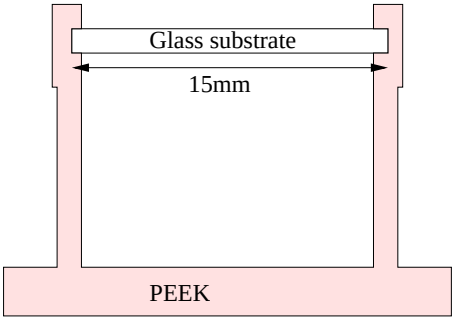

Figure 2.1 The first glass substrate holder, seen from the side. The heater can not bee seen, it is on top of the glass substrate.

With the glass substrate in this holder, I also tried to measure the thermal properties of the glass, and of a liquid on top of the glass but the results were impossible to interpret. As will be shown in chapter 6, there will be a static temperature difference between the heater and the cryostate. The size of this temperature DC offset of the heater, depend on the thermal coupling between the heater and the cryostate. Since the coupling with the PEEK holder was relatively week, the temperature DC ofset was relatively large. Also the coupling is not easy to model. Therefore I had a new holder fabricated, where the glass substrate is glued onto a copper backing in good thermal contact with the cryostate. (This will be described

in more detail in chapters 9 and 10. The measuring cell is shown on figure 9.1, page 55.)

The new copper backing improved the data significantly, and I was beginning to be able to interpret the measured data. At that time (about 2 years after I started the project), the resistance of my carbon heaters was between 1 and 2 $k\Omega$, and it was necessary to fabricate heaters with lower resistance in order to get enough power released in the heaters (the maximum output voltage of the frequency generator is $10V$). This was difficult with the carbon sources I used in the electron beam evaporation chamber, but after a while, I found a way to change them, making this possible.

I thought that I was finally about to reach the first goal: to make a setup using the stiff planar heater and 3ω detection technique, and measure c_l. And I was hoping that the quality of the data would be better than the ones already published. This was also about time, since with a little more than one year left time was running out quickly.

But, I was soon disappointed. Still there were problems. The data were noisy and did not look exactly as predicted by model. The rest of this story includes some unfortunate experimental conditions, and it is hard to bare thinking of the amount of time I "wasted" on these problems.

But, before I looked more into these problems I spend three months at the Department of Physics – Katholieke Universiteit Leuven in the city Leuven, Belgium. I worked with Prof. Dr. Christ Glorieux and Ph.D. student Hassane Bentefour. This was truly 3 wonderful months for me and my family.

After returning from Belgium I found that there were problems with the frequency generator. It could not deliver the effect that was needed, and as a result a lot of higher harmonics was present in the input signal, and everything changed as function of frequency. I began looking for a possible amplifier. Several months passed by before I found out that there already was one in the setup. It was a question of changing from one coaxial plug to another. Had I known this from the beginning, and been aware of the problems with the frequency generator, I could have saved a lot of time. At least I learned that is important also to check the things that one are sure off are working properly.

I think this lesson helped me find the next error, though it also took quit some time. It turned out that there was a electric leak between the heating stage in the cryostate and electrical ground. This caused the temperature of the cryostate to be unstable, $\pm$ a few degrees. The cryostate needed total renovation and after briefly using another one, which I also found did not work properly, I changed to the one which has been used for all the data presented in this report. This was at the end of January, 2003 and I had about 4 months left. At that time I thought I had a setup

that was working properly, heaters with the right resistance and a well designed measuring cell. Still I cannot say that I was satisfied with the results. The data was very noisy and did still not look exactly as predicted by model.

In order to understand why this was so, I made a lot of measurements, replacing the heater by a ordinary temperature–independent resistor. Among other things, I compared the 3ω signal, already present in the input signal, to the one in the output signal (it should just be reduced with the same factor as the 1ω signal). The results were strange, but reproducible. For this reason I was worried about the linearity of the voltmeter. I tried comparing different voltmeters, but no difference was found. After trying to change the wiring of the setup, I finally found that the metal body of the home–built relay box, that I used, was, by mistake, not grounded. After fixing this problem the measurements looked much better, and all other more or less strange hypotheses, that was thought of in order to explain the data, were no longer needed.

Especially at high frequencies there were still quite some scatter in the data, but at least this was understandable. Over $\approx 6Hz$ the voltmeter lost 1 digit. This has been improved somewhat by letting the voltmeter sample only 128 in stead of 512 times per period. Around may 20^{th} 2003 (less than 2 weeks before turning in this report) the electronic workshop finished a new frequency generator and it was possible to sample only 16 times per period. Unfortunately I have not had the time to explore these new possibilities completely.

Other last minutes changes was made. Originally I used a $1mm$ thick substrate for my heaters. But from April 17^{th} 2003 I started using $6mm$ thick substrates instead. This turned out to be necessary, since it was necessary to correct for the finite width of the heaters, and in order for these corrections to be correct the substrate had to be thick (compared to the thermal diffusion length). The final equations describing these corrections was worked out by Tage Christensen just a few weeks before turning in this report.

Even during the last week I was still making measurements. All measurements presented in this report have been made in the period 12/4–2003 till 29/5–2003, and the measurements on super–cooled liquids in the period 16/5–2003 till 29/5–2003. The report was turned in 30/5–2003.

2.4 Success?

Has this work been a success? If the criteria is whether or not I fulfill all the objectives set out from the beginning, this work is not a success. It may be possible to reach these objectives based on the work presented here, but more work is

needed to reach them. Still I will call it a success. I believe that in this report I present results that brings one closer to these objectives, and that can be very useful for anyone with the same goals. It was impossible from the beginning to predict the exact cause of things, and there was only one way to find out how much could be accomplished during the following three years – try!

Personally I have learned a lot, and I believe that others can extract important knowledge from this work.

3 Highly viscous liquids and the glass transition

In this chapter some details of the phenomenology of the glass transition will be given. Linear measurements done in this regime can be treated in linear response theory, and a short introduction to this is given in the following chapter. Several excellent introductions to these things are available. I can recommend: [Brawer, 1985], [Harrison, 1976] and [Debenedetti, 1996]. This and the following chapter build on these unless noted.

3.1 Glass transition

When a liquid is cooled from above to below its melting point it may super-cool (or under–cool as it is sometimes maybe more appropriately called). If it super-cools it does not crystallize, and it still has the properties of a liquid. Some liquids super–cool very easy and may be difficult to crystallize, other crystallize very easy and may be difficult to super-cool. The conditions that determine whether the liquid super-cools or crystallizes may be things like cooling rate and purity.

If the liquid does not crystallize and is cooled further, its viscosity will become larger and larger and at some temperature (the glass transition temperature, T_g) the liquid will fall out of equilibrium, and become a glass. T_g is not a fixed quantity, it depend on the cooling rate: the faster cooling the higher T_g. Thus the glass transition is not a phase transition (despite its confusing name), but a dynamic phenomena, arising from the fact that the time needed for the system to come into equilibrium becomes larger than the time–scale of the experiment. This is not something that we human beings can come about just by waiting long enough, since the time it takes the system to come to equilibrium effectively becomes infinite, on time–scales relevant to mortal scientists.

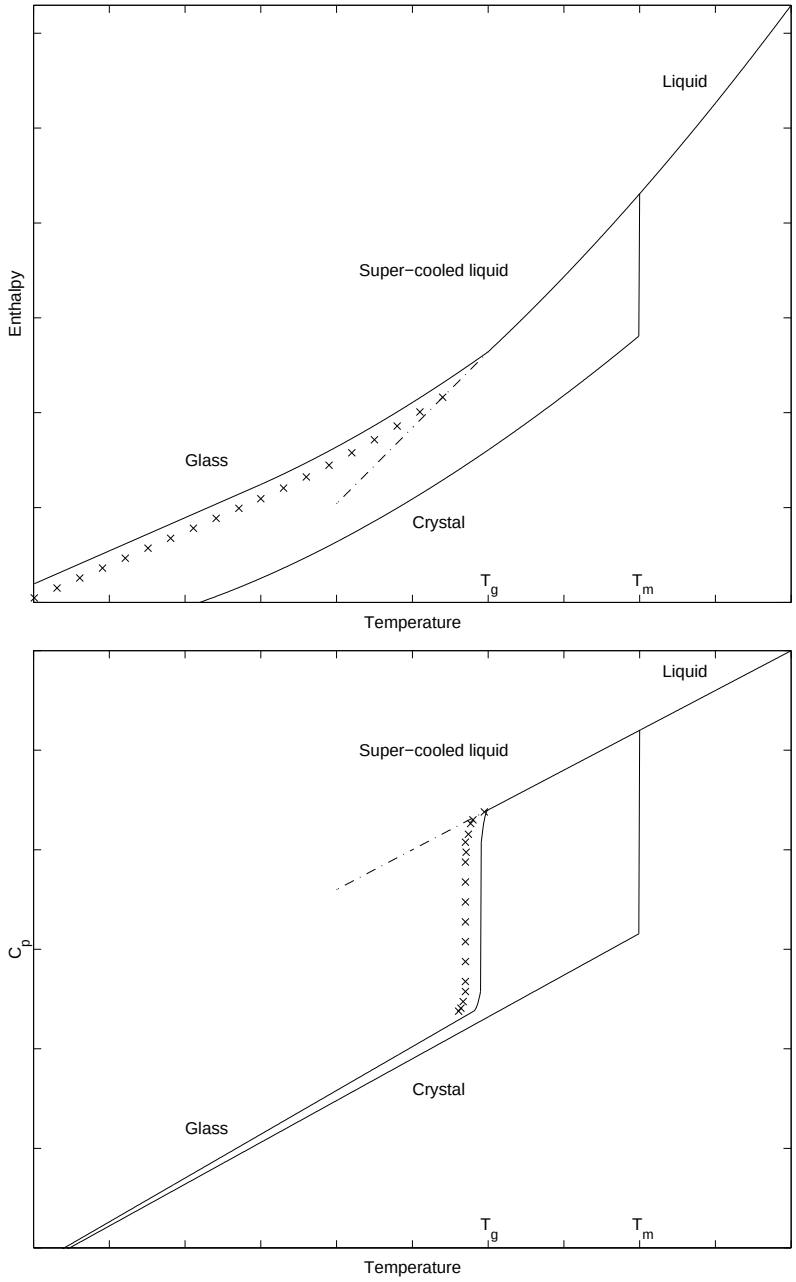

Figure 3.1 Schematic figure showing the enthalpy and heat capacity from above the melting point to below the glass transition temperature. T_m is the melting temperature and T_g the glass transition temperature. T_g depend on the cooling rate. The points marked "x" represent a lower cooling rate than the straight line. If the cooling rate is made even lower, one can imagine that the system will follow the dotted line. But, since the viscosity grows dramatically near T_g, the time needed to follow the dotted line grows enormously and becomes effectively infinite on time–scales relevant for mortal scientists. Similar figures can be found in many textbooks e.g. [Brawer, 1985, p. 8-9], and [Debenedetti, 1996, 244].

The glass transition is associated with large changes of physical quantities such as heat capacity, bulk and shear modulus, thermal expansion coefficient, and dielectric constant (for dielectric liquids). On figure 3.1 this is schematic shown for the enthalpy (H) and specific heat capacity at constant pressure: $c_p = \left(\frac{\partial H}{\partial T}\right)_p$.

Under some circumstances a super–cooled liquid can crystallize, e.g. if it is disturbed mechanically. This is made use of in some hand–heaters: a little plastic bag contain a super–cooled liquid and a little piece of metal. When the metal is clicked, the disturbance makes the liquid crystallize and heat is released (see figure 3.1). Since the liquid inside the bag has a melting point somewhere between room temperature and $100°C$, it can be boiled and used again.

3.2 Relaxation and frequency dependent heat capacity

If a small amount of heat is given as a input to a low viscous liquid (in equilibrium), and the liquid afterwards is held at adiabatic conditions, the result will be a instantaneous temperature rise to the new equilibrium temperature. By instantaneous is here understood instantaneous on time–scales much longer than phonon times ($\approx 10^{-12}s$), and that the time is long enough, so that the temperature is uniform throughout the system. If the experiment is instead performed on a highly viscous liquid (such as a super–cooled liquid near T_g), the result will also be a instantaneous temperature rise, but followed by a relaxation towards a lower temperature (e.g. [Fujimori and Oguni, 1994], [Fujimori et al., 1992]). The two situations are illustrated on figure 3.2.

The relaxation phenomena can be understood in terms of fast and slow degrees of freedom. When the heat is supplied, it will be distributed among the fast degrees of freedom. As time goes on, some of the energy will be distributed to the slower degrees of freedom, and the temperature decreases.

Instead of the above described time–domain experiment, a frequency–domain experiment could be performed, where the liquid is periodically heated and cooled. The amplitude and phase of the resulting temperature oscillations will then depend on frequency. At low frequencies (corresponding to long times) all the degrees of freedom come into play and a relatively high heat capacity will be measured, while at high frequencies (corresponding to short times) only the fast degrees of freedom are fast enough to come into play, and a lower heat capacity is measured. This is illustrated on figure 3.3

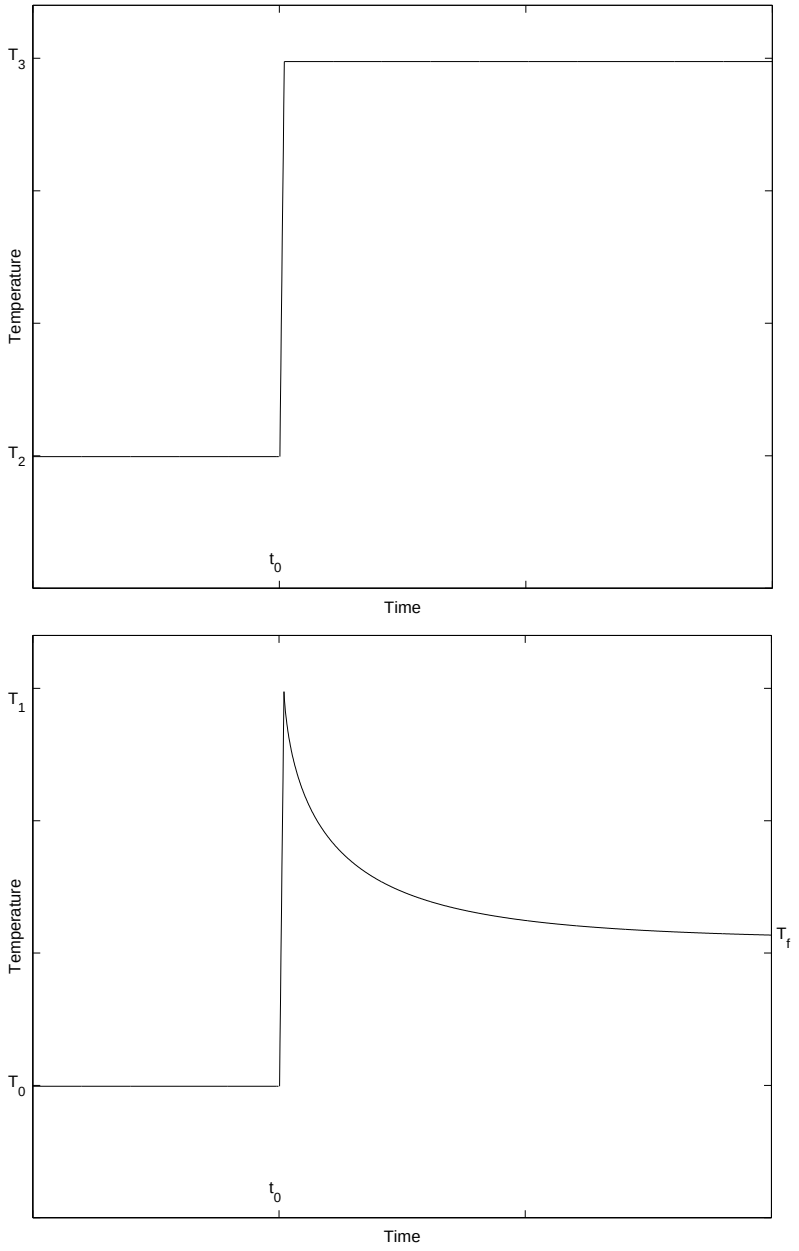

Figure 3.2 If a small amount of heat is supplied to a low viscous liquid (at time t_0) which afterwards is held at adiabatic conditions, the result will be a instantaneous temperature rise of the liquid (top curve). If the same experiment is performed on a highly viscous liquid, relaxation will follow a instantaneous temperature rise (lower curve).

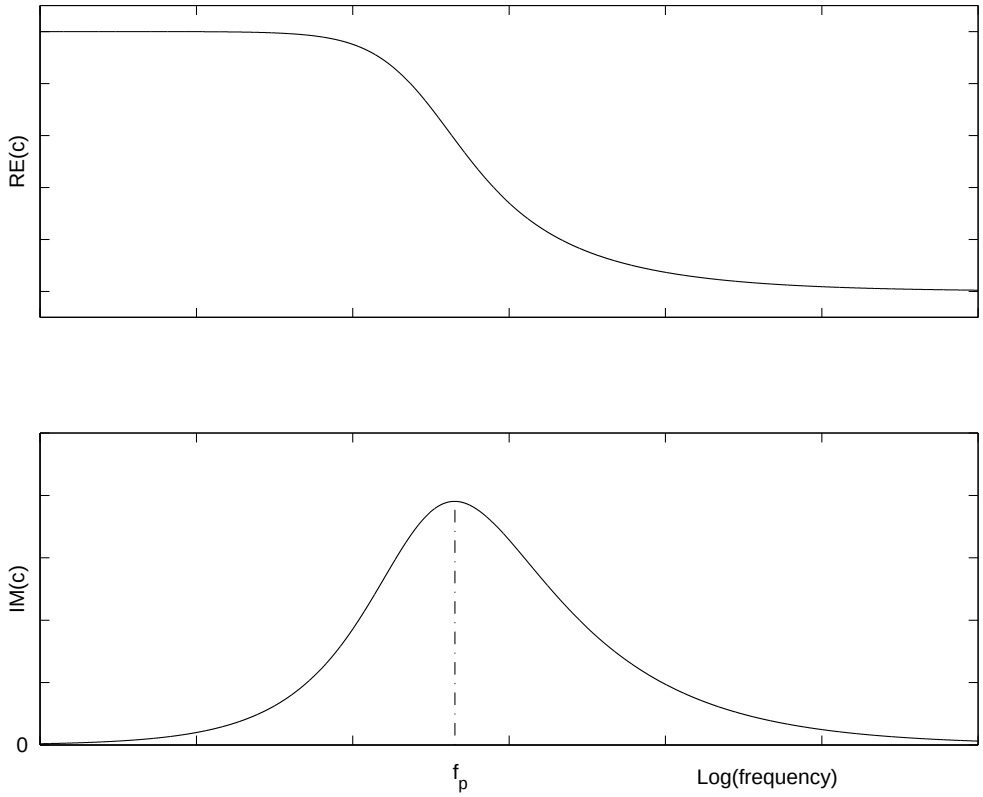

Figure 3.3 Real and imaginary part of the heat capacity (c) as function of the logarithm of frequency. At low frequencies, compared to high frequencies, a higher heat capacity is measured. At intermediate frequencies, relaxation is observed. The peak in the imaginary part of c is a result of the phase of the temperature oscillations lacking behind the phase of the heat current input (more about this in chapter 5).

Some times a glass transition temperature (T_g') is defined as the temperature at which $\tau_p \equiv 1/f_p = 1000s$ (or $\tau_p = 100s$), where f_p is the loss peak frequency (see figure 3.3) of the quantity in question, e.g. heat capacity (here a distinction is made between T_g and T_g'). Thus not only is T_g' a dynamic quantity, it may depend on the physical quantity in question. τ_p varies with temperature, and typical variations around T_g is that it becomes 10 times larger when the temperature is lowered $5K$. Note that this definition of T_g' is not based on the liquid falling out of equilibrium (as the definition of T_g mentioned earlier) but on measurements made on the equilibrium liquid. Of course T_g and T_g' may coincide, if the cooling rate is properly chosen. No matter how the glass transition temperature is defined, the substance is only called a glass when fixed in a non–equilibrium state (in other words if the substance is in equilibrium it is still a super–cooled liquid even at

temperatures lower than T_g').

One striking feature of the glass transition is the non-Arrhenius behavior of $\tau_p(T)$ (e.g. [Harrison, 1976, p. 20], [Brawer, 1985, p. 196], [Debenedetti, 1996, p. 257]). That is, it is not in general a simple thermal activated process governed by: $\tau_p = \tau_0 e^{E/k_B T}$, where τ_0 and E are constants, $k_B = 1.38066 \times 10^{-23} JK^{-1}$ Boltzmanns constant, and T the temperature.

Another striking feature of the glass transition is that the relaxation cannot in general be described by a single relaxation time: a single exponential decay. Thus, the bottom curve in figure 3.2 is not a simple exponential decay. This feature is sometimes explained by saying that a distribution of relaxation times is needed, meaning that the total relaxation is a weighted sum of several exponential decays (e.g. [Harrison, 1976, p. 52], [Brawer, 1985, p. 42]).

4 Linear response theory

In this chapter a short introduction to linear response theory is given. This in not an attempt to give a complete overview of the field. Hopefully it can be used as a reminder to those who have seen it before, and at the same time serve the purpose of defining some of the terminology used. Those familiar with all this can just skip it.

Linear response theory can be used to describe the experiments mentioned in the previous chapter. As the name indicates, the relation between input (I) and output (O) is considered linear. This means that, if the input is multiplied by some constant, then the output will be multiplied by the same constant (and thus that the output, coming from the sum of two inputs, must correspond to the sum of the output that would result from each of the two inputs). This linearity criterion is usually only fulfilled if the input is sufficiently small.

For a relaxing system there is a delay between the input (I) and the output (O) of the system, and thus in calculating the output at a given time not only the input at that time, but also at past times, needs to be considered. Thus the input dI at a time t' earlier than t: $dI(t-t')$, gives a contribution dO to the output at time t:

$$dO(t) = R(t')dI(t-t'),$$

where the response function (R) only depend on the time difference (t') between the output and input, and of course not on the absolute time.

The total output at time t is then:

$$O(t) = \int_0^\infty R(t')dI(t-t') = \int_0^\infty R(t')\dot{I}(t-t')dt', \tag{4.1}$$

$$\Updownarrow$$

$$O(t) = R \circ I, \tag{4.2}$$

where $\dot{I} \equiv dI/dt'$, and the symbol "$\circ$" is defined as the convolution with the time derivative, given by equation 4.1.

In the experiment shown on figure 3.2 the input is the supplied heat and the process of keeping the system at adiabatic conditions, and the output is the temperature

rise. The input is thus a step function which can be described by:

$$I(t) = \begin{cases} I_0 E(t) = (I_0)1 \text{ for } t > 0 \\ I_0 E(t) = (I_0)0 \text{ for } t \leq 0 \end{cases} \tag{4.3}$$

$$\Downarrow$$

$$\dot{I}(t) = I_0 \delta(t_+), \tag{4.4}$$

where E is a unit Heaviside stepinput, I_0 the amplitude of the input, and δ the Dirac delta function.[1]

Equation 4.1 gives:

$$O(t) = I_0 \int_0^\infty R(t')\delta(t-t')dt' = I_0 R(t)$$

It is seen that the response function in the example (figure 3.2) is one divided with the heat capacity of the system.

In the frequency–domain experiment, the input is given by a periodic varying function (in the example on figure 3.3 the input is the heat current). Below it will just be considered to be a simple cosine function (with amplitude I_0 and cyclic frequency Ω), but in general it can be any periodic function, and the equations must apply for every Fourier component:

$$I(t) = I_0 \cos(\Omega t) = \text{RE}\left\{ I_0 e^{i\Omega t} \right\}$$

Equation 4.1 gives:

$$O(t) = \text{RE}\left\{ I_0 e^{i\Omega t} i\Omega \text{LT}\left[R(t')\right](s) \right\}, \tag{4.5}$$

where $s = i\Omega$ and LT is the Laplace transform defined as (e.g. [Chow, 2000, p. 372], [Arfken, 1985, p. 795]):

$$\text{LT}[f](s) \equiv \int_0^\infty f(t)e^{-st}dt \qquad \text{Laplace transform} \tag{4.6}$$

The output will oscillate at the same frequency as the input, and can be written:

$$O(t) = \text{RE}\left\{ \tilde{O}_0 e^{i\Omega t} \right\}, \tag{4.7}$$

[1] The Dirac delta function is defined as (e.g [Arfken, 1985, p. 81]):

$$\delta(t) = 0, \text{ for } t \neq 0$$
$$\int f(t)\delta(t)d\tau = f(0),$$

but here $f(0)$ is understood as $f(0_+) \equiv \lim_{t\to 0_+} f(t)$, (that is, the limit coming from positive t) indicated by the subscript "+" on t in equation 4.4.

where the amplitude $\tilde{O}_0$ can be complex, which shows that there can be a phase difference between the in– and output. Since the equations are linear there are no higher order harmonics i.e. there are no terms of the type $e^{in\Omega t}$, with $n > 1$. Thus the calculations can just be done using the complex in– and output, and remembering that the actual physical signal is the real part. Using equations 4.5 and 4.7:

$$\begin{aligned} \tilde{O}_0 &= I_0 i\Omega \mathrm{LT}\left[R(t')\right](s) \\ \Updownarrow & \\ \frac{\tilde{O}_0}{I_0} &\equiv \tilde{R}(\Omega) = i\Omega \mathrm{LT}\left[R(t')\right](s), \end{aligned} \tag{4.8}$$

where $\tilde{R}(\Omega)$ is the complex frequency dependent response function.

It is seen that the response function in the example (figure 3.3) describes what is called the thermal impedance (this will be defined in more detail in chapter 5).

4.1 6 different response functions

For the in– and output there are four possibilities:

Type	Generalized	Symbol
A	Force (voltage)	e
A	Momentum	$p = \int e dt$
B	Velocity (current)	f
B	Displacement (charge)	$q = \int f dt$

If the input is of type A the output is of type B and vise versa. This gives 8 possible combinations in equation 4.2, but two of them are identical with two other (since $p = \int e dt$ and $q = \int f dt$), and only 6 possibilities remain:

Input type	Response function	Given by
A	Compliance, J	$q = J \circ e$
A	Admittance, Y	$f = Y \circ e$
A	"Lightness", F	$f = F \circ p$
B	Modulus, G	$e = G \circ q$
B	Impedance, Z	$e = Z \circ f$
B	Inertia, M	$p = M \circ f$

Note that:

$$\begin{aligned}[ef] &= [\text{Energy/time}],\\ [eq] &= [\text{Energy}],\\ [pf] &= [\text{Energy}],\end{aligned}$$

from which it is seen that the experimental situations described is different ways of exchanging energy with the system.

4.2 Note on Fourier and Laplace transform

If the time–dependent response function is known, the frequency dependent response function can be found using equation 4.8. Instead of using the Laplace transform the Fourier transform can be used (e.g. [Chow, 2000, p. 166], [Arfken, 1985, p. 794]):

$$\text{FT}[f](\Omega) \equiv k\int_{-\infty}^{\infty} f(t)e^{-i\Omega t}dt, \quad \text{Fourier transform} \tag{4.9}$$

$$\text{FT}^{-1}\left[\tilde{f}(\Omega)\right](t) \equiv \frac{1}{2\pi k}\int_{-\infty}^{\infty} \tilde{f}(\Omega)e^{i\Omega t}d\Omega, \text{Inverse Fourier transform} \tag{4.10}$$

where the constant k can be chosen freely. Here $k = 1$ is chosen so that the Fourier and Laplace transform tally.

As can be seen from equation 4.6 and equation 4.9 the Fourier transform can be used instead of the Laplace transform if $R(t) = 0$ for $t < 0$ (and $s = i\Omega$), which is usually the case.

It can be shown (by doing integration by parts) that, if f(t) in equation 4.6 is of exponential order, then (e.g. [Chow, 2000, p. 382]):

$$\text{LT}\left[\dot{f}(t)\right] = s\text{LT}[f(t)] - f(0)$$

In the usual physical cases $f(0) = 0$ as in equation 4.3.

For the transformation of an integral (e.g. [Chow, 2000, p. 383]):

$$\text{LT}\left[\int f(t)dt\right] = \frac{1}{s}\text{LT}[f(t)],$$

and thus integration and differentiation in time–domain is in frequency–domain replaced by dividing or multiplying by s, respectively.

Part II

Measuring technique and modeling

5 Thermal impedance

The quantity measured in many thermal experiments is thermal impedance. In this chapter this quantity will be defined. Subsequent chapters will show how it can be measured in some cases and what information can be extracted from it.

Imagine that in some material there is a temperature gradient and as a result a heat flow along this gradient. This could for example be realized via a small heater with temperature T_p surrounded by a liquid inside a cryostate of temperature T_k. If this is in the linear limit (and equilibrium has been reached) then:

$$\begin{aligned} \Delta T &\equiv T_p - T_k = I_T Z_{T,DC} \\ \Updownarrow & \\ Z_{T,DC} &= \frac{\Delta T}{I_T}, \end{aligned} \tag{5.1}$$

where the proportionallity factor $(Z_{T,DC})$ between ΔT and the heat current (I_T) is the thermal impedance .

Equation 5.1 is a sort of generalized "Ohm's law". ΔT plays the role of a generalized voltage, I_T plays the role of a generalized current and $Z_{T,DC}$ the role of a generalized resistance (impedance). This equation is only valid in the linear limit where the temperature difference ΔT is small. (In the linear limit, a small change in ΔT results in exactly such a change in I_T that equation 5.1 gives the same result for $Z_{T,DC}$. Thus it is easy to check experimentally, whether or not the assumption of linearity is valid.)

Since in this case it is a static generalized voltage (ΔT), this thermal impedance will be called the DC thermal impedance. In the following it will be shown how to define a more general complex thermal impedance, which must be used if the temperature (T_p) and the heat current (I_T) are time–dependent.

Imagine that the heat current has a DC part (I_{Tm}) and a harmonic time–dependent part, so that the heat current $(I_T(t))$ varies around the average value (I_{Tm}), with frequency $f = \Omega/2\pi$ and amplitude (I_{TA}):

$$\begin{aligned} I_T(t) &= I_{Tm} + \Delta I_T(t) \\ \Delta I_T(t) &= I_{TA}\cos(\Omega t + \varepsilon) = \tfrac{1}{2}\left(\tilde{I}_{TA}e^{i\Omega t} + \tilde{I}^*_{TA}e^{-i\Omega t}\right), \quad \tilde{I}_{TA} \equiv I_{TA}e^{i\varepsilon} \end{aligned} \tag{5.2}$$

The temperature of the heater T_p will vary around some average temperature (T_{pm}) with the same frequency f. But there may be a phase difference (χ) between I_T and T_p, and therefore:

$$\begin{aligned} T_p(t) &= T_{pm} + \Delta T_p(t), \\ \Delta T_p(t) &= T_A \cos(\Omega t + \chi + \varepsilon) = \tfrac{1}{2}\left(\tilde{T}_A e^{i\Omega t} + \tilde{T}_A^* e^{-i\Omega t}\right), \quad \tilde{T}_A \equiv T_A e^{i\chi} e^{i\varepsilon} \end{aligned} \tag{5.3}$$

Now, the complex thermal impedance ($\tilde{Z}_T$) can be defined as:

$$\begin{aligned} & \tilde{Z}_T \equiv \frac{\tilde{T}_A}{\tilde{I}_{TA}} = \frac{T_A e^{i\chi}}{I_{TA}} \\ \Updownarrow & \\ & \tilde{Z}_T = |\tilde{Z}_T| e^{i\chi}, \;\; |\tilde{Z}_T| = \frac{T_A}{I_{TA}}, \end{aligned} \tag{5.4}$$

(where $|\tilde{Z}_T|$ is the modulus of the complex $\tilde{Z}_T$). Equation 5.4 tells us that if we can measure the amplitude (T_A) and phase shift (χ) of the temperature oscillations resulting from a known heat current input (I_T), then we can obtain $\tilde{Z}_T$.

Again, equation 5.4 is only valid in the linear limit, but it is easy experimentally to check whether or not the assumption of linearity is valid, since then the same result must be obtained for $\tilde{Z}_T$ for different I_{TA}.

It is interesting to note that:

$$\mathrm{RE}\left\{\tilde{Z}_T\right\} = \frac{1}{2}\left(\frac{T_A e^{i\chi}}{I_{TA}} + \frac{T_A e^{-i\chi}}{I_{TA}}\right) = \frac{T_A}{I_{TA}}\cos(\chi) = |\tilde{Z}_T|\cos(\chi) \tag{5.5}$$

$$\mathrm{IM}\left\{\tilde{Z}_T\right\} = \frac{1}{2i}\left(\frac{T_A e^{i\chi}}{I_{TA}} - \frac{T_A e^{-i\chi}}{I_{TA}}\right) = \frac{T_A}{I_{TA}}\sin(\chi) = |\tilde{Z}_T|\sin(\chi) \tag{5.6}$$

$$\Updownarrow$$

$$\tilde{Z}_T = |\tilde{Z}_T|\left(\cos(\chi) + i\sin(\chi)\right)$$

$$\Downarrow$$

$$\frac{\mathrm{IM}\left\{\tilde{Z}_T\right\}}{\mathrm{RE}\left\{\tilde{Z}_T\right\}} = \tan(\chi) \tag{5.7}$$

At low frequencies there will be no phase shift (χ) between I_T and T_p, since on this time–scale the system is able to respond immediately with a temperature jump to a heat current input. But when the frequency gets so high that the system response time is not fast enough to follow the heat current input, there will be a phase difference between I_T and T_p. As can be seen from equation 5.6, a result of this phase difference will be a non–zero imaginary part of $\tilde{Z}_T$.

Equations 5.5 and 5.6 show that:

$$\chi = 0 \quad \Rightarrow \quad \mathrm{RE}\left\{\tilde{Z}_T\right\} = \frac{T_A}{I_{TA}},\ \mathrm{IM}\left\{\tilde{Z}_T\right\} = 0$$

$$\chi = \frac{-\pi}{2} \quad \Rightarrow \quad \mathrm{RE}\left\{\tilde{Z}_T\right\} = 0,\ \mathrm{IM}\left\{\tilde{Z}_T\right\} = -\frac{T_A}{I_{TA}}$$

In the first case ($\chi = 0$) the temperature (T_p) varies in–phase with the heat current (I_T), while in the second case they are $\pi/2$ (maximum, $\chi = -\pi/2$) out of phase. For this reason, the real part is sometimes called the in–phase component and the imaginary part is called the out–of–phase component.

The phase difference χ must be in the interval $-\pi/2 \leq \chi \leq 0$. The simple physical argument for this is that $\chi < -\pi/2$ would mean that the temperature should fall at the same time as heat is supplied, which is unphysical.

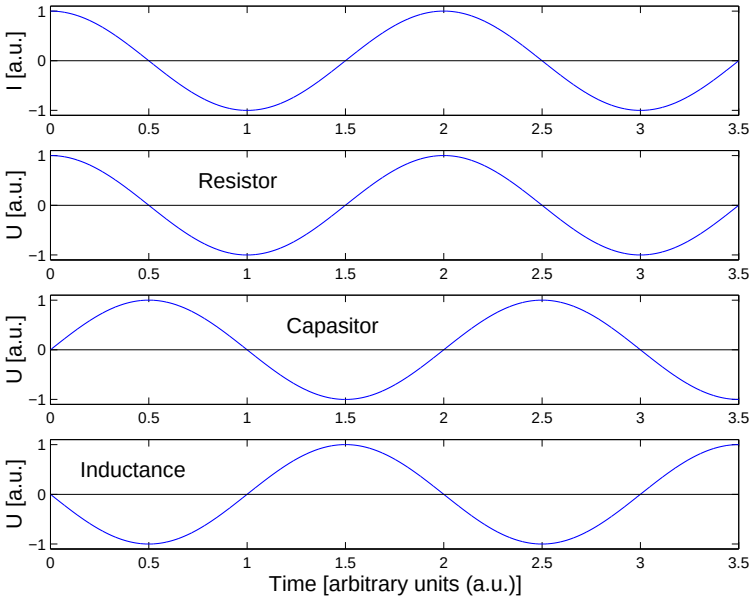

Figure 5.1 The top curve shows the time–dependent current in the electrical circuit of a resistor, a capacitor and an inductance in series. The three other curves show the voltage across the resistor, capacitor and inductance, respectively. (The numbers on the axis are arbitrarily chosen.)

Another way of saying this is that there is no thermal analog to inductance: imagine a small electrical circuit consisting of a resistor, a capacitor and an inductance in series. If $I(t) \propto \cos(\omega t)$ is the time–dependent current in the circuit (varying as a cosine function with time), then the voltage across the resistor, across the capacitor

and across the inductance will vary as $\cos(\omega t)$, $\cos(\omega t - \pi/2)$ and $\cos(\omega t + pi/2)$, respectively. This is shown in figure 5.1. Now, the thermal analogs to a resistor and a capacitor are heat resistance (inverse thermal conductivity) and heat capacity, respectively, but there is no analog to inductance.

Finally, it is worth noting that, if the experimental setup is such that the surroundings some distance from R_p has the constant temperature T_k, then (in equilibrium):

$$\chi \to 0 \text{ for } \omega \to 0$$
$$T_A \to \Delta T = T_{pm} - T_k \text{ for } \omega \to 0,$$

since on that long time–scale (at low frequencies) the system responds "immediately" and the minimum temperature of T_p will thus be equal to T_k (and the temperature amplitude is $T_{pm} - T_k$). Together with equations 5.1 and 5.5, this shows that:

$$Z_{T,DC} = \lim_{\omega \to 0} \left(\mathrm{RE} \left\{ \tilde{Z}_T \right\} \right)$$

6 3ω detection technique

The main idea in the 3ω detection technique is to use a temperature–dependent electrical resistor as heater and thermometer simultaneously. It functions as a heater since it has a electrical resistance, thus a time–dependent voltage across the resistor will result in a time–dependent thermal current in the sample surrounding the resistor. At the same time it functions as a thermometer, since the resistance depend on temperature. As will be shown in the following, information about the complex thermal impedance can then be extracted from the part of the voltage across the heater that varies with three times the frequency of the input–voltage (the third harmonic). This fact, of course, is the origin of the name 3ω detection technique (or 3ω method).

Then, depending on the details of the setup (geometry, frequency, range etc.) the complex thermal impedance can be related to thermal properties of the heater and its surroundings. This will be discussed in more detail in the following chapters.

Sometimes "the 3ω method" is used as a name for an experiment that uses the information contained in the third harmonic in a planar geometry. But since the detection of the third harmonic and the extraction of the thermal impedance from this signal is not connected to any specific geometry, the name "3ω detection technique" will in this report be used for any technique that uses the third harmonic signal to measure the thermal impedance. (For the history of the technique, see chapter 8.)

Now, imagine that a temperature–dependent resistor (R_p) is placed in a small electrical circuit as illustrated on figure 6.1.

The following notation is used. The input and output–voltage are designated U and V, respectively, and can be a sum of several harmonics, in general:

$$U = U_0 + \tfrac{1}{2}\sum_{n=1}^{\infty}\left(\tilde{U}_n e^{in\omega t} + \tilde{U}_n^* e^{-in\omega t}\right) = U_0 + \sum_{n=1}^{\infty} U_n \cos(n\omega t + \varphi_n)$$

$$V = V_0 + \tfrac{1}{2}\sum_{n=1}^{\infty}\left(\tilde{V}_n e^{in\omega t} + \tilde{V}_n^* e^{-in\omega t}\right) = V_0 + \sum_{n=1}^{\infty} V_n \cos(n\omega t + \psi_n)$$

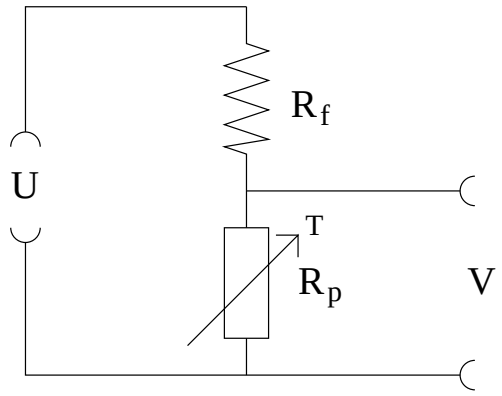

Figure 6.1 "R_p" and "R_f" both designate the resistors and the value of their electrical resistance. Thus, R_p is the temperature–dependent resistor with electrical resistance R_p, and R_f is the temperature–independent resistor with electrical resistance R_f. U is the input voltage and V is the output–voltage measured across R_p.

The complex amplitudes ($\tilde{U}_n$, $\tilde{V}_n$) are just the combination of the amplitudes and phase shifts (e.g. $\tilde{U}_n \equiv U_n e^{i\varphi_n}$, $U_n = |\tilde{U}_n|$ and φ_n is the phase shift).

In the ideal case, U is a harmonic time–dependent voltage of frequency $f = \omega/2\pi$ and given by:

$$U = U_1 \tfrac{1}{2}\left(e^{i\omega t} + e^{-i\omega t}\right)$$

It may not be easy to produce an input signal that does not contain any other harmonics, with no phase shifts and with no DC offset (U_0). Therefore, all the calculations will be done assuming that U is given by:

$$U = \tfrac{1}{2}\left(\tilde{U}_1 e^{i\omega t} + \tilde{U}_1^* e^{-i\omega t} + \tilde{U}_3 e^{i3\omega t} + \tilde{U}_3^* e^{-i3\omega t}\right) + U_0 \qquad (6.1)$$

Of course, U can also contain other harmonics (e.g. 2ω, 4ω), but doing the calculations with U given by equation 6.1 will show that the other harmonics are not relevant.

U depends on time, and thus the power (P) released in R_p depends on time. The temperature (T_p) and resistance $(R_p(T_p))$ of R_p will therefore also depend on time. The variation of R_p can be written as:

$$R_p(t) = R_{pm} + \Delta R_p(t), \qquad (6.2)$$

where R_{pm} is the mean (time–independent) value of R_p, and $\Delta R_p(t)$ the deviation from this mean value.

The temperature coefficient (α) of R_p is defined by:

$$\alpha \equiv \frac{d\ln R_p}{dT_p} = \frac{1}{R_p}\frac{dR_p}{dT_p} \Leftrightarrow dR_p = R_p \alpha dT_p \tag{6.3}$$

Now, if ΔR_p is so small that $\alpha \approx$ constant, then:

$$\Delta R_p \approx R_{pm}\alpha\Delta T_p$$

Inserting this into equation 6.2 yields:

$$R_p(t) \approx R_{pm}(1+\alpha\Delta T_p), \tag{6.4}$$

(ΔT_p is the temperature deviation from the mean value T_{pm}; cf. equation 5.3).

Since R_p varies with time, V does not just vary the same way as U with time, but, as will be shown below, there will be a 3ω contribution to V not coming from the 3ω component of U. But since $R_{pm} \gg \Delta R_p(t)$, this contribution is very small and can be neglected when the power released in R_p is calculated.

$V_{1\omega}$ is the part of V that varies with ω:

$$V_{1\omega} = \tfrac{1}{2}\left(\tilde{V}_1 e^{i\omega t} + \tilde{V}_1^* e^{-i\omega t}\right) \tag{6.5}$$

The heat flow (I_T) from R_p to the surroundings is simply equal to the power (P) released in R_p (after equilibrium has been reached). Thus:

$$\begin{aligned}
I_T &= P = \frac{V^2}{R_p} \approx \frac{V_{1\omega}^2}{R_{pm}} \\
&= \frac{1}{4R_{pm}}\left[\tilde{V}_1 e^{i\omega t} + \tilde{V}_1^* e^{-i\omega t}\right]^2 \\
&= \frac{1}{R_{pm}}\left[(\tilde{V}_1)^2 e^{i2\omega t} + (\tilde{V}_1^*)^2 e^{-i2\omega t} + 2\tilde{V}_1\tilde{V}_1^*\right] \\
&= \frac{V_1^2}{2R_{pm}}\frac{1}{2}\left[e^{i(2\omega t+2\psi_1)} + e^{-i(2\omega t+2\psi_1)} + 2\right] \\
&= I_{Tm} + \frac{1}{2}\left(\tilde{I}_{TA}e^{i2\omega t} + \tilde{I}_{TA}^* e^{-i2\omega t}\right), \quad \tilde{I}_{TA} = I_{TA}e^{i2\psi_1} \\
&= I_{Tm} + \Delta I_T(t),
\end{aligned} \tag{6.6}$$

where the average value (I_{Tm}) and amplitude (I_{TA}) of I_T are given by:

$$I_{TA} = I_{Tm} \approx \frac{V_1^2}{2R_{pm}} \tag{6.7}$$

Note that, besides the DC offset (I_{Tm}), I_T has a part that varies with twice the frequency (2ω) as the input voltage. Also, if equation 6.6 is compared with equation 5.2, it is seen that in this case $\varepsilon = 2\psi_1$.

I_{Tm} can be expressed in terms of quantities that are either known or measured by noting that the electrical current is the same through R_p and R_f:

$$\begin{aligned} & \frac{V_{1\omega}}{R_{pm}} \approx \frac{U_{1\omega}}{R_{pm}+R_f} \approx \frac{U_{1\omega}-V_{1\omega}}{R_f} \\ & \Updownarrow \\ & R_{pm} \approx R_f \frac{V_1}{U_1-V_1}, \end{aligned} \tag{6.8}$$

where $U_{1\omega}$ is the 1ω component of U and since $U_{1\omega}$ and $V_{1\omega}$ have approximately the same phase ($\varphi_1 \approx \psi_1$. See equation 6.1 and equation 6.5). The combination of equation 6.7 and equation 6.8 yields:

$$I_{Tm} \approx \frac{V_1^2(U_1-V_1)}{2R_fV_1} = \frac{V_1(U_1-V_1)}{2R_f} \tag{6.9}$$

The goal is to write an equation for V:

$$V = \frac{UR_p}{R_p+R_f} \tag{6.10}$$

Now, inserting equation 6.4 for R_p gives:

$$V \approx \frac{UR_{pm}(1+\alpha\Delta T_p)}{R_{pm}(1+\alpha\Delta T_p)+R_f} = \left(\frac{UR_{pm}(1+\alpha\Delta T_p)}{R_{pm}+R_f}\right)\left(\frac{1}{1+\frac{R_{pm}\alpha\Delta T_p}{R_{pm}+R_f}}\right)$$

$1 \gg \alpha\Delta T_p$ and the expansion to the 1^{st} order in the two small terms $\left(\alpha\Delta T_p \text{ and } \frac{R_{pm}\alpha\Delta T_p}{R_{pm}+R_f}\right)$ yields:

$$V \approx \frac{UR_{pm}}{R_{pm}+R_f} + \frac{R_fR_{pm}\alpha}{(R_{pm}+R_f)^2}\Delta T_pU \tag{6.11}$$

ΔT_p can be expressed by inserting $\tilde{T}_A$ from equation 5.4 into equation 5.3:

$$\Delta T_p(t) = \tfrac{1}{2}\left(\tilde{Z}_T\tilde{I}_{TA}e^{i2\omega t} + \tilde{Z}_T^*\tilde{I}_{TA}^*e^{-i2\omega t}\right), \tag{6.12}$$

where $\Omega = 2\omega$ is the angular frequency of the heat current and temperature oscillations.

$\Delta T_p U$ is needed for insertion into equation 6.11. This can be calculated using equations 6.12 and 6.1:

$$\begin{aligned}\Delta T_p U &= \tfrac{1}{4}\left(\tilde{Z}_T\tilde{I}_{TA}e^{i2\omega t}+\tilde{Z}_T^*\tilde{I}_{TA}^*e^{-i2\omega t}\right)\left(\tilde{U}_1e^{i\omega t}+\tilde{U}_1^*e^{-i\omega t}\right.\\ &\quad\left.+\tilde{U}_3e^{i3\omega t}+\tilde{U}_3^*e^{-i3\omega t}+2U_0\right)\\ &= \tfrac{1}{4}\left[\tilde{Z}_T\tilde{I}_{TA}\tilde{U}_1e^{i3\omega t}+\tilde{Z}_T\tilde{I}_{TA}\tilde{U}_1^*e^{i\omega t}+\tilde{Z}_T\tilde{I}_{TA}\tilde{U}_3e^{i5\omega t}\right.\\ &\quad+\tilde{Z}_T\tilde{I}_{TA}\tilde{U}_3^*e^{-i\omega t}+2\tilde{Z}_T\tilde{I}_{TA}U_0e^{i2\omega t}+\tilde{Z}_T^*\tilde{I}_{TA}^*\tilde{U}_1e^{-i\omega t}+\tilde{Z}_T^*\tilde{I}_{TA}^*\tilde{U}_1^*e^{-i3\omega t}\\ &\quad\left.+\tilde{Z}_T^*\tilde{I}_{TA}^*\tilde{U}_3e^{i\omega t}+\tilde{Z}_T^*\tilde{I}_{TA}^*\tilde{U}_3^*e^{-i5\omega t}+2\tilde{Z}_T^*\tilde{I}_{TA}^*U_0e^{-i2\omega t}\right]\end{aligned} \tag{6.13}$$

Thus, if U contains an $m\omega$ component (a harmonic of order m), this will of course result in a harmonic of order m in V (first term in equation 6.11). But besides this, it will result in a harmonic of order $(m+2)$ and, if $(m-2)\geq 0$, also a harmonic of order $(m-2)$. This is a consequence of the mixing with the 2^{nd} harmonic (harmonic of order 2) of I_T (second term in equation 6.11). Since the 1^{st} harmonic of U is much larger than any other harmonic of U, it is only necessary to consider the mixing with this component. For example when we look at the 3^{rd} harmonic of V, we will only need to consider the 1^{st} and 3^{rd} harmonic of U. Of course, a 5ω component of U will also produce a 3ω contribution to V, but this will be much smaller that the other contributions.

The different harmonics can be found by doing a Fourier transformation. V can be written as a Fourier series:

$$\begin{aligned}V(t) &= \frac{c_0}{2}+\sum_{n=1}^{\infty}\frac{1}{2}\left(\tilde{c}_ne^{in\omega t}+\tilde{c}_n^*e^{-in\omega t}\right)\\ &= \frac{a_0}{2}+\sum_{n=1}^{\infty}a_n\cos(n\omega t)+\sum_{n=1}^{\infty}b_n\sin(n\omega t)\end{aligned}$$

where:
$$\begin{cases}\tilde{c}_n = a_n - ib_n\\ a_0 = \frac{2}{T}\int_0^T V(t)dt\\ a_n = \frac{2}{T}\int_0^T V(t)\cos(n\omega t)dt\\ b_n = \frac{2}{T}\int_0^T V(t)\sin(n\omega t)dt\\ T = \frac{2\pi}{\omega}\end{cases}$$

A Fourier transformation of V ($\mathrm{FT}[V]$) will give:

$$\mathrm{FT}[V(t)] = c_0,\ \tilde{c}_1,\ \tilde{c}_2,\ldots,\ \tilde{c}_n,\ldots \tag{6.14}$$

The following notation is used: The nth Fourier component is designated $\mathrm{FT}[V,n]$, and $V_{1\omega}$, $V_{2\omega}$ and $V_{3\omega}$ are the 1^{st}, 2^{nd} and 3^{rd} harmonic of V, respectively. Thus,

from equations 6.11 and 6.13:

$$V_{1\omega} = \frac{R_{pm}}{R_{pm}+R_f}\frac{1}{2}\left(\tilde{U}_1 e^{i\omega t} + \tilde{U}_1^* e^{-i\omega t}\right)$$
$$+\frac{R_f R_{pm}\alpha}{(R_{pm}+R_f)^2}\frac{1}{4}\left(\tilde{Z}_T\tilde{I}_{TA}\tilde{U}_1^* e^{i\omega t} + \tilde{Z}_T\tilde{I}_{TA}\tilde{U}_3^* e^{-i\omega t} + \tilde{Z}_T^*\tilde{I}_{TA}^*\tilde{U}_1 e^{-i\omega t} + \tilde{Z}_T^*\tilde{I}_{TA}^*\tilde{U}_3 e^{i\omega t}\right)$$
$$\Downarrow$$
$$\tilde{V}_1 = \mathrm{FT}[V,1] \approx \frac{R_{pm}}{R_{pm}+R_f}\tilde{U}_1 + \frac{R_f R_{pm}\alpha}{2(R_{pm}+R_f)^2}\tilde{Z}_T\tilde{I}_{TA}\tilde{U}_1^*, \tag{6.15}$$

where the small term $(\tilde{Z}_T^*\tilde{I}_{TA}^*\tilde{U}_3)$ is neglected in equation 6.15. Also:

$$V_{2\omega} = \frac{R_{pm}}{R_{pm}+R_f}\frac{1}{2}\left(\tilde{U}_2 e^{i2\omega t} + \tilde{U}_2^* e^{-i2\omega t}\right)$$
$$+\frac{R_f R_{pm}\alpha}{(R_{pm}+R_f)^2}\frac{1}{4}\left(2\tilde{Z}_T\tilde{I}_{TA}U_0 e^{i2\omega t} + 2\tilde{Z}_T^*\tilde{I}_{TA}^*U_0 e^{-i2\omega t}\right)$$
$$\Downarrow$$
$$\tilde{V}_2 = \mathrm{FT}[V,2] \approx \frac{R_{pm}}{R_{pm}+R_f}\tilde{U}_2 + \frac{R_f R_{pm}\alpha}{(R_{pm}+R_f)^2}\tilde{Z}_T\tilde{I}_{TA}U_0, \tag{6.16}$$

where the term $\tilde{U}_2$ is the complex amplitude of the 2ω component of U. (This term was not included in equation 6.1.) And:

$$V_{3\omega} = \frac{R_{pm}}{R_{pm}+R_f}\frac{1}{2}\left(\tilde{U}_3 e^{i3\omega t} + \tilde{U}_3^* e^{-i3\omega t}\right)$$
$$+\frac{R_f R_{pm}\alpha}{(R_{pm}+R_f)^2}\frac{1}{4}\left(\tilde{Z}_T\tilde{I}_{TA}\tilde{U}_1 e^{i3\omega t} + \tilde{Z}_T^*\tilde{I}_{TA}^*\tilde{U}_1^* e^{-i3\omega t}\right)$$
$$\Downarrow$$
$$\tilde{V}_3 = \mathrm{FT}[V,3] \approx \frac{R_{pm}}{R_{pm}+R_f}\tilde{U}_3 + \frac{R_f R_{pm}\alpha}{2(R_{pm}+R_f)^2}\tilde{Z}_T\tilde{I}_{TA}\tilde{U}_1 \tag{6.17}$$

From equation 6.7:

$$\tilde{I}_{TA} \approx \frac{(\mathrm{FT}[V,1])^2}{2R_{pm}}$$

Combining this with equation 6.17:

$$\tilde{Z}_T \approx \frac{\mathrm{FT}[V,3] - \frac{R_{pm}}{R_{pm}+R_f}\mathrm{FT}[U,3]}{\mathrm{FT}[U,1]}\frac{4(R_{pm}+R_f)^2}{(\mathrm{FT}[V,1])^2 R_f\alpha} \tag{6.18}$$

(where R_{pm} is given by equation 6.8).

This is the 3ω detection technique: by measuring the 3^{rd} harmonic of the output signal one can measure the thermal impedance.

As can be seen from equation 6.16, it is also possible to measure the thermal impedance by measuring the 2^{nd} harmonic if U has a DC offset. This can be called the 2ω detection technique. This is to my knowledge not a technique that has been used. But in some cases this may have advantages over the 3ω detection technique: Usually, one wants to keep the temperature amplitudes low, in order to stay in the linear regime. But from equations 5.4, 6.7, 6.16 and 6.17, it can be seen that:

$$\begin{aligned} T_A &\propto I_{Tm} \propto U_1^2 \\ |\mathrm{FT}[V,2]| &\propto U_1^2 U_0 \\ |\mathrm{FT}[V,3]| &\propto U_1^3 \end{aligned}$$

This means that, if T_A is made smaller, then at the same time $|\mathrm{FT}[V,2]|$ and $|\mathrm{FT}[V,3]|$ are also made smaller. But in $|\mathrm{FT}[V,2]|$ this can actually be compensated for by making the DC offset larger (than the amplitude of the 1^{st} harmonic of the input signal). The problem is that a large DC component in U will result in a large overall temperature rise (T_{DC}) of R_p. There is already a temperature DC offset (T_{DC}) due to the fact that it is only possible to add heat and not cool with R_p (see equation 6.6 and equation 6.7). Now, the size of the temperature DC offset of course depends on the thermal impedance between R_p and the surrounding temperature bath. So the size of T_{DC} and whether or not a large T_{DC} will present a problem will depend on the exact experimental situation. Therefore, the question of which technique will be most advantageous, the 2ω detection technique or the 3ω detection technique, depends on the exact experimental situation.

6.1 Sensitivity

It is interesting to look at the relation between the first and third harmonic, since this quantity sets a minimum requirement of the measuring equipment.

The first term in equation 6.17 is just the 3ω signal already present in U, thus the measured 3ω signal corrected for this is:

$$\tilde{V}_{3c} = \tilde{V}_3 - \frac{R_{pm}}{R_{pm}+R_f}\tilde{U}_3 \tag{6.19}$$

Combining this with equations 6.17 and 6.15, and using equation 5.4 for $\tilde{Z}_T$:

$$\frac{\tilde{V}_1}{\tilde{V}_{3c}} = \frac{2(R_{pm}+R_f)}{R_f \alpha \tilde{T}_A} + \frac{\tilde{U}_1^*}{\tilde{U}_1}$$

$$\Updownarrow$$

$$\frac{\tilde{V}_{3c}}{\tilde{V}_1} \approx \frac{R_f}{2(R_{pm}+R_f)}\alpha\tilde{T}_A, \tag{6.20}$$

since:

$$\frac{\tilde{U}_1^*}{\tilde{U}_1} \approx 1 \ll \frac{2(R_{pm}+R_f)}{R_f\alpha\tilde{T}_A}$$

Equation 6.20 could mislead one to think that it is desirable to make R_{pm} as small as possible. But it must be remembered that the sensitivity of the technique comes from the fact that R_p, and therefore also V, change with temperature. Thus, it is dV/dT_p that must be maximized. From the definition of α (cf. equation 6.3):

$$dT = \frac{dR_p}{\alpha R_p},$$

and thus (using equation 6.10):

$$\frac{dV}{d\left(\frac{dR_p}{\alpha R_p}\right)} = \frac{\alpha R_p dV}{dR_p} = \frac{\alpha U R_f R_p}{(R_f+R_p)^2} \tag{6.21}$$

Equation 6.21 is maximized by letting $R_f = R_p$, and thus the two resistances should be chosen as close to one another as possible, in order to maximize the sensitivity of the experiment. (Also, it is seen that the sensitivity increases with α.)

The required resolution of the measuring equipment can be calculated from equation 6.20 if α and $|\tilde{T}_A|$ is known (where $|\tilde{T}_A|$ is so small that the measurements still are in the linear regime).

Some typical values could be:

$\alpha = 5\times10^{-3}K^{-1}$,

$|\tilde{T}_A| = 5\times10^{-2}K$,

and thus (letting $R_f = R_p$):

$$\left|\frac{\tilde{V}_{3c}}{\tilde{V}_1}\right| \approx 6\times10^{-5}$$

6.2 Measuring the temperature coefficient (α)

In equation 6.18, α is needed. Below it is shown how α can be found if the heater (R_p) has been calibrated.

If the resistor R_p is a semiconductor, it is expected that:

$$R_p(T_p) = R_0 e^{\left(\frac{T_0}{T_p}\right)}$$

$$\Updownarrow$$

$$\ln R_p = \ln R_0 + T_0 \frac{1}{T_p}, \tag{6.22}$$

where R_0 and T_0 are constants. Substituting this into equation 6.3:

$$\alpha = \frac{d(\ln R_0 + \frac{T_0}{T_p})}{dT_p} = -\frac{T_0}{T_p^2} \tag{6.23}$$

Using equation 6.22 again:

$$\alpha = \frac{-1}{T_0} \ln^2 \left(\frac{R_p}{R_0}\right)$$

Now, again, looking only at small variations of R_p ($\Delta R_p \ll R_{pm}$, cf. equation 6.2), so that α can be considered constant, R_p can be substituted with R_{pm}, given by equation 6.8:

$$\alpha = \frac{-1}{T_0} \ln^2 \left(\frac{R_f(V_1)}{R_0(U_1 - V_1)}\right) \tag{6.24}$$

Thus, if R_p have been calibrated and T_0 and R_0 found, then α can easily be obtained.

If R_p is a thin metal film, then, instead of equation 6.22, it is expected that:

$$R_p(T_p) = AT_p + B \tag{6.25}$$

$$\Downarrow$$

$$\alpha_m \equiv \frac{1}{R_p}\frac{dR_p}{dT_p} = \frac{A}{R_p}, \tag{6.26}$$

where A and B are constants and subscript m on α is short for "metal". Combining equation 6.25 and equation 6.26, gives α_m as function of T_p:

$$\alpha_m = \frac{1}{T_p + \frac{B}{A}} \tag{6.27}$$

If R_{pm}, given by equation 6.8, is substituted for R_p in equation 6.26, then:

$$\alpha_m = \frac{A(U_1 - V_1)}{R_f V_1}$$

So, if the film has been calibrated and A found, it is easy to obtain α.

7 Modeling

In the preceding chapter the principles behind the 3ω detection technique, and how it can be used to measure a thermal impedance, was described. There, no special geometry of the heater was assumed. But when thermal information, like heat capacity and thermal conductivity, is to bee extracted from the measured thermal impedance this becomes essential. In this chapter a simple planar geometry will be considered, and it will be shown what thermal information can be extracted from the thermal impedance in this case.

In order to introduce to the modeling, the planar geometry will first be modeled in a simple manner using an electrical network analogy. In this model, only one infinitely thick layer of material is considered. After this, a more general approach that can be used for any number of layers of material of any thickness, will be introduced. Of course, the result of the first way of modeling will turn out to be a simple case of the more general approach.

7.1 Planar heater

In the case of a planar heater a one–dimensional geometry will be assumed. This means that it is assumed that heat only flows in the direction perpendicular to the heater. Here, this assumption is not questioned (its limitations will be discussed in chapter 12). But the assumption is a good one as long as $L_D \ll W_{heater}$, where W_{heater} is the width of the heater, and L_D is the thermal diffusion length[1]:

$$L_D \equiv \sqrt{\frac{D}{\Omega}}, \quad D \equiv \frac{\kappa}{c}, \tag{7.1}$$

where D is the diffusion constant, c ($[c] = [Jm^{-3}K^{-1}]$) is the specific heat capacity per unit volume, and κ ($[\kappa] = [Wm^{-1}K^{-1}]$) the thermal conductivity.

[1] L_D can be defined in various ways. E.g. in [Moon et al., 1996, p. 30] it is defined as: $L_D \equiv \sqrt{D/2\Omega}$, and in [Chirtoc et al., 2001, p. 106] it is defined as $L_D \equiv \sqrt{2D/\Omega}$. In [Menon, 1996, p. 5249-5250] a expression similar to 7.1 is used, and this definition will be used in this report.

The planar heater can be realized by a electrical conducting thin film on a glass substrate (see figure 7.1). It is assumed that heat only flows into the glass (there is vacuum on the other side of the heater, and the radiation of heat is negligible). Further it is assumed that the heater itself is infinitely thin, with no heat capacity, and that the glass is infinitely thick (which means that $L_D \ll l_1$, where l_1 is the thickness of the glass substrate).

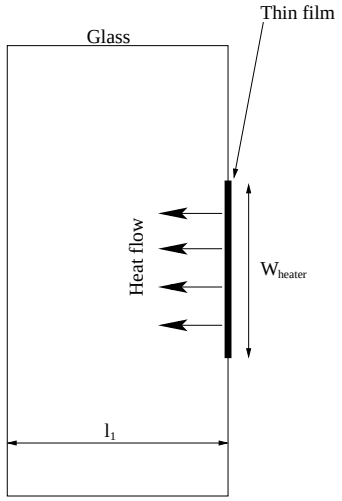

Figure 7.1 The planar heater realized as an electrical conducting thin film on a glass substrate. It is assumed that heat only flow in the direction perpendicular to the heater, and only into the glass (there is vacuum on the other side of the heater, and the radiation of heat is negligible). Further it is assumed that the heater itself is infinitely thin, with no heat capacity, and that the glass is infinitely thick.

This situation corresponds to heat diffusion in one dimension, and can be modeled by the electrical network shown on figure 7.2. A heat current is then modeled by an electrical current, a thermal impedance $(\tilde{Z})$ by an electrical impedance (and therefore a thermal admittance $(\tilde{Y} = 1/\tilde{Z})$ by an electrical admittance), and a heat capacity by an electrical capacitor.

Here, the elements in the model is just referred to as if they are thermal elements (and not electrical elements).

Every set of $\tilde{Y}_e dx$, $\tilde{Z}_e dx$ corresponds to an infinitely thin slice of material (glass). The heat capacity (C_{slice}) and thermal conductivity of the slice (κ_{slice}) is given by:

$$\begin{aligned} C_{slice} &= cAdx, \\ \kappa_{slice} &= \frac{\kappa A}{dx}, \end{aligned}$$

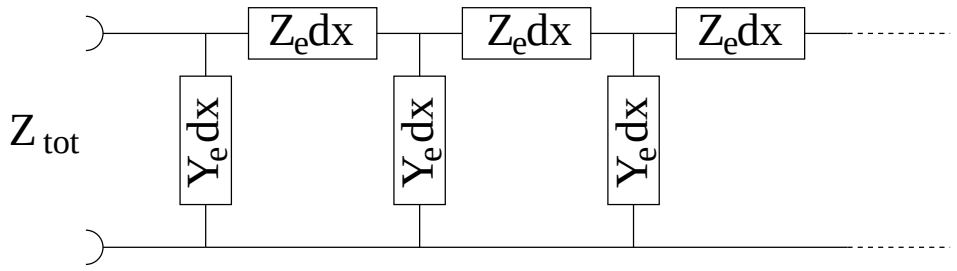

Figure 7.2 The electrical model for heat diffusion in one dimension. The elements in the model are referred to as thermal elements (not electrical elements). Z_{tot} is the thermal impedance seen from the end (where the heater is situated) of the infinitely long chain. The elements are drawn in a very general way, but in the electrical model the horizontal elements $(Z_e dx)$ can be thought of as resistors, and the vertical elements $(Y_e dx)$ as capacitors. Thereby both the storage property (heat capacity) and the conducting property (thermal conductivity) of the material is modeled.

where A is the area of the slice.

Here, only one Fourier component $(e^{i\Omega t})$ will be considered. The result will be similar for any other Fourier component. In general an admittance is defined as the generalized current (f) divided by the generalized voltage (e), which is the reciprocal of a thermal impedance (see page 21, it is important to note that in the model on fig. 7.2: $Y_e \neq 1/Z_e$). From the definition of the admittance and the definition of a capacitor (C):

$$\begin{aligned} Y &\equiv \frac{f}{e}, \\ C &\equiv \frac{q}{e}, \\ f &\equiv \frac{\partial q}{\partial t}, \qquad q = q_0 e^{i\Omega t} \\ \Downarrow & \\ f &= q_0 i\Omega e^{i\Omega t} = i\Omega q, \end{aligned}$$

where q is the charge on the capacitor varying with the amplitude q_0. From this it is seen that the admittance of a capacitor (C) is $i\Omega C$, thus:

$$\tilde{Y}_e dx = i\Omega C_{slice} = i\Omega c A dx, \tag{7.2}$$

$$\tilde{Z}_e dx = \frac{1}{\kappa_{slice}} = \frac{dx}{\kappa A}, \tag{7.3}$$

where Ω is the cyclic frequency of the temperature oscillations.

Since the chain is infinity long, the network in figure 7.2 can be replaced by the one on figure 7.3. From this figure:

$$\frac{1}{\tilde{Z}_{tot}} = \tilde{Y}_e dx + \frac{1}{\tilde{Z}_e dx + \tilde{Z}_{tot}} = \frac{\tilde{Y}_e dx(\tilde{Z}_e dx + \tilde{Z}_{tot}) + 1}{\tilde{Z}_e dx + \tilde{Z}_{tot}}$$

$$\Updownarrow$$

$$\frac{\tilde{Z}_e dx}{\tilde{Z}_{tot}} + 1 = \tilde{Y}_e \tilde{Z}_e (dx)^2 + \tilde{Y}_e dx \tilde{Z}_{tot} + 1$$

$$\Downarrow$$

$$\frac{\tilde{Z}_e dx}{\tilde{Z}_{tot}} \approx \tilde{Y}_e dx \tilde{Z}_{tot} \quad \text{(The small second order term is neglected)}$$

$$\Updownarrow$$

$$\tilde{Z}_{tot} \approx \sqrt{\frac{\tilde{Z}_e}{\tilde{Y}_e}} \tag{7.4}$$

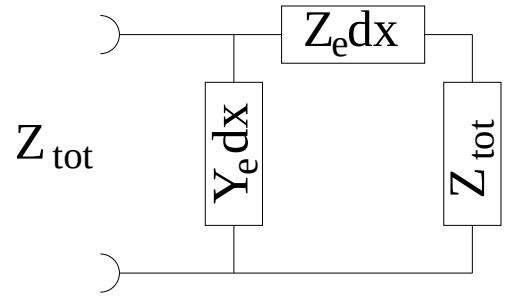

Figure 7.3 This figure just illustrates that the impedance of this infinitely chain does not change if the first link is removed.

Inserting equations 7.2 and 7.3 in equation 7.4 yields:

$$\tilde{Z}_{tot} \approx \frac{1}{A\sqrt{i\Omega\kappa c}} \tag{7.5}$$

Equation 7.5 gives the thermal impedance of one infinitely thick layer of material. In many cases, though, the thermal impedance of a multi layered system is needed. Therefore a more general approach, based on a transfer matrix, is developed in the following. Of course, as will be seen, equation 7.5 is just a special simple case of multi layer systems.

7.2 Transfer matrix

The derivation of the transfer matrix, given in this section, is due to and taken almost directly from [Christensen, 1989, p. 63-72].

In order to understand the transfer matrix, the heat diffusion equation and how it can be derived is needed. This is shown below. A continuity equation for the heat can be written as:

$$\frac{\partial \rho_Q}{\partial t} + \nabla \cdot \overline{J_Q} = 0, \tag{7.6}$$

where $[\rho_Q] = [Jm^{-3}]$ is the heat density, and $[J_Q] = [Js^{-1}m^{-2}]$ is the heat current density. In the linear case, the heat current density is given by Fouriers law:

$$\overline{J_Q} = -\kappa \overline{\nabla T} \tag{7.7}$$

The change in heat density with time can be written in terms of the heat capacity per unit volume (c):

$$\frac{\partial \rho_Q}{\partial t} = c\frac{\partial T}{\partial t} \tag{7.8}$$

Inserting equations 7.8 and 7.7 in equation 7.6 gives the heat diffusion equation:

$$\begin{aligned} & c\frac{\partial T}{\partial t} + \nabla \cdot (-\kappa \overline{\nabla T}) = 0 \\ \Updownarrow & \\ & \frac{\partial T}{\partial t} = D\nabla^2 T, \end{aligned} \tag{7.9}$$

where D is the diffusion constant (cf. equation 7.1). Now, it is important to notice that this equation *does not* hold if c and/or κ is time–dependent. The reason for this is that, equation 7.8 only holds if c is constant in time, and equation 7.7 only holds if κ is constant in time. If this is not the case, the following integrals must be used (cf. equation 4.2):

$$\begin{aligned} \rho_Q(t) &= \int_0^\infty c(t')\dot{T}(t-t')dt' \\ J_Q(t) &= -\int_0^\infty \kappa(t')\dot{\nabla T}(t-t')dt' \end{aligned}$$

It should be noted that though it is widely accepted that at the glass transition the heat capacity can be time (or frequency) dependent, it is also widely accepted that the thermal conductivity is time independent.

So, actually the diffusion constant (D) in equation 7.9 does not make any sense in the case where both the heat capacity and the thermal conductivity is time–dependent.

The solution to this problem is to look at it in frequency–domain, instead of time–domain:

$$\begin{aligned} \tilde{T} &= \tilde{T}_A e^{i\Omega t} \\ \tilde{J}_Q &= \tilde{J}_{QA} e^{i\Omega t}, \end{aligned} \tag{7.10}$$

where $\tilde{T}_A$ and $\tilde{J}_{QA}$ is the complex amplitudes of the temperature $(\tilde{T})$ and heat current density $(\tilde{J}_Q)$, varying with cyclic frequency Ω (the amplitudes are allowed to be complex in order to allow phase shifts). Again, of course, the temperature and heat current can vary in any complicated periodic way. But it is only necessary to look at one Fourier component, since the result will be similar for any other Fourier component.

In the calculations in frequency–domain there is no problem with c and κ being frequency dependent since all the calculations in principle are done for one frequency (at the time). But since this one frequency is not any specific frequency, the calculations are valid for any frequency, and therefore it does not matter whether or not c and κ change with frequency. So instead of c and κ, one can just write $\tilde{c}$ and $\tilde{\kappa}$.

Again, the problem is simplified to heat diffusion in one dimension. Equations 7.7 and 7.8 can be used for each Fourier component:

$$\left\{ \begin{array}{l} \tilde{J}_Q = -\tilde{\kappa}\frac{\partial \tilde{T}}{\partial x} \\ \frac{\partial \rho_Q}{\partial t} = \tilde{c}\frac{\partial \tilde{T}}{\partial t} = -\frac{\partial \tilde{J}_Q}{\partial x} \end{array} \right.$$

$$\Updownarrow$$

$$\left\{ \begin{array}{l} -\tilde{J}_Q \frac{1}{\tilde{\kappa}} dx = \frac{\partial \tilde{T}}{\partial x} dx = \frac{\tilde{T}_{x+dx} - \tilde{T}_x}{dx} dx = \tilde{T}_{A,x+dx} - \tilde{T}_{A,x} \\ -\tilde{c}\frac{\partial \tilde{T}}{\partial t} dx = \frac{\partial \tilde{J}_Q}{\partial x} dx = \frac{\tilde{J}_{Q,x+dx} - \tilde{J}_{Q,x}}{dx} dx = \tilde{J}_{Q,x+dx} - \tilde{J}_{Q,x} \end{array} \right.$$

Inserting the expressions for $\tilde{T}$ and $\tilde{J}_Q$ (equation 7.10):

$$\left\{ \begin{array}{l} -J_{QA} e^{i\Omega t} \frac{1}{\tilde{\kappa}} dx = (\tilde{T}_{A,x+dx} - \tilde{T}_{A,x}) e^{i\Omega t} \\ -\tilde{c}\frac{\partial \tilde{T}_A e^{i\Omega t}}{\partial t} dx = (\tilde{J}_{Q,x+dx} - \tilde{J}_{Q,x}) e^{i\Omega t} \end{array} \right.$$

$$\Updownarrow$$

$$\left\{ \begin{array}{ll} -\tilde{Z} dx \tilde{J}_x = \tilde{T}_{A,x+dx} - \tilde{T}_{A,x}, & \tilde{Z} \equiv \frac{1}{\tilde{\kappa} A}, \quad \tilde{J} \equiv J_{QA} A \\ -\tilde{Y} dx \tilde{T}_{A,x} = \tilde{J}_{x+dx} - \tilde{J}_x, & \tilde{Y} \equiv i\Omega \tilde{c} A, \end{array} \right. \tag{7.11}$$

where $\tilde{J}$ is the heat current through the area A ($[\tilde{J}] = [W]$), $\tilde{Z}$ is the heat resistance per unit length ($[\tilde{Z}] = [(\tilde{\kappa}dx)^{-1}/dx)] = [KW^{-1}m^{-1}]$), and $\tilde{Y}$ is $i\Omega$ times the heat capacity per unit length ($[\tilde{Y}] = [i\Omega\tilde{c}Vol/dx] = [WK^{-1}m^{-1}]$). This can be written in matrix form as:

$$\begin{pmatrix} \tilde{T}_{A,x+dx} \\ \tilde{J}_{x+dx} \end{pmatrix} = \begin{pmatrix} 1 & -\tilde{Z}dx \\ -\tilde{Y}dx & 1 \end{pmatrix} \begin{pmatrix} \tilde{T}_{A,x} \\ \tilde{J}_x \end{pmatrix}$$

or

$$\begin{pmatrix} \tilde{T}_{A,x} \\ \tilde{J}_x \end{pmatrix} = \begin{pmatrix} 1 & \tilde{Z}dx \\ \tilde{Y}dx & 1 \end{pmatrix} \begin{pmatrix} \tilde{T}_{A,x+dx} \\ \tilde{J}_{x+dx} \end{pmatrix} \tag{7.12}$$

since:

$$\begin{pmatrix} 1 & -\tilde{Z}dx \\ -\tilde{Y}dx & 1 \end{pmatrix} \begin{pmatrix} 1 & \tilde{Z}dx \\ \tilde{Y}dx & 1 \end{pmatrix} = \begin{pmatrix} 1-\tilde{Z}\tilde{Y}dx^2 & 0 \\ 0 & 1-\tilde{Z}\tilde{Y}dx^2 \end{pmatrix} \approx \begin{pmatrix} 1 & 0 \\ 0 & 1 \end{pmatrix}$$

The 2×2 matrix in equation 7.12 is the transfer matrix $(\underline{\underline{\tilde{A}}}(dx))$ for a heat conductor of infinitesimal length (dx):

$$\underline{\underline{\tilde{A}}}(dx) \equiv \begin{pmatrix} 1 & \tilde{Z}dx \\ \tilde{Y}dx & 1 \end{pmatrix} \tag{7.13}$$

$\underline{\underline{\tilde{A}}}(dx)$ gives the temperature and heat current at x, given the values at $x+dx$ (or visa versa). Of course what is needed is the transfer matrix $(\underline{\underline{\tilde{A}}}(l))$ for a heat conductor of some length (l):

$$\begin{pmatrix} \tilde{T}_0 \\ \tilde{J}_0 \end{pmatrix} = \begin{pmatrix} \tilde{A}_{11} & \tilde{A}_{12} \\ \tilde{A}_{21} & \tilde{A}_{22} \end{pmatrix} \begin{pmatrix} \tilde{T}_l \\ \tilde{J}_l \end{pmatrix} = \underline{\underline{\tilde{A}}}(l) \begin{pmatrix} \tilde{T}_l \\ \tilde{J}_l \end{pmatrix}, \tag{7.14}$$

where $\tilde{T}_0$, $\tilde{J}_0$ and $\tilde{T}_l$, $\tilde{J}_l$ is the temperature and heat current at $x = 0$ and $x = l$ (iteration of equation 7.12 shows that the linear relationship in equation 7.14 exists).

Now, if two materials A and B of length l_1 and l_2 are in thermal contact, see figure 7.4, and $\underline{\underline{\tilde{A}}}$ and $\underline{\underline{\tilde{B}}}$ are the transfer matrix for the two materials then:

$$\left.\begin{aligned} \begin{pmatrix} \tilde{T}_0 \\ \tilde{J}_0 \end{pmatrix} &= \underline{\underline{\tilde{A}}}(l_1) \begin{pmatrix} \tilde{T}_{l1} \\ \tilde{J}_{l1} \end{pmatrix} \\ \begin{pmatrix} \tilde{T}_{l1} \\ \tilde{J}_{l1} \end{pmatrix} &= \underline{\underline{\tilde{B}}}(l_2) \begin{pmatrix} \tilde{T}_{l2} \\ \tilde{J}_{l2} \end{pmatrix} \end{aligned}\right\} \Rightarrow \begin{pmatrix} \tilde{T}_0 \\ \tilde{J}_0 \end{pmatrix} = \underline{\underline{\tilde{A}}}(l_1)\underline{\underline{\tilde{B}}}(l_2) \begin{pmatrix} \tilde{T}_{l2} \\ \tilde{J}_{l2} \end{pmatrix} \tag{7.15}$$

Since equation 7.15 also is valid if A and B are made of the same material:

$$\underline{\underline{\tilde{A}}}(l_1+l_2) = \underline{\underline{\tilde{A}}}(l_1)\underline{\underline{\tilde{A}}}(l_2) = \underline{\underline{\tilde{A}}}(l_2)\underline{\underline{\tilde{A}}}(l_1)$$

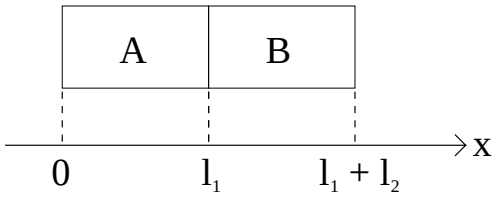

Figure 7.4 Two materials A and B in good thermal contact at $x = l_1$.

It is necessary to look at the derivative of $\underline{\underline{\tilde{A}}}(l)$ in order to find $\underline{\underline{\tilde{A}}}(l)$:

$$\begin{aligned}\frac{\partial \underline{\underline{\tilde{A}}}}{\partial l} &= \frac{\underline{\underline{\tilde{A}}}(l+dl)-\underline{\underline{\tilde{A}}}(l)}{dl} = \underline{\underline{\tilde{A}}}(l)\frac{\underline{\underline{\tilde{A}}}(dl)-\underline{\underline{1}}}{dl} = \underline{\underline{\tilde{A}}}(l)\underline{\underline{\tilde{D}}} \\ &= \begin{pmatrix} \tilde{A}_{11} & \tilde{A}_{12} \\ \tilde{A}_{21} & \tilde{A}_{22} \end{pmatrix}\begin{pmatrix} 0 & \tilde{Z} \\ \tilde{Y} & 0 \end{pmatrix} = \begin{pmatrix} \tilde{Y}\tilde{A}_{12} & \tilde{Z}\tilde{A}_{11} \\ \tilde{Y}\tilde{A}_{22} & \tilde{Z}\tilde{A}_{21} \end{pmatrix}, \quad (7.16)\end{aligned}$$

$$\text{where: } \underline{\underline{1}} \equiv \begin{pmatrix} 1 & 0 \\ 0 & 1 \end{pmatrix}, \quad \underline{\underline{\tilde{D}}} \equiv \begin{pmatrix} 0 & \tilde{Z} \\ \tilde{Y} & 0 \end{pmatrix}$$

Equation 7.16 gives four differential equations. The derivative with respect to dl of these four equations are:

$$\left.\begin{aligned} \tfrac{\partial^2 \tilde{A}_{11}}{\partial l^2} &= \tilde{Y}\tfrac{\partial \tilde{A}_{12}}{\partial l} = \tilde{Y}\tilde{Z}\tilde{A}_{11} \\ \tfrac{\partial^2 \tilde{A}_{12}}{\partial l^2} &= \tilde{Z}\tfrac{\partial \tilde{A}_{11}}{\partial l} = \tilde{Y}\tilde{Z}\tilde{A}_{12} \\ \tfrac{\partial^2 \tilde{A}_{21}}{\partial l^2} &= \tilde{Y}\tfrac{\partial \tilde{A}_{22}}{\partial l} = \tilde{Y}\tilde{Z}\tilde{A}_{21} \\ \tfrac{\partial^2 \tilde{A}_{22}}{\partial l^2} &= \tilde{Z}\tfrac{\partial \tilde{A}_{21}}{\partial l} = \tilde{Y}\tilde{Z}\tilde{A}_{22} \end{aligned}\right\} \Rightarrow \frac{\partial^2 \tilde{A}_{ij}}{\partial l^2} = \tilde{Y}\tilde{Z}\tilde{A}_{ij} \quad (7.17)$$

Equation 7.17 have the general solution:

$$\tilde{A}_{ij}(l) = \tilde{C}_{ij}\cos\left(l\sqrt{-\tilde{Y}\tilde{Z}}\right) + \tilde{S}_{ij}\sin\left(l\sqrt{-\tilde{Y}\tilde{Z}}\right), \quad (7.18)$$

and of course:

$$\underline{\underline{A}}(0) = \begin{pmatrix} 1 & 0 \\ 0 & 1 \end{pmatrix}, \text{ since: } \begin{pmatrix} \tilde{T}_0 \\ \tilde{J}_0 \end{pmatrix} = \underline{\underline{A}}(0)\begin{pmatrix} \tilde{T}_0 \\ \tilde{J}_0 \end{pmatrix}$$

$\cos(0) = 1$, and $\sin(0) = 0$, and therefore $\underline{\underline{C}} = \underline{\underline{A}}(0)$. From equation 7.17 it is seen that:

$$\tilde{A}_{11}(l) = \frac{1}{\tilde{Z}}\frac{\partial \tilde{A}_{12}}{\partial l}$$

$$\tilde{A}_{22}(l) = \frac{1}{\tilde{Y}}\frac{\partial \tilde{A}_{21}}{\partial l}$$

Using equation 7.18 for $\tilde{A}_{ij}$, and the fact that $\underline{\underline{C}} = \underline{\underline{A}}(0)$:

$$\cos\left(l\sqrt{-\tilde{Y}\tilde{Z}}\right) + \tilde{S}_{11}\sin\left(l\sqrt{-\tilde{Y}\tilde{Z}}\right) = \frac{\sqrt{-\tilde{Y}\tilde{Z}}}{\tilde{Z}}\tilde{S}_{12}\cos\left(l\sqrt{-\tilde{Y}\tilde{Z}}\right)$$

$$\Downarrow$$

$$\tilde{S}_{11} = 0,\ \ \tilde{S}_{12} = \frac{\tilde{Z}}{\sqrt{-\tilde{Y}\tilde{Z}}},$$

and

$$\cos\left(l\sqrt{-\tilde{Y}\tilde{Z}}\right) + \tilde{S}_{22}\sin\left(l\sqrt{-\tilde{Y}\tilde{Z}}\right) = \frac{\sqrt{-\tilde{Y}\tilde{Z}}}{\tilde{Y}}\tilde{S}_{21}\cos\left(l\sqrt{-\tilde{Y}\tilde{Z}}\right)$$

$$\Downarrow$$

$$\tilde{S}_{22} = 0,\ \ \tilde{S}_{21} = \frac{\tilde{Y}}{\sqrt{-\tilde{Y}\tilde{Z}}}$$

And so finally the transfer matrix can be written as:

$$\underline{\underline{\tilde{A}}}(l) = \begin{pmatrix} \cos\left(l\tilde{k}\right) & \frac{\tilde{Z}}{\tilde{k}}\sin\left(l\tilde{k}\right) \\ \frac{\tilde{Y}}{\tilde{k}}\sin\left(l\tilde{k}\right) & \cos\left(l\tilde{k}\right) \end{pmatrix}, \quad \tilde{k} \equiv \sqrt{-\tilde{Y}\tilde{Z}} \tag{7.19}$$

(The same expression can be found in [Carslaw and Jaeger, 1959, p. 110].)

It may seem quite complicated to derive equation 7.19, but it turns out to be worth the effort. With equation 7.19 the one–dimensional heat diffusion problem has been solved once and for all. No matter the number of layers of material that must be considered it is just a question of matrix multiplication (as is seen from equation 7.15). A special simple case is considered in the following.

Again the two materials in figure 7.4 are considered. $\tilde{e}_A$ and $\tilde{e}_B$ is the effusivity of A and B, respectively. The effusivity is defined as:

$$\tilde{e} \equiv \sqrt{\tilde{c}\tilde{\kappa}}$$

If $\tilde{e}_B \gg \tilde{e}_A$, and B is in good thermal contact with a temperature bath, then B short–circuit A to the temperature bath. This will for example be the case, if A is glass, and B is copper in contact with the temperature bath since:

$$\begin{aligned} \kappa_{glass} &\approx 0.9 W m^{-1} K^{-1}, c_{glass} \approx 2.1 \times 10^6 J K^{-1} m^{-3} \\ \Rightarrow e_{glass} &\approx 1.4 \times 10^3 J m^{-2} K^{-1} s^{-1/2} \end{aligned}$$

and

$$\begin{aligned} \kappa_{copper} &\approx 400 W m^{-1} K^{-1}, c_{copper} \approx 3.4 \times 10^6 J K^{-1} m^{-3} \\ \Rightarrow e_{copper} &\approx 3.7 \times 10^4 J m^{-2} K^{-1} s^{-1/2} \end{aligned}$$

[Nordling and Österman, 1996, p. 28,33].

Thus, the thermal impedance $(\tilde{Z}_B)$ of B can be considered zero:

$$\tilde{Z}_B \equiv \frac{\tilde{T}_{l1}}{\tilde{J}_{l1}} = 0$$

Equation 7.14 shows that the thermal impedance $(\tilde{Z}_{tot})$, seen from $x = 0$, is given by:

$$\tilde{Z}_{tot} \equiv \frac{\tilde{T}_0}{\tilde{J}_0} = \frac{\tilde{A}_{11}(l_1)\tilde{T}_{l1} + \tilde{A}_{12}(l_1)\tilde{J}_{l1}}{\tilde{A}_{21}(l_1)\tilde{T}_{l1} + \tilde{A}_{22}(l_1)\tilde{J}_{l1}} = \frac{\tilde{A}_{11}(l_1)\tilde{Z}_B + \tilde{A}_{12}(l_1)}{\tilde{A}_{21}(l_1)\tilde{Z}_B + \tilde{A}_{22}(l_1)} = \frac{\tilde{A}_{12}(l_1)}{\tilde{A}_{22}(l_1)}$$

Inserting the result from equation 7.19:

$$\tilde{Z}_{tot} = \frac{\frac{\tilde{Z}}{\tilde{k}}\sin(l\tilde{k})}{\cos(l\tilde{k})} = \frac{\tilde{Z}}{\tilde{k}}\tan(l\tilde{k}) \tag{7.20}$$

Using the definitions of $\tilde{Z}$ and $\tilde{Y}$ from equation 7.11, and the definition of $\tilde{k}$ (equation 7.19):

$$\tilde{Z}_{tot} = \frac{1}{A\sqrt{i\Omega\tilde{c}\tilde{\kappa}}}\tanh\left(l_1\sqrt{\frac{i\Omega\tilde{c}}{\tilde{\kappa}}}\right) \tag{7.21}$$

Equation 7.21 gives the thermal impedance of a finite, one–dimensional diffusion chain of length l_1, that is held at isothermal conditions at the end (at $x = l_1$). It is seen that equation 7.21 corresponds to equation 7.5, when $l_1 \to \infty$, as expected.

Equation 7.21 shows that in the case where the one dimensional diffusion model is valid, and where the length (l_1) can be considered infinite, there only the effusivity can be obtained, not the heat capacity alone.

7.3 Thermal properties of a liquid

Above it was only discussed how to extract the thermal properties of the glass substrate. But the focus of this report is how to measure the thermal properties of a liquid. The way to do this, of course, is to measure the thermal impedance with and without liquid on the other side of the heater, see figure 7.5.

If there is a liquid on the heater, the heat can both flow into the glass substrate (and into whatever is on the other side of the substrate) and into the liquid. The

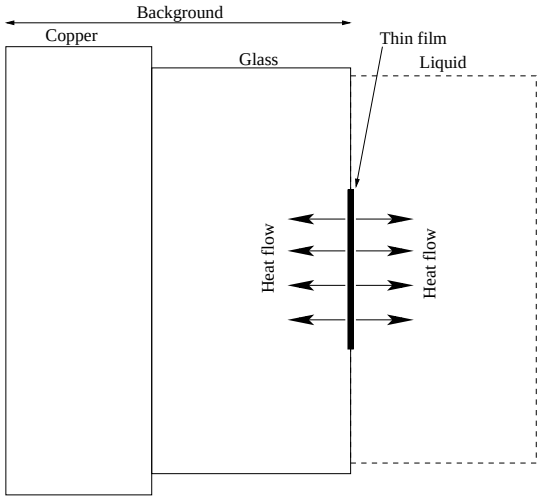

Figure 7.5 If a liquid is placed in contact with the heater heat can flow both into the substrate (e.g. glass on copper) and into the liquid.

substrate may be any layered material e.g. glass on copper[2]. $\tilde{Y}_S$ is the thermal admittance (reciprocal thermal impedance) of the substrate, $\tilde{Y}_L$ the thermal admittance of the liquid, and $\tilde{Y}_{LS}$ is the total thermal admittance that is measured with liquid on the heater. The total heat current $(\tilde{J}_Q)$ generated by the heater is the sum of the heat currents into the liquid $(\tilde{J}_{QL})$ and into the substrate $(\tilde{J}_{QS})$. Then, if $\tilde{T}$ is the temperature at the heater:

$$\begin{cases} \tilde{Y}_L = \frac{\tilde{J}_{QL}}{\tilde{T}}, \quad \tilde{Y}_S = \frac{\tilde{J}_{QS}}{\tilde{T}}, \quad \tilde{Y}_{LS} = \frac{\tilde{J}_Q}{\tilde{T}} \\ J_Q = J_{QL} + J_{QS} \end{cases}$$

$$\Updownarrow$$

$$\tilde{Y}_{LS} = \tilde{Y}_L + \tilde{Y}_S \tag{7.22}$$

If $\tilde{Y}_S$ is measured without liquid on the heater, $\tilde{Y}_L$ can be found from equation 7.22 if measurements with and without liquid have been made. Then the appropriate model for the heat diffusion in the liquid must be applied, in order to extract the thermal parameters of the liquid. If, for example, the liquid layer can be considered infinitely thick, and a one–dimensional model is adequate for the heat diffusion, then equation 7.5 must be used, with $\tilde{c}$ and $\tilde{\kappa}$ being the thermal properties of the liquid.

[2]The example of glass on copper (figure 7.5) is not chosen at random. In the planar heater experiments, I have made, this was in fact the configuration. More details on this in chapters 9 and 10.

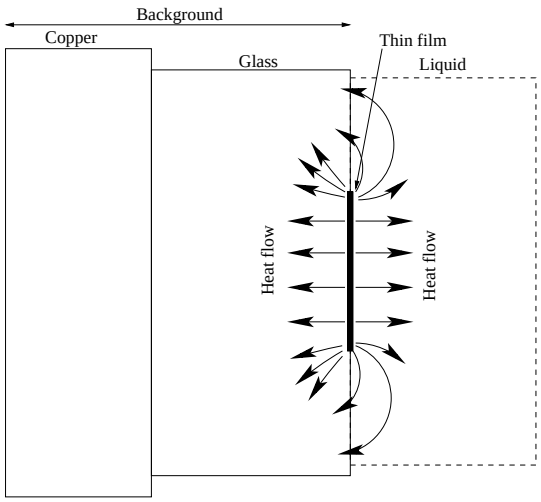

Figure 7.6 If heat diffuses in three dimensions, heat can flow across the liquid substrate interface.

It is important to realize that equation 7.22 holds when heat only diffuses in the direction perpendicular to the heater, but not necessary in all other cases. Here, $\tilde{Y}_S$ is defined as the thermal admittance measured without liquid on the heater. Thus, if heat diffusion from the heater must be described in three dimensions, and the thermal parameters of the liquid and substrate are different in a way that the temperature becomes higher in the liquid than in the substrate, then at the liquid substrate interface, some distance away from the heater itself, heat will diffuse from the liquid into the substrate, see figure 7.6 (this is referred to as a boundary mismatch in [Moon et al., 1996, p. 31]). Thus, $\tilde{Y}_S$ (measured without liquid) will not satisfy equation 7.22.

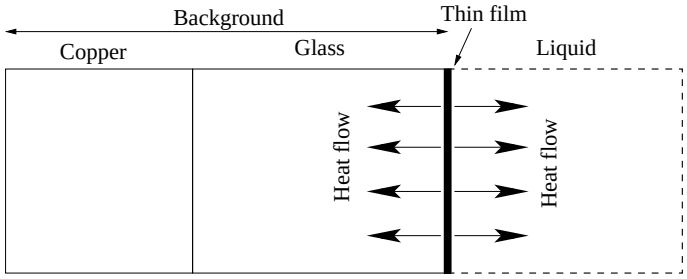

Figure 7.7 The problem with heat flow across the liquid substrate interface can be overcome if the heater fills all the interface. There must be a thermal isolating "medium" (e.g. vacuum) around the setup, and radiation of heat must be negligible.

This problem with heat flow across the liquid substrate interface may be overcome, if it is possible to fabricate a heater that fills all the area of the substrate, and, if it is possible to have the liquid to fill exactly the same area, see figure 7.7. This will, however, not be so easy to realize in practice.

8 Measurements of dynamic heat capacity from the literature

In this chapter the history of the 3ω detection technique will be considered, and references to the most important articles in the field will be given. The 3ω detection technique is not the only technique used to measure frequency dependent specific heat capacity, and therefore some other techniques will be briefly considered first.

Only dynamic calorimetry methods are considered, that is, methods that study relaxation phenomena [Jung et al., 1999, S1359]. These methods may also be used to study other physical phenomena, e.g. phase transitions, but this is not included. As shown in chapter 3, the methods can roughly be divided into two groups that can be called "time–domain methods" (in which the relaxation phenomena is studied as function of time after a perturbation of the system), and "frequency–domain methods" (in which the system is perturbated in a oscillatory manner and the system response is studied as function of the perturbation frequency). Two time–domain methods are mentioned: isothermal (where the heat flow to the system is measured after a temperature jump) and adiabatic (where the temperature of the system is measured after a heat input). Besides the 3ω detection technique (that have its one section in the end of this chapter) three frequency–domain methods are mentioned: traditional AC calorimetry, the photoacoustic, and the photopyroelectric technique. Some review articles are available on the techniques e.g. [Gmelin, 1997], [Jung et al., 1999], and [Jeong, 1997]. For the photo–techniques see [Thoen and Glorieux, 1997] and [Chirtoc et al., 2001].

8.1 Time–domain methods

The time–scale of the time–domain methods is usually much longer than for the frequency–domain methods. Where in frequency–domain the lowest frequencies usually are around $1mHz$, which corresponds to $1000s \approx 1/4$hour, the time–domain methods operate with times from around $10s$ to $10^6 s \approx 12$days (e.g. [Fu-

jimori and Oguni, 1994, p. 603], [Suga and Matsuo, 1989, p. 1123]). The limit on how short times can be observed in a time–domain experiment is set by the time needed for the system to "equilibrate"[1] after a temperature jump or heat input, while the long time limit is set by the stability of the setup over long times, and the patience of the experimentalist.

The most common time–domain method [Fujimori and Oguni, 1994, p. 601, 602] is the adiabatic method where a known amount of heat is supplied to the system in thermodynamic equilibrium, after which the evolution of the systems temperature with time is monitored under adiabatic conditions. In the isothermal method a step in temperature is made from the equilibrium state (of course this step is also made by supplying some heat), and then the flow of heat to the system that is needed in order to keep the temperature constant is monitored [Fujimori and Oguni, 1994, p. 602]. In both the adiabatic and isothermal case the calorimeter used must be very well shielded from the surroundings in order to avoid unknown quantities of heat to flow into the system. No perfect thermal insulator exists, and there will always be radiation of heat, thus, much care must be taken to minimize the thermal leak to the surroundings (e.g. [Jeong, 1997, p. 87], [Jung et al., 1999, p. S1361], [Suga and Matsuo, 1989, p. 1127], [Kobashi et al., 1998, p. 668], [Fujimori and Oguni, 1993, p. 272]).

For other adiabatic measurements see e.g. [Atake et al., 2000A], [Atake et al., 2000B].

8.2 Frequency–domain methods

Traditional AC calorimetry is fundamentally different from the 3ω detection technique, in that the heat source and temperature detector are not one and the same, and thus heat is supplied in one place and the temperature is measured somewhere else (usually very close to the heat source). In the cases discussed here the frequency dependence of the heat capacity (or effusivity) is desired and this method works well for low frequencies, where the thermal diffusion length (L_D) is long compared to the distance between the heat source and the temperature sensor (e.g. [Christensen, 1985], [Minakov et al., 2001]). For higher frequencies the measured temperature amplitude and phase shift can not be taken as a measure of these quantities at the heat source. Christensen [1985] (and Christensen [1989]) report measurements of the normalized heat capacity (assuming that the thermal conductivity is frequency independent) on supercooled glycerol near the glass transition

[1] "Equilibrate" must here be understood in the sense that the temperature of the system is uniform throughout the system. The system is not equlibrated in the sense that the system is fully relaxed, since the relaxation phenomena is in fact the phenomena that is studied.

in the frequency range $[2.4mHz; 35mHz]$, while Minakov et al. [2001] report measurements, also on glycerol, in the frequency range $[40mHz; 10Hz]$. Minakov et al. [2001] has a special arrangement with two sensors, and they can measure both the thermal conductivity and the heat capacity simultaneously. Since these techniques has a rather narrow frequency range, other methods are desired.

In photoacoustic and photopyroelectric measurements the sample (e.g. a supercooled liquid) is heated periodically with a pulsed laser. Due to the thermal expansion, an acoustic wave can be measured with a microphone in a gas above the sample [Thoen and Glorieux, 1997, p. 139], [Büchner and Korpium, 1987, p. 31]. This is done in a photoacoustic experiment, and information on the phase and amplitude of the temperature oscillations in the sample is extracted from the acoustic signal [Thoen and Glorieux, 1997], [Büchner and Korpium, 1987]. The extraction of the sample properties may be somewhat complicated. The thermal properties of the gas and backing is involved, and also the frequency response of the microphone and electronics is usually not flat. Therefore a calibration procedure, using a sample with known thermal properties, is needed [Thoen and Glorieux, 1997, p. 141]. Büchner and Korpium [1987] report measurements of the effusivity of a supercooled salt melt $(0.4Ca(NO_3)_2 - 0.6KNO_3)$ near the glass transition for three frequencies (as function of temperature): $9.6Hz, 55Hz, 512Hz$.

In a photopyroelectric experiment the temperature amplitude and phase are measured by a pyroelectric material [Bentefour, 2002], [Bentefour et al., 2001], [Chirtoc et al., 2001], [Caerels et al., 1998], [Thoen and Glorieux, 1997], [Dădârlat et al., 1990], [Chirtoc and MihăIlescu, 1989]. In one configuration of the setup, the heat is absorbed at the liquid pyroelectric interface, and thus the heat source and thermometer is in the same place (as in the 3ω detection technique), which makes it possible to go to higher frequencies. Bentefour [2002], Bentefour et al. [2001] (Chirtoc et al. [2001]) report effusivity measurements on glycerol and Bentefour [2002] on propylene glycol in the frequency range $[0.05Hz; 100kHz]$.

One minor drawback of this technique is that the exact amount of power released in the liquid is not known (some of the laser light is reflected and not absorbed). Thus a reference point for each curve ((frequency, effusivity) or (temperature, effusivity)) must be known in advance.

8.3 3ω detection technique

The 3ω detection technique is also a frequency–domain technique, but is given this separate section, since it is the central technique in this report. Here, a brief sketch of the history of the technique is given.

The first to use the 3ω detection technique was Von O. M. Corbino in 1911 [Corbino, 1911] (e.g. see [Gmelin, 1997, p. 1] or [Moon et al., 1996, p. 29]), and it has been used for studying thin wire (filament) properties such as specific heat capacity of titanium by L. R. Holland and others [Holland, 1963], [D. Gerlich, 1965], [Holland and Smith, 1966], [Rosenthal, 1961]. In 1985 S. R. Nagel and N. O. Birge published results where the technique was used with a nickel planar heater on a glass substrate. This was the first time the technique was used to study the frequency dependence of the heat capacity of a supercooled liquid (glycerol) [Birge and Nagel, 1985][2]. Since then a number of articles have been published from the Nagel group, including data on glycerol and propylene glycol [Birge, 1986] (where also a wire experiment is included) and [Birge and Nagel, 1987], *o*–Terphenyl Mixtures [Dixon and Nagel, 1988], di–*n*–butylphthalate [Menon, 1996] ([Birge et al., 1997] – review article), salol [Dixon, 1990] ([Wu et al., 1991] – comparison with other liquids and dielectric susceptibility). The frequency range of the measurements is something like [2mHz;4kHz] [Birge et al., 1997], and thus much wider than the traditional AC calorimetry measurements.

Other groups have used this technique as well. The German group around Donth have used a nickel heater with nickel electrodes, but on a polymer substrate (e.g. [Korus et al., 1997A, p. 100]) that has an effusivity smaller than the effusivity of glass, which enlarge the resolution of the experiment (cf. chapter 10) (e.g. [Donth et al., 1996], [Beiner et al., 1996], [Korus et al., 1997A], [Korus et al., 1997B], [Beiner et al., 1998]).

Also in South Korea this technique has been used quite a lot, with Y. H. Jeong and I. K. Moon as central persons. Data on supercooled $[Ca(NO_3)_2]_{0.4}(KNO_3)_{0.6}$ can be found in [Jeong and Moon, 1995], on potassium-calcium nitrate in [Moon et al., 1996] and [Jeong, 1997], and on polypropylene glycol in [Moon et al., 2001] (for other uses of the technique e.g. study of the Curie point see [Jung et al., 1992], [Jeong et al., 1991],[Bae et al., 1993],[Bae et al., 1994]). Finally it should be mentioned that also Inada et al. [1990] have used the technique to study the frequency dependent heat capacity of glycerol, propylene glycol and their mixtures, and Cahill [1990] study thermal conductivity of dielectric solids.

As mentioned in chapter 1, one of the aims of the work reported here has been to measure more accurately with less scatter in the data, even if that would mean narrowing the frequency range. Therefore I have tried to estimate the size of the scatter of the measurements mentioned above. This has been done simply by looking at the data plotted in the mentioned articles, and from them judging how large the scatter of the data points are ($\Delta_s(e)$, where e is the effusivity). The result

[2]Note that some of the axis of the plots in this article are not correct. They are corrected in [Birge, 1986, p. 1635].

$\Delta_s(e)/e$, estimated from the (frequency,*e*) curves around the loss peak frequency in the imaginary part of *e*, is around 10% for the best 3ω measurements (based on [Birge, 1986, p. 1636], [Birge and Nagel, 1987, p. 1470], [Menon, 1996, p. 5252], [Dixon, 1990, p. 8181], [Dixon and Nagel, 1988, p. 342]), and probably a bit more for the photopyroelectric measurements (based on [Bentefour et al., 2001], [Bentefour, 2002, p. 124, 131]). Of course this is only a rough estimate and a more direct comparison of new measurements to the old will be useful, but it seems that in order to improve on this point the measured $\Delta_s(e)/e$ must be less than 10%.

9 Design of the measuring cell

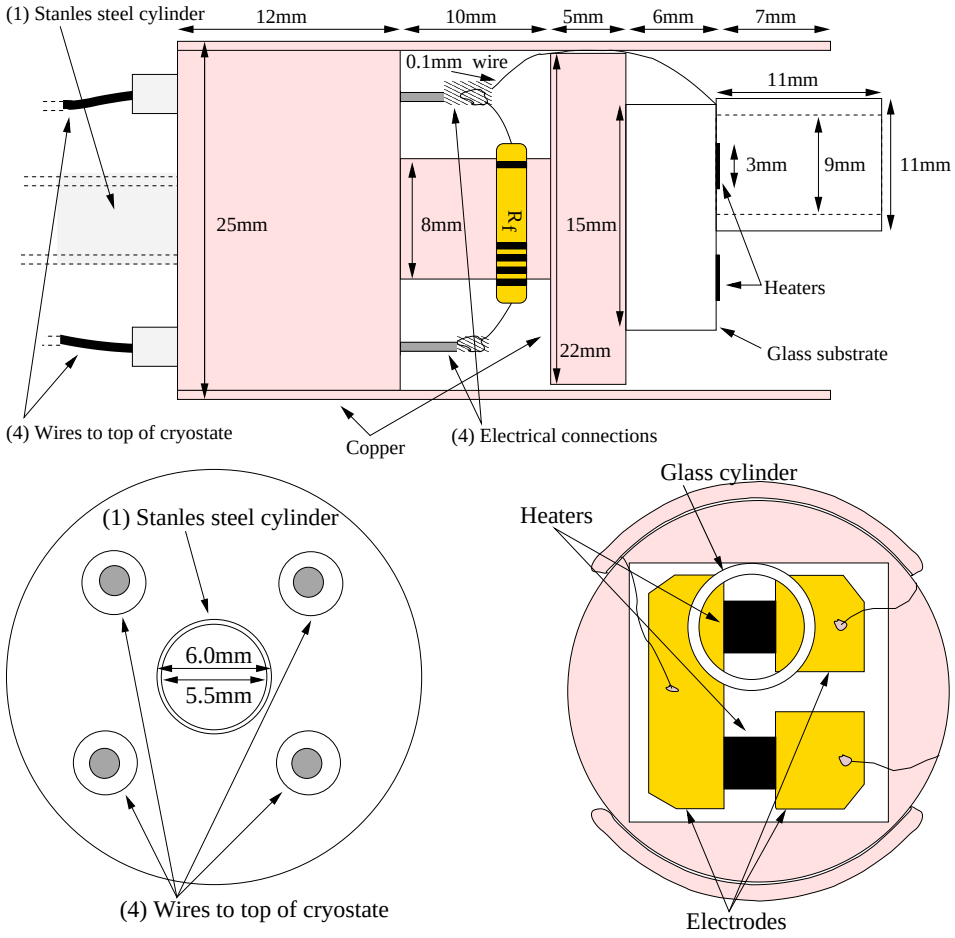

Figure 9.1 The top figure shows the measuring cell seen from the side. The cell is placed vertically inside the cryostate (turned 90° clockwise – the top–end is the one on the left). The lower left and right figure shows the cell seen from the top and the bottom, respectively. The heaters measure $3mm \times 3mm$.

In this chapter the design of the measuring cell will be described. Even though the

detailed arguments for designing it in exactly this way will not be presented until the following chapters, it is convenient to present the design here.

The cell is shown on figure 9.1. The heaters measure $3mm \times 3mm$ and the glass substrate is $6mm$ thick. It is glued onto the copper backing[1]. The glue layer is very thin.

The cell is placed vertically inside the cryostate (turned 90° clockwise: the top–end is the one on the left). The copper of the cell is in good thermal contact with the cryostate, and thus, the temperature of the copper backing will be equal to that of the cryostate (T_k).

The liquid is placed inside a glass cylinder that is glued[2] to the substrate and placed around the heater. In all the liquids I have used the surface tension of the liquid can keep the liquid inside the cylinder when the cell is turned (with the opening pointing down). In some cases, though, the liquid will flow out of the cylinder if it is shaken just a little bit, which is impossible to avoid when putting the cell into the cryostate. In these cases, the part of liquid closest to the cylinder opening is just cooled a little before the cell is put inside the cryostate. This is done by dipping the tip of the cylinder with liquid into liquid nitrogen, and sealing the liquid in that way.

The temperature–independent resistor (R_f) is placed just above the copper backing inside the cryostate. In this way long wires are avoided and everything is kept at constant temperature during a frequency scan. This is, though, done primary for practical reasons and is not very important. I have tried placing it outside the cryostate and no changes in the measurements could be observed.

The stainless steel cylinder is $\approx 40cm$ long and goes to the top of the cryostate. Stainless steel have a relatively low thermal conductivity compared to other alloys and metals.[3] At the same time the material is thin $(0.25mm)$, making it a poor thermal conductor, and thus only a little amount of heat will be transported from the top of the cryostate (at room temperature) to the cell.

The electrical connections through the copper to the wires that goes to the top of the cryostate are, of course, electrically isolated from the copper. The electrical connections are actually made with a little plug, and the "T–shaped" copper part has a thread and can bee taken off (by turning it counterclockwise). Thus it is rather easy to replace the substrate and film.

[1] The glue that I have used is: Torr Seal (Low Vapor Pressure Resin) from Varian Associates, Vacuum Products Division, Lexington, MA, USA.

[2] Using the same glue as for gluing the substrate to the copper backing.

[3] The stainless steel that is used is type AISI 304, and it has a thermal conductivity of $\approx 16.3 W m^{-1} K^{-1}$ at room temperature (this value is taken from a catalogue from the company Goodfellow. Similar values can be found elsewhere).

There are two heaters on each substrate, but in the measurements reported here only one is used at the time. Originally the idea was to use two heaters: one with liquid and one without liquid. If the two heaters are coupled in series and the output signal are measured across one of them, then the 3ω signal will be zero if the two heaters are exactly alike and, if $Z_1 = Z_2$, where Z_1 and Z_2 are the thermal impedance heater 1 and heater 2 "look into", respectively (the calculations showing this can be found in A appendix on page 157). The problem is that the 3ω signal resulting from $Z_1 \neq Z_2$ does not solely depend on the thermal impedance of the liquid $(Z_L \equiv 1/Y_L)$ but also on the thermal impedance of the substrate $(Z_S \equiv 1/Y_S)$:

$$V_{3\omega} \propto Z_1 - Z_2 = \frac{1}{Y_L + Y_S} - \frac{1}{Y_S},$$

if heater 1 is the one with liquid (see page 45). Thus, the thermal impedance of the substrate needs to be measured separately anyway, and nothing is gained compared to the use of just one heater with and without liquid.

Actually the method of using two heaters would be somewhat more difficult, since also the current through the heater must be measured in order to have enough information to calculate the thermal impedance of the liquid (of course this does not present any major problem). The reason why this is necessary is that the power released in the heater must be known and thus besides the voltage across the heater also the resistance of the heater or the current through the heater must be known. In the case with a fixed resistor (R_f) in series with the heater this can be calculated, since also the input–voltage is known. But, when the fixed resistor is replaced with a $2^{nd.}$ temperature–dependent resistor (heater) this information is no longer available. This is not something that can easily be calibrated, since the temperature of the heaters depend on the power released in them. One could imagine that a heater was calibrated with a fixed R_f, and thus a set of T_k, R_{pm} values are known at a given input–voltage. But when the fixed R_f is replaced with a temperature–dependent resistor ($2^{nd.}$ heater) then these values can no longer be used, unless one is certain that the resistance of R_f is exactly the same as the resistance of the $2^{nd.}$ heater, and of course this will only be the case at one specific temperature, if at any temperature at all. Another drawback of this method is that if the heaters are not exactly alike (have the same resistance and temperature coefficient), the 3ω signal will not be zero when measurements are made without liquid.

10 Optimizing the cell dimensions

10.1 Temperature gradients in the sample

Since it is only possible to supply heat, not to cool, with the thin film heater (cf. equations 6.6 and 6.7), the average temperature (T_{pm}) of the heater will be higher than the temperature (T_k) of the surrounding temperature bath (cryostate): $T_{pm} - T_k = I_{Tm} Z_{T,DC}$ (cf. equation 5.1).

It is important how the coupling between the heater and the temperature bath is made, that is, the geometry of the setup. In what shall be called the gradient–method, the coupling is made through the liquid, and there will be a temperature gradient through the liquid. This gradient may present a problem, since the properties of the liquid will be different at different distances from the heater. As will be shown below this does not seem to be a problem when only the thermal properties of the liquid are considered, but this is somewhat misleading. It actually does play an important role, as can be seen when the thermo–mechanical problem mentioned in chapter 1 (page vi) is considered.

For the *DC* part of the heat current (I_{Tm}):

$$I_{Tm} = -\kappa_L \frac{dT}{dx}, \tag{10.1}$$

where κ_L is the thermal conductivity of the liquid.

At low frequencies the one–dimensional approximation fails due to edge effects. These edge effects play a significant role when the diffusion length (L_D) becomes comparable to the width (W) of the heater. Even if a first order approximation can be made and these edge effects taken into account, this approximation will not hold down to frequencies where L_D becomes significant larger than W. Thus at least $L_{D,max} \leq W$. This means that the maximum relevant distance (dx) in equation 10.1 is W:

$$I_{Tm} = -\kappa_L \frac{\Delta T_W}{W},$$

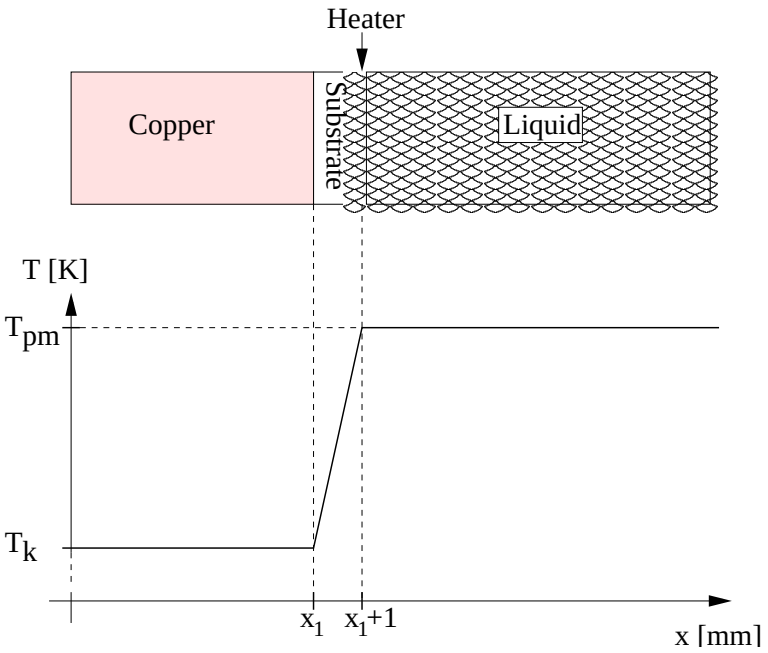

Figure 10.1 With a copper backing that is clamped to the cryostate (temperature bath) the average temperature is constant through the liquid. The DC heat is lead away through the glass substrate. This is the non-gradient–method.

where ΔT_W is the temperature difference between the heater and the liquid a distance W (perpendicular) away from the heater.

From equation 5.4 (with $\tilde{Y}_L \equiv 1/\tilde{Z}_T$):

$$I_{TA} = T_A|\tilde{Y}_L|,$$

and since $I_{Tm} = I_{TA}$ (cf. equation 6.7):

$$\begin{aligned} T_A|\tilde{Y}_L| &= \kappa_L \frac{\Delta T_W}{W} \\ \Updownarrow & \\ \Delta T_W &= T_A|\tilde{Y}_L|\frac{W}{\kappa_L} = \frac{W}{L_{D,max}} T_A, \end{aligned} \tag{10.2}$$

where equation 7.5 has been used for $\tilde{Y}_L$ (with $\tilde{Y} = 1/\tilde{Z}_{tot}$)), and equation 7.1 for L_D.

From equation 10.2 it is seen that in the worst case (the lowest used frequency, where $L_D = L_{D,max} = W$): $T_W = T_A$. If T_A is small enough so that the measurements are in the linear regime, as must be the case, then also T_W is so small that the

thermal properties of the liquid does not change (from the heater to W away from the heater): of course the thermal properties do change through the liquid, but the thermal waves do not travel very far and therefore do not "feel" the changes. Thus, the gradient through the liquid does not seem to present a problem viewed from this perspective.

As mentioned in chapter 1, the liquid expands (and contracts) while heated (and cooled), and this results in a mechanical sound wave. The wavelength of this sound wave is probably somewhere between $1m$ and $1km$, depending on frequency[1] (and it is really not appropriate to speak of a wave, since the thickness of the liquid layer is much smaller than the wavelength). Thus the mechanical disturbance reaches much further than the thermal, and the temperature gradient through the liquid becomes important. $T_{pm} - T_k$ will be several degrees, and while the substance is still a liquid at the heater, it can be deep into the glass at liquid temperature bath interface.

Therefore the thermo–mechanical problem becomes extremely complicated in the gradient–method, and it will not be a well defined quantity that is measured. Thus, in order to deal properly with the thermo–mechanical problem, a non–gradient–method must be used. With such a method, at least in some cases, it will be the longitudinal heat capacity (c_l) that is measured (see page v).

For these reasons it is desirable to get rid of the DC heat through the substrate rather than through the liquid. Therefore, I have designed the setup with a copper backing behind the substrate (see figure 10.1). Also, with such a backing it is well controlled how the DC heat is lead away when measurements are made without liquid, and it is lead away the same way for measurements with and without liquid.

The copper backing is clamped to the cryostate, and the temperature of the copper backing is the cryostate temperature (T_k, cf. chapter 9). In this way the average temperature of the liquid is the same through all the liquid, and this method is a non–gradient–method. If there is air between the liquid and the cryostate (there could be vacuum) of course heat can diffuse through that to the cryostate. Also there will be radiation of heat. But, if the conduction of heat through the glass substrate is much larger, then these contributions are negligible. The conditions needed to fulfilled this is discussed in section 10.2.

[1]The group velocity (v_g) of a longitudinal wave is given by: $v_g = \sqrt{Y_o/\rho}$, where Y_o and ρ are Young's modulus and the density, respectively [Nordling and Österman, 1996, p. 224]. $Y_o > G$ (where G is the shear modulus) [Nordling and Österman, 1996, p. 153] and is typical $10^9 Pa$ near T_g. With ρ around $10^3 kgm^{-3}$ the velocity becomes $v_g \approx 10^3 ms^{-1}$, and thus, the wavelength is around $1m$ at $1kHz$ and $1km$ at $1Hz$.

10.2 Maximum thickness of the glass substrate

If the heater was a half spherical shell and the surrounding temperature bath also was spherical, then it was easy to compute Z_{Tair}. Letting the radius (R) to the temperature bath be of the order of the smallest distance from the heater to the cryostate, and setting the radius of the heater equal to the length (L) of the heater, and estimating Z_{Tair} this way, under estimates Z_{Tair} (especially if $W < L$, and thus the estimate is conservative, since the demand is that Z_{Tair} must be large). Integrating from L to R yields:

$$Z_{Tair} \approx \frac{2}{\kappa_L 4\pi} \int_L^R \frac{1}{r'^2} dr' = \frac{2}{\kappa_{air} 4\pi} \left(\frac{1}{L} - \frac{1}{R} \right) \approx \frac{1}{\kappa_{air} 2\pi L} \text{ , if } L \ll R, \quad (10.3)$$

where κ_{air} is the thermal conductivity of air ($\kappa_{air} \approx 0.026 W m^{-1} K^{-1}$ at $292K$ [Nordling and Österman, 1996, p. 36-37]), and the number 2 (after the first $\approx$) comes from the fact that only half a sphere is used. In the measurements reported here the relevant numbers are: $R \approx 1 \times 10^{-2} m$, $L = 3 \times 10^{-3} m$, and equation 10.3 gives: $Z_{Tair} \approx 2 \times 10^3 K W^{-1}$.

$Z_{T,DC}$ is given by:

$$Z_{T,DC} = \frac{l_S}{A \kappa_S} = \frac{l_S}{L^2 \kappa_S},$$

where l_S is the thickness of the glass substrate, A the area of the heater, and κ_S the thermal conductivity of the substrate. Thus the demand $Z_{T,DC}/Z_{Tair} \ll 1$ can be written as:

$$\frac{Z_{T,DC}}{Z_{Tair}} = \frac{\kappa_{air} 2\pi l_S}{L \kappa_S} \approx \frac{l_S}{6L} \ll 1, \quad (10.4)$$

where the table value for κ_{glass} (given on page 43) is used for κ_S, and the value for κ_{air} (given above) is used. As mentioned Z_{Tair} is probably under estimated and the $\ll$ in equation 10.4 can be taken somewhat loosely.

Equation 10.4 gives a rough estimate of the upper limit of the thickness of the glass substrate (l_S), for a given heater length (L).

Radiation of heat has not been considered, since, as is shown below, the thermal impedance related to the radiation of heat (Z_{Trad}) is large compared to Z_{Tair}. According to Stefan–Boltzmann formula for a black body: $\frac{\partial P}{\partial A} = \sigma T^4$, where $\sigma = 5.6705 \times 10^{-8} W m^{-2} K^{-4}$, P is the power through the area ($A = L^2$), and T is the temperature of the body (for a non black body the right hand side must be multiplied with the emissivity, but this is neglected here). The net heat current

(I_{Trad}) from the heater to the surroundings, due to radiation of heat, is given by the difference between the radiation from the heater to the cryostate $(P(T_{pm}))$ and the radiation coming from the cryostate to the heater $(P(T_k))$:

$$\begin{aligned} I_{Trad} &= P(T_{tm}) - P(T_k) \\ &\approx A\sigma T_{pm}^4 - (A\sigma T_{pm}^4 + A\sigma 4 T_{pm}^3 (T_k - T_{pm})) \end{aligned}$$

$$\Downarrow$$

$$Z_{Trad} = \frac{T_{pm} - T_k}{I_{Trad}} \approx \frac{1}{L^2 \sigma 4 T_{pm}^3},$$

(where $P(T_k)$ is Taylor expanded around T_{pm}).

From this and equation 10.3 it is seen that:

$$\frac{Z_{Tair}}{Z_{Trad}} = \frac{L 2\sigma T_{pm}^3}{\kappa_{air}\pi} \approx 20 m^{-1} L \text{ , for } T_{pm} = 250K$$

Thus, if L is less than a few *cm* it is reasonable to neglect the heat flow coming from radiation of heat.

10.3 Minimum thickness of the glass substrate

Now, the minimum thickness of the substrate will be considered. At high frequencies (Ω large) the glass substrate can be considered infinitely thick ($L_D(\Omega) \ll l_S$). But, at some frequency (coming from high to low frequencies) the thermal waves travels so far that the copper behind the glass substrate becomes important. At low frequencies (when $L_D(\Omega) \gg l_S$) the glass substrate is not important, and (almost) all the heat will flow into the copper backing and none into the liquid, and the resolution of the experiment will be lost. *Therefore, the minimum thickness of the glass substrate is set by the lower frequency limit of the experiment*.

With liquid on the heater the total admittance $(\tilde{Y}_{LS})$ is measured: $\tilde{Y}_{LS} = \tilde{Y}_L + \tilde{Y}_S$ (cf. equation 7.22).

It is desirable that the thermal admittance of the substrate $(\tilde{Y}_S)$ is as small as possible compared to the thermal admittance of the liquid $(\tilde{Y}_L)$, so that as much of the signal as possible is due to the liquid. For the thickness of the glass substrate (or the liquid layer) the two limiting cases are thermal thick or thermal thin, that is, either it is thick or thin compared to the diffusion length (see equation 7.1):

$$\text{Thermal thin:} \quad l_x \ll \sqrt{\frac{\kappa_x}{\Omega_{max} c_x}} = L_{D,x} \tag{10.5}$$

$$\text{Thermal thick:} \quad l_x \gg \sqrt{\frac{\kappa_x}{\Omega_{min} c_x}} = L_{D,x} \tag{10.6}$$

where subscript x indicates either substrate (S) or liquid (L), and Ω_{min} and Ω_{max} are the minimum and maximum cyclic frequency of the heat current in the experiment. Thus, the maximum thickness of the liquid layer is given by equation 10.5, if the layer can be considered thermal thin, and the minimum thickness of the layer by equation 10.6, if the layer can be considered thermal thick.

Here, it will be assumed that the one–dimensional diffusion model can be used (and for simplicity of notation that c_x and κ_x are real). If the thermal admittance in the thermal thick case is designated $\tilde{Y}_{thick}$, then (from equation 7.5):

$$\tilde{Y}_{thick} = A\sqrt{i\Omega c_x \kappa_x} \tag{10.7}$$

In the thermal thin case the thermal admittance ($\tilde{Y}_{thin}$) is different for the liquid and the glass, since the glass is just a thermal conductor between the heater and the copper backing (it is at isothermal conditions at the end of the diffusion chain), while the liquid functions as a capacitor (it is at adiabatic conditions at the end of the diffusion chain). Thus:

$$\begin{aligned} Y_{thin,S} &= \frac{A\kappa_S}{l_S}, \\ \tilde{Y}_{thin,L} &= i\Omega C_L A l_L \end{aligned}$$

From this and equation 10.7 all the possible combinations of thermal thin and thick liquid layer and glass substrate can be obtained. This is shown in figure 10.2.

	Liquid thermal thick	Liquid thermal thin
Substrate thermal thick	A $r_A \equiv \frac{\tilde{Y}_L}{\tilde{Y}_S} = \sqrt{\frac{c_L \kappa_L}{c_S \kappa_S}}$	B $r_B \equiv \frac{\tilde{Y}_L}{\tilde{Y}_S} = \sqrt{\frac{i\Omega c_L^2}{c_S \kappa_S}} l_L$
Substrate thermal thin	C $r_C \equiv \frac{\tilde{Y}_L}{\tilde{Y}_S} = \frac{\sqrt{i\Omega c_L \kappa_L}}{\kappa_S} l_S$	D $r_D \equiv \frac{\tilde{Y}_L}{\tilde{Y}_S} = \frac{i\Omega c_L}{\kappa_S} l_L l_S$

Figure 10.2 $\tilde{Y}_L/\tilde{Y}_S$ in the thermal thin and thick cases.

As can be seen from the equations in figure 10.2, not surprisingly, only in case A (where both the liquid layer and glass are thermal thick) is $\tilde{Y}_L/\tilde{Y}_S$ independent of

both l_L and l_S. More interesting is the fact that in the tree other cases is $\tilde{Y}_L/\tilde{Y}_S \propto l_x$ when x is thermal thin. Thus, it seems that the best result for the tree cases is to make l_x as large as possible. Of course l_x can as a maximum attain the value given by equation 10.5.

Calculating the ratios of r_B, r_C and r_D with respect to r_A and combining with the criteria given by equation 10.5 gives:

$$\begin{aligned}
\frac{r_B}{r_A} &= \sqrt{i}\frac{l_L}{L_{D,L}}, \quad \text{equation 10.5 for } x = L \quad \Rightarrow \quad \left|\frac{r_B}{r_A}\right| \ll 1 \\
\frac{r_C}{r_A} &= \sqrt{i}\frac{l_S}{L_{D,S}}, \quad \text{equation 10.5 for } x = S \quad \Rightarrow \quad \left|\frac{r_C}{r_A}\right| \ll 1 \\
\frac{r_D}{r_A} &= i\frac{l_L l_S}{L_{D,L}L_{D,S}}, \quad \text{equation 10.5 for } x = L,S \quad \Rightarrow \quad \left|\frac{r_D}{r_A}\right| \ll 1
\end{aligned}$$

This clearly illustrates that there is no hope that $\tilde{Y}_L/\tilde{Y}_S$ will be larger in case B,C or D than in case A. *Therefore, the optimum is to have both a thermal thick liquid layer and a thermal thick substrate.*

Thus, in order to set the minimum thickness of the glass substrate and liquid layer, the lowest cyclic frequency of the heat current (Ω_{min}), used in the experiment is needed to insert in equation 10.6.

10.4 Relation between Ω_{min} and W

Ω_{min} (using equation 10.6) is needed to set the minimum thickness of the glass substrate and liquid layer, and L is needed to set the maximum thickness of the glass substrate (using equation 10.4).

However Ω_{min} and W are not independent, and if W is not very different from L, then Ω_{min} and L are not independent.

As mentioned, even if a first order approximation can be made and the edge effects can be taken into account, this approximation will not hold down to frequencies where L_D becomes significantly larger than W. The problem of the edge effect will be discussed in more detail in chapter 12, and it turns out that if such a first order approximations must be used, then a reasonable minimum requirement is:

$$L_{D,max} = \sqrt{\frac{\kappa_S}{\Omega_{min} c_S}} = \frac{1}{3}W, \tag{10.8}$$

where $L_{D,max}$ is the maximum diffusion length obtained in the experiment, and the thermal parameters for the substrate can be used, since the diffusion length in

the glass substrate is usually longer than in the liquid (e.g. table values for glycerol are: $\kappa_{glys} = 0.285 W m^{-1} K^{-1}$, $c_{p,glys} = 3.024 \times 10^6 J m^{-3} K^{-1}$ around room temperature [Nordling and Österman, 1996, p. 36-37]).

Now, given some width (W) of the heater, Ω_{min} can be calculated, which then sets the minimum thickness of the glass substrate (l_S). The combination of equations 10.8 and 10.6 yields:

$$\frac{1}{3}W \ll l_S$$

Given this and equation 10.4:

$$\frac{1}{3}W \ll l_S \ll 6L \tag{10.9}$$

(Remembering that the second $\ll$ can be taken somewhat loosely).

From figure 9.1 it is seen that the dimensions of the measuring cell obey equation 10.9. The thickness of the glass $(l_S = 6mm)$ and $W = L = 3mm)$.

11 Properties of the thin films

In designing the planar heater experiment one must consider what properties the heater must possess and how it can be fabricated. In this chapter some possible materials for the thin film heater and electrodes will be discussed. Also the problem of how to get good electrical contact to the electrodes will be discussed. In later chapters (chapter 13 and chapter 14) it will be described how the films can be fabricated using an electron beam evaporation chamber.

11.1 Optimal properties

Before looking at what materials should be chosen it is useful to list what properties are optimal, if there are no limitations on what can actually be fabricated.

The resistance R_{pm} of the heater should have a suitable size, since this is measured in the experiment. It is both difficult to accurately measure a very high and a very low resistance. If it is too low, the resistance of the connecting wires and of the electrodes will interfere. If it is too high, it will require a large voltage to drive a reasonable current through it and, since a given effect must be released in the heater, a high resistance requires a high voltage.

It is of course not possible to set an exact lower limit for R_{pm}, but the resistance of the connecting wires is probably below 1Ω (a copper wire of diameter $0.1mm$ has a length specific resistance of $\approx 2\Omega m^{-1}$, since the resistivity of copper is $\approx 1.67 \times 10^{-8}\Omega m$ [Nordling and Österman, 1996, p. 46]). If this must be low compared to R_{pm}, then it will be reasonable to require that $100\Omega \leq R_{pm}$.

The maximum desired value ($R_{pm,MAX}$) is set by the maximum voltage available and the required effect that must be released in the film, which is set by the minimum required temperature amplitude ($T_{A,MIN}$). The maximum voltage available in the setup described in this report is $10V$. The maximum voltage across the heater $(V_{out,MAX})$ will then be $\approx 5V$, since the heater is in series with a temperature–independent resistor (R_f, see figure 6.1, page 26) with similar resistance (in section 6.1 it was shown that there are good reasons to chose the

resistance of $R_f \approx R_{pm}$). The temperature amplitude (T_A) of the temperature oscillations is given by equation 5.4. If it is assumed that the thermal impedance is given by equation 7.5, then the required effect (I_{tm}) can be calculated. For this rough estimate it is assumed that the thermal impedance of the substrate and the liquid are of similar size, and thus, the measured thermal impedance with liquid on the heater will be $1/2$ the value of the thermal impedance of the glass (see equation 7.22). Thus $AR_{pm,MAX}$ is given by:

$$AR_{pm,MAX} = \left| \frac{V_{out,MAX}^2}{2T_{A,MIN}\sqrt{i\Omega_{MAX} c_S \kappa_S}} \right| = \frac{V_{out,MAX}^2}{2T_{A,MIN}\sqrt{\Omega_{MAX} c_S \kappa_S}}$$

If the table values for glass given on page 43 are used for c_S and κ_S, the maximum cyclic frequency (Ω_{MAX}) is set to $1000s^{-1}$, and a temperature amplitude of minimum $20mK$ is needed, then $AR_{pm,MAX} \approx 1.4 \times 10^{-2}\Omega m^2$. In the experiments reported in this report, the area of the heater is $A = 9 \times 10^{-6}m^2$, therefore, it is reasonable to require $R_{pm} \leq 1k\Omega$.

Since the temperature is measured by measuring R_p, another important property of the heater is the temperature coefficient ($\alpha \equiv (1/R_p)(dR/dT)$, cf. equation 6.26, page 33). The larger $|\alpha|$, the better temperature resolution. This can be seen from equation 6.17 (page 30), where the 3ω signal is proportional to α. Therefore, the goal is to have as high a $|\alpha|$ as possible.

For the electrodes it must be required that $R_{elec.} \ll R_{pm}$, where $R_{elec.}$ is the resistance of the electrodes. If this is not so, an appreciable amount of heat will be released in the electrodes, and further, the voltage at one end of the heater will differ from the voltage at the other end, and the heat will not be uniformly distributed across the heater (see figure 11.1).

Also, since the heat must be distributed uniformly across the heater, it is important that there is no holes in the film and that it has a uniform thickness. One way to quantify this is to require that it is uniform on the length scale set by the diffusion length ($L_D \approx 2 \times 10^{-5}m$, if $\Omega = 1000s^{-1}$, and the values for the heat capacity and thermal conductivity of glass given on page 43 is used, cf. equation 7.1). Also, the temperature variations across the heater due to a non uniform heater must be small compared to T_A (the temperature variations across the heater must be so small that the relaxation time of the liquid does not change across the heater (within the resolution of the experiment)). Ultimately to check this, the temperature variation across the heater should be measured. This could probably be done using IR photography (see [Mailly et al., 2001, p. 34]).

In connection with this it is worth to consider whether the average value of the resistance of the heater ($R_{pm} = \langle R \rangle$), that is measured, corresponds to the average

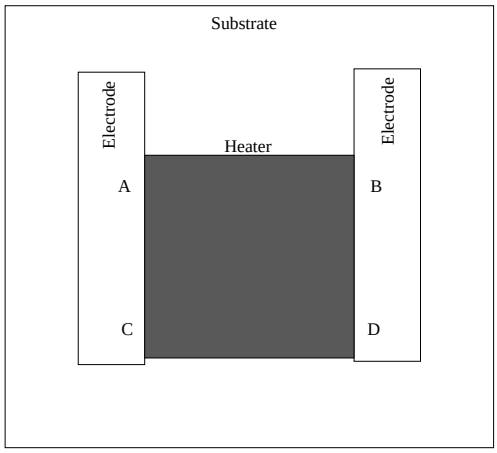

Figure 11.1 If the electrodes have a high resistance, then the voltage between points *A* and *B* will differ from the voltage between *C* and *D*.

temperature across the heater also, if there is a temperature difference from one end of the heater to the other. If the heater is slightly warmer at the left side in figure 11.1 (at the points *A* and *C*) than at the right side (at the points *B* and *D*), then it can be considered as a serial connection of resistors (R_n). Thus what is measured is the average value of such a series connection: $\langle R\rangle = \langle\sum_n(R_n)\rangle$. If $R_n = R_{n0} + \Delta R_n$, where R_{n0} is the average value and ΔR_n the deviation from this value then:

$$\langle R\rangle = \left\langle \sum_n (R_{n0}) \right\rangle \tag{11.1}$$

If, on the other hand, the heater is slightly warmer at the top end in figure 11.1 (at the points *A* and *B*) than at the bottom (at the points *C* and *D*), then it can be considered as a parallel connection of resistors (R_n). Thus, what is measured is the average value of such a parallel connection:

$$\begin{aligned} \frac{1}{\langle R\rangle} &= \left\langle \frac{1}{R} \right\rangle = \left\langle \sum_n \left(\frac{1}{R_{n0} + \Delta R_n} \right) \right\rangle \approx \left\langle \sum_n \left(\frac{1}{R_{n0}} \left(1 - \frac{\Delta R_n}{R_{n0}} \right) \right) \right\rangle \\ &\approx \frac{1}{\langle \sum_n (R_{n0}) \rangle}, \quad \text{since: } \frac{\Delta R_n}{R_{n0}} \ll 1 \end{aligned} \tag{11.2}$$

Equation 11.1 and equation 11.2 shows that in both cases $\langle R\rangle \approx \langle\sum_n(R_{n0})\rangle$, thus, the average value of the resistance corresponds in both cases to the average value of the temperature across the heater.

For obvious reasons there must be good electrical contact to the heater electrodes

and between the electrodes and the heater. The optimal properties of the thin films are summarized in figure 11.2.

Resistance of heater (R_{pm})	$100\Omega \leq R_{pm} \leq 1k\Omega$
Resistance of electrodes $(R_{elec.})$	$R_{elec.} \ll R_{pm}$
$\lvert\alpha\rvert$	High
Good electrical contact	Yes
Homogeneous film	Yes

Figure 11.2 The optimal properties of the heater and electrodes.

In the following sections it will be discussed if and how the listed properties can be obtained. First the properties of the heater itself.

11.2 Heater

In all cases that I'm aware of, a metal has been used for the heater. Nickel (Ni) is the most widely used. Probably because it is the element with the highest temperature coefficient $(\alpha_{Ni} \approx 6.75 \times 10^{-3} K^{-1}$ [Nordling and Österman, 1996, p. 45-47]), and that it is accessible and relatively easy to work with. Also it has a relative high resistivity [Menon, 1996, p. 5248] at least compared to metals like aluminum, silver, and gold (see figure 11.3). I have made thin films of aluminum (Al), chromium (Cr), indium (In), gold (Au), nickel (Ni), platinum (Pt), and silver (Ag). In all cases, I have measured a lower temperature coefficient than the table value (for a example of $\alpha_{Ni}(T)$, that I have measured, see figure 16.3 page 119). Consistent with this is the value for $\alpha_{Ni} = 3 \times 10^{-3} K^{-1}$ found by Birge et. al. [Birge et al., 1997, p. 55], $\alpha_{Ni} = 1 - 2 \times 10^{-3} K^{-1}$ found by Beiner et. al. [Beiner et al., 1996, p. 5184] and $\alpha_{Ni} \approx 2 \times 10^{-3} K^{-1}$ found by [Jonsson et al., 2000, p. 48].

The fact that α is lower in the thin film than in the bulk is probably due to defects in the thin film. These defects can lower α in two ways. Firstly, the reason why the resistance becomes higher with temperature, can roughly be explained by the fact that the thermal vibrations of the metal lattice becomes larger as the temperature is raised. Thus, the free electrons will bump into the lattice molecules more often at higher temperatures. Defects in the lattice will also raise the resistance, but since these defects are present at all temperatures (as long as they are

Element	Resistivity $[10^{-8}\Omega m]$	$\alpha\,[10^{-3}K^{-1}]$
Al	2.65	4.29
Cr	13	3
In	8.37	5.1
Au	2.35	3.98
Ni	6.84	6.75
Pt	10.6	3.92
Ag	1.59	4.10

Figure 11.3 Resistivity and temperature coefficient of selected elements. [Nordling and Österman, 1996, p. 45-47]

not annealed away), the part of the resistance coming from these defects will not be temperature–dependent. Of course the presence of more or less defects will not affect dR/dT, but since $\alpha \equiv (1/R_p)(dR/dT)$ it will affect α. Secondly, it is possible that the defects in the film are of a nature that make them work like a semiconductor. That is, the number of current carrying electrons are thermally activated. Thus the resistance will drop as the temperature is raised (α is negative). Of course, if this effect is present, the negative α of the defects will partly or totally suppress the positive α of the bulk. There is no doubt that an effect of negative α can be present in a very thin film. I have made nickel films with a resistance of $7-10k\Omega$ per square and a (small but) negative α. To my experience, α comes closer to the table value, the thicker the film. Also, if the thin film is annealed (e.g. at $100^{\circ}C$ for several hours) α gets closer to the table value, which can be attributed to the annealing away of defects. For some metals, like nickel, it is problematic to anneal in air atmosphere, since they will oxidize. Thus annealing the film may be complicated. I do not have enough experience and knowledge about annealing to give guidelines on how to reach the best result (and how good that will be). Though, I have tried to anneal thin films under vacuum (not very high vacuum, only around $0.1mbar = 10Pa$), but still oxidation of Ni took place and ruined the film. Probably annealing in a protecting atmosphere (e.g. argon) will give better results. This I have no experience with.

Even though nickel has a relatively high resistance it is a metal, and it is not possible to make thin films with a reasonable α and a high resistance (per square) at the same time: the thinner film, the higher resistance, but lower α. This problem can, to my experience and knowledge, not be overcome by choosing another metal (but may be, at least partly, overcome if the film is annealed. To my knowledge non of

the experimentalists using metal films and the 3ω detection technique anneal their films.).

Birge et. al. use heaters with a resistance of approximately 2.5Ω per square and a film thickness of approximately $30-40nm$ [Birge et al., 1997, p. 57] (and as mentioned $\alpha_{Ni} = 3\times10^{-3}K^{-1}$ [Birge et al., 1997, p. 55]). By making their film rectangular they have heaters of approximately 10Ω, 20Ω and 40Ω [Birge et al., 1997, p. 57], [Menon, 1996, p. 5249].

In order to get heaters with better properties I have made heaters of carbon[1]. The resistance of the carbon thin films vary with temperature as it does for a semiconductor (see equation 6.22). They have a negative temperature coefficient (α_C), and they have two advantages over metal heaters. Firstly, $|\alpha_C| > |\alpha_{Ni}|$ (at least at temperatures lower that $300K$). α_C is typical between $-3\times10^{-3}K^{-1}$ and $-6\times10^{-3}K^{-1}$ in the temperature interval $[300K, 180K]$ for a heater with resistance $\approx 500\Omega$ per square at room temperature (for a heater with resistance $\approx 1.5k\Omega$ per square at room temperature, α_C is typical between $-6\times10^{-3}K^{-1}$ and $-10\times10^{-3}K^{-1}$). (For an example of $\alpha_C(T)$, that I have measured, see figure 16.3 page 119). Secondly, it is possible to make carbon films with resistances in a large interval. By varying the thickness I have made carbon films with resistances between 100Ω and $500k\Omega$ per square. Thus, it is possible to fabricate a film with a resistance in the desired interval $([100\Omega, 1k\Omega])$ without making it very long and thin.

For a carbon film with resistance $\approx 500\Omega$ per square (at room temperature) I have measured the thickness to $30nm \pm 15\%$ (measured with a simple interferometer[2]). This is in agreement with the table value of $1.3\times10^{-5}\Omega m$ at $300K$ [Nordling and Österman, 1996, p. 45] for the resistivity of carbon, graphite.

A possible problem with the carbon (or metal) thin film heaters is whether or not the heat is distributed homogeneously across the heater. Of course the best way to check this is to measure the temperature profile across the heater. As mentioned (page 68) it may be possible to do this with IR photography. I have not had the possibility (time and equipment) to do this, and I can not quantify how homogeneous the thin films are. This is something that ought to bee looked into more carefully.

[1] I got this idea almost by accident. I had deals (where the metal to be evaporated is placed) in the electron beam evaporation chamber made of carbon, and found, that a small amount of the deal material also ended up on the substrate. That discovery led to experiments with no metals in the deals, and finally to the thin carbon films. For more "historical" details see chapter 2.

[2] A Å-Scope Interferometer, model nr. 980-4020 from Ångstrom Technology, California.

11.3 Electrodes

Making good electrodes is not difficult. Gold is a good candidate, since it has a low resistivity, can easily be evaporated, is easy accessible, and do not oxidize. Birge et. al. uses gold electrodes with a resistance of about $2-5\%$ of the heater resistance and a thickness of approximately $200nm$ [Birge et al., 1997, p. 55-56], [Menon, 1996, p. 5248]. I have also used gold electrodes but made them thicker (probably around $500nm$). The electrodes I have made have a resistance of less that 0.1Ω (less than 0.05Ω per square). Thus since the resistance of the carbon heaters I have used is more than 100Ω, then $R_p/R_{elec.} < 0.1\%$.

11.4 Connecting wires to the electrodes

First I tried using silver epoxy[3] to connect wires to the gold electrodes, but it was difficult getting good durable electrical contact this way. Birge et. al. seems to share this experience, and have at least in the later versions of the experiment used standard 60Sn40Pb solder[4] [Birge et al., 1997, p. 56], [Menon, 1996, p. 5248].

Unfortunately it is not possible to solder thin gold films with 60Sn40Pb solder [AWS, 1978, p. 107-108], [Beiser, 1954, p. 180-183], [Indium, n.d.]. The gold dissolves very quickly into the solder [AWS, 1978, p. 107-108]. If one is quick with the soldering ion (I have tried this myself) it may be possible to solder a wire on to a gold thread of $1mm$ in diameter (or thicker) with 60Sn40Pb solder, but even then it is easy to see that a lot of the gold is dissolved. Soldering on a gold film less that $1\mu m$ thick with this solder is impossible. My guess is that, the reason Birge et. al. has success with a 60Sn40Pb solder is that they probably have Ni underneath the gold thin film (Ni can be soldered with 60Sn40Pb solder [Indium, n.d.]). If this is the case, it can look as if they have soldered on the gold, but really the gold is dissolved into the solder and the connection is made to the Ni film underneath.

Fortunately it is possible to solder on gold with indium (In) based solders. I have obtained very good results with a 80In15Pb5Ag solder (from a solder kit from Indium Corporation of America [Indium, n.d.], with a melting point of $154°C$). Other alloys should work as well, such as 53Sn29Pb17In0.5Zn, 95In5Bi [AWS,

[3] I used the two component "Eccobond 57 C" from Grace N.V., Nijverheidsstraat 7, 2260 Westerlo Belgium.

[4] 60Sn40Pb solder (sometimes just written 60-40 or $60/40$) means that it is made of 60% tin (Sn) and 40% lead (Pb).

1978, p. 108], and other In based solders without Sn [Indium, n.d.]. For operation temperatures above $125°C$ solders like 80Au20Sn or 88Au12Ge can be used [Indium, n.d.].

The wires I have soldered on to the gold electrodes are made of copper, with a diameter of $0.1mm$, and covered with lacquer for electrical isolation (the lacquer is removed before soldering. For details see below).

11.4.1 Details on the soldering procedure

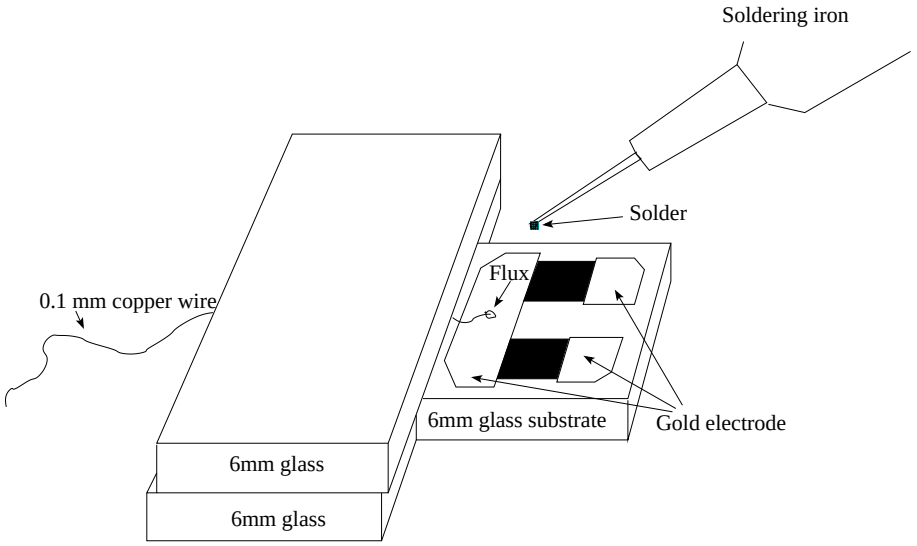

Figure 11.4 The $0.1mm$ thick wire is held in place by the two $6mm$ thick glass plates.

Below the exact soldering procedure that I have used is described. Not that it is difficult, but if anyone needs to do the same, I think that this description can be helpful: it is easy and it works every time.

After cutting the wire in suitable length, the lacquer is removed from the ends where the wires have to be soldered. This can be done by heating the soldering ion to the maximum temperature ($\approx 450°C$) and use a 62Sn36Pb2Ag solder (the solder I use is from Farnell, order code:419540). Of course a small amount of this solder will then be on the wire, but it is a very small amount, and it does not damage the final result. I have chosen the 62Sn36Pb2Ag solder because it is more "friendly" to gold than the 60Sn40Pb solder, it was easy to get hold of, and it was inexpensive. The reason that I do not simply use the 80In15Pb5Ag solder is that

it contains no flux. Of course the lacquer can also be removed with a knife or similar, but I found the other method much easier.

The wire is then placed on the gold film (see figure 11.4) and a small drop of flux is added on top of the wire, where the lacquer has been removed. I use the flux # 5*R* from Indium. A small amount of 80In15Pb5Ag is placed on the tip of the soldering iron, that is now $\approx 210°C$. The tip with solder is then "dipped" into the flux on top of the wire for $\approx 1s$.

12 Edge effects

As mentioned (e.g. page 59), the one–dimensional diffusion model does only hold as long as edge effects can be neglected, that is, as long as $L_D \ll W$, where W is the width of the heater. Jonsson and Andersson [1998] have made numerical calculations (finite element modeling) for a heater with $W \ll L$, where L is the length of the heater. These calculations show that L_D must be smaller than $\approx 0.024W$ in order to keep the error resulting from using the one–dimensional model below 1% [Jonsson and Andersson, 1998, p. 1880].

Thus, for a given heater the one–dimensional model will break down when the frequency becomes sufficiently low (and this lower frequency limit for the one–dimensional model is surprisingly high). But it is actually possible to calculate the contribution from the edge effects, and in most of the published data that has been measured using a planar heater and the 3ω detection technique some correction for the edge effect has been made.

Consider a heater with $W \ll L$. For such a heater without liquid the following expression is given [Cahill, 1990, p. 803], [Bae et al., 1993, p. 138], [Moon et al., 1996, p. 30], [Korus et al., 1997A, p. 104]:

$$\tilde{Z}_S = \frac{1}{\tilde{Y}_S} = \frac{4}{\pi\tilde{\kappa}_S L W^2}\int_0^\infty \frac{\sin^2(\frac{1}{2}Wu)}{u^2\sqrt{u^2+\tilde{q}^2}}du, \quad \text{for } W \ll L, \quad \tilde{q} = \sqrt{\frac{i\Omega\tilde{c}_S}{\tilde{\kappa}_S}}, \tag{12.1}$$

where $\tilde{Z}_S$ is the measured thermal impedance of the infinitely thick substrate, and $\tilde{\kappa}_S$ and $\tilde{c}_S$ is for the substrate.

Equation 12.1 reduces to the one–dimensional expression ($\tilde{Z}_S = \tilde{Z}_{tot}$, given by equation 7.5) in the limit $\Omega \to \infty$, that is $\tilde{q} \to \infty$, as expected:[1]

$$\begin{aligned} \tilde{Z}_S &\approx \frac{4}{\pi\tilde{\kappa}_S L W^2 \tilde{q}}\int_0^\infty \frac{\sin^2(\frac{1}{2}Wu)}{u^2}du, \quad \text{for } \tilde{q} \to \infty \\ &= \frac{1}{A\sqrt{i\Omega\tilde{c}_S\tilde{\kappa}_S}} \end{aligned}$$

[1] $\int_0^\infty \frac{sin^2(px)}{x^2}dx = \frac{p\pi}{2}$ [Spiegel, 1995, p. 96].

where $LW = A$ is the area of the heater.

(Equation 12.1 is the result of regarding the heater as a superposition of line sources. The result for the line source is integrated over the width of the heater.)

Equation 12.1 is for the heater without liquid. In order to treat the data measured with liquid a simple addition hypothesis is assumed. This addition hypothesis is only valid if the heat diffusion is one–dimensional (or the thermal parameters of the liquid and substrate are equal). I will return to this point at the end of this section.

Fortunately my supervisor Tage Christensen has been able to solve the problem more generally[2] [Behrens et al., n.d.]:

$$\tilde{Z}_{LS} = \frac{1}{\tilde{Y}_{LS}} = \frac{4}{\pi L W^2} \int_0^\infty \frac{\sin^2(\frac{1}{2}Wu)}{u^2 \left(\tilde{\kappa}_S \sqrt{u^2 + \tilde{q}_S^2} + \tilde{\kappa}_L \sqrt{u^2 + \tilde{q}_L^2} \right)} du, \text{for } W \ll L, \quad (12.2)$$

(subscript S and L is short for substrate and liquid, respectively). As can be seen equation 12.2 reduces to equation 12.1 if $\tilde{\kappa}_L = 0$, which corresponds to the heater without liquid, as expected.

Also, the problem for a heater, where $W \ll L$ does not hold, has been solved by Tage Christensen [Behrens et al., n.d.]:

$$\tilde{Z}_{LS} = \frac{1}{\pi^2 A^2} \int_0^\infty \int_0^\infty \frac{\sin^2(\frac{1}{2}Wu)\sin^2(\frac{1}{2}Lv)}{u^2 v^2 \left(\tilde{\kappa}_S \sqrt{u^2 + v^2 + \tilde{q}_S^2} + \tilde{\kappa}_L \sqrt{u^2 + v^2 + \tilde{q}_L^2} \right)} du dv, \quad (12.3)$$

In principle equations 12.2 and 12.3 can be used in the data analysis, but it will require a fitting routine including numerical evaluations of the integrals. The evaluation of the double integral in equation 12.3 can be very time consuming. It will be shown in section 12.2 that equation 12.3 might be rewritten so that the repeated evaluation of the double integral (e.g. in a fitting routine) can be speeded up significantly. In some cases, though, it will be convenient to have an approximation that can be used. For the substrate alone (i.e. $\kappa_L = 0$ in equation 12.3) the following expansion can be used [Behrens et al., n.d.]:

$$\tilde{Z}_S \approx \frac{1}{A\sqrt{i\Omega\tilde{\kappa}_S\tilde{c}_S}} \left(1 - \frac{2}{\pi} \sqrt{\frac{\tilde{D}_S}{i\Omega}} \left(\frac{1}{L} + \frac{1}{W} \right) \right), \quad \text{for } L_D < \frac{1}{3}W \quad (12.4)$$

If $W \ll L$, then the term $(1/L)$ can be ignored. In chapter 16 it will be shown that equation 12.4 break down at low frequencies. If the deviations from equation

[2] The calculations are rather lengthy and complicated, and will not be given here.

12.4 must be within $\approx 1\%$ it can be used down to frequencies around where L_D becomes $1/3$ of the heater width.

For the heater with liquid equation 12.3 must be expanded and it becomes more complicated [Behrens et al., n.d.]:

$$\tilde{Z}_{LS} \approx \frac{1}{A\sqrt{i\Omega}\left(\sqrt{\tilde{\kappa}_S\tilde{c}_S}+\sqrt{\tilde{\kappa}_L\tilde{c}_L}\right)}\left(1-\frac{2}{\pi\sqrt{i\Omega}}\left(\frac{1}{W}+\frac{1}{L}\right)F\right), \qquad (12.5)$$

for $L_D < \frac{1}{3}W$, and where:

$$F = \left(\sqrt{\tilde{\kappa}_S\tilde{c}_S}+\sqrt{\tilde{\kappa}_L\tilde{c}_L}\right)\left[\frac{\tilde{\kappa}_S\tilde{c}_L-\tilde{\kappa}_L\tilde{c}_S}{\tilde{\kappa}_L\tilde{c}_L-\tilde{\kappa}_S\tilde{c}_S}\frac{\sqrt{\tilde{\kappa}_S\tilde{\kappa}_L}}{\sqrt{(\tilde{\kappa}_L\tilde{c}_L-\tilde{\kappa}_S\tilde{c}_S)(\tilde{\kappa}_S\tilde{c}_L-\tilde{\kappa}_L\tilde{c}_S)}}\right.$$
$$\ln\left(\frac{(\tilde{c}_S+\tilde{c}_L)\sqrt{\tilde{\kappa}_S\tilde{\kappa}_L}+\sqrt{(\tilde{\kappa}_L\tilde{c}_L-\tilde{\kappa}_S\tilde{c}_S)(\tilde{\kappa}_S\tilde{c}_L-\tilde{\kappa}_L\tilde{c}_S)}}{(\tilde{\kappa}_S+\tilde{\kappa}_L)\sqrt{\tilde{c}_S\tilde{c}_L}}\right)$$
$$\left.+\frac{\tilde{\kappa}_L-\tilde{\kappa}_S}{\tilde{\kappa}_L\tilde{c}_L-\tilde{\kappa}_S\tilde{c}_S}\right]$$

As mentioned several authors have used equation 12.1 and a simple addition hypothesis in order to treat the measured data. It is assumed that equation 12.1 can be used both for $\tilde{Y}_S$ as well as for $\tilde{Y}_L$, and the addition hypothesis: $\tilde{Y}_{LS} = \tilde{Y}_L + \tilde{Y}_S$, corresponding to equation 7.22, page 45. Of course if equation 12.1 is valid for a substrate it also valid if the substrate is replaced by a liquid. But, as mentioned in section 7.3, equation 7.22 is not valid if the heat diffusion is not one–dimensional (or the thermal parameters of the liquid and substrate are equal) (since heat can flow across the liquid substrate interface). Thus this way of treating the data are not entirely correct. As mentioned this problem is referred to as a boundary mismatch in [Moon et al., 1996, p. 31].

Further, disregarding this boundary mismatch problem, the expressions given in [Birge et al., 1997, p. 60] and [Menon, 1996, p. 5251] seems to be not entirely correct. Using the addition hypothesis, equation 12.4 with $W \ll L$, and defining $\tilde{Y}_{x,1d} \equiv A\sqrt{i\Omega\tilde{c}_x\tilde{\kappa}_x}$ (where x is either S or L):

$$\begin{aligned}
\tilde{Y}_{LS} &= \tilde{Y}_{S,1d}\left(1+\frac{2}{\pi W}\sqrt{\frac{\tilde{D}_S}{i\Omega}}\right)+\tilde{Y}_{L,1d}\left(1+\frac{2}{\pi W}\sqrt{\frac{\tilde{D}_L}{i\Omega}}\right)\\
&= \tilde{Y}_{S,1d}+\tilde{Y}_{L,1d}+\frac{2A}{\pi W}(\tilde{\kappa}_S+\tilde{\kappa}_L)\\
&= (\tilde{Y}_{S,1d}+\tilde{Y}_{L,1d})\left(1+\frac{2}{\pi}\frac{A}{W}\frac{\tilde{\kappa}_S+\tilde{\kappa}_L}{\tilde{Y}_{S,1d}+\tilde{Y}_{L,1d}}\right)
\end{aligned}$$

In the corresponding equation in [Birge et al., 1997, p. 60] and [Menon, 1996, p. 5251] the factor $2/\pi$ is missing.

12.1 Data analysis: Approximation

In this section the data analysis using the approximate equations (12.4 and 12.5) will be considered. In the next section the data analysis using the exact expressions will be considered.

To analyze the data measured without liquid equation 12.4 can be used. For the substrate κ_S and c_S is expected to be frequency–independent. Thus, equation 12.4 gives:

$$\tilde{Z}_S A\sqrt{i\Omega} \approx \frac{1}{\sqrt{\kappa_S c_S}}\left(1-\frac{\sqrt{2}(1-i)}{\pi\sqrt{\Omega}}\left(\frac{1}{L}+\frac{1}{W}\right)\sqrt{\frac{\kappa_S}{c_S}}\right)$$

$$\Downarrow$$

$$\begin{cases} \mathrm{RE}\left\{\tilde{Z}_S A\sqrt{i\Omega}\right\} \approx \frac{1}{\sqrt{\kappa_S c_S}}\left(1-\frac{\sqrt{2}}{\pi\sqrt{\Omega}}\left(\frac{1}{L}+\frac{1}{W}\right)\sqrt{\frac{\kappa_S}{c_S}}\right) \\ \mathrm{IM}\left\{\tilde{Z}_S A\sqrt{i\Omega}\right\} \approx \frac{\sqrt{2}}{\pi\sqrt{\Omega}}\left(\frac{1}{L}+\frac{1}{W}\right)\frac{1}{c_S} \end{cases} \tag{12.6}$$

From equation 12.6 it is seen that, if the real and imaginary part of $\tilde{Z}_S A\sqrt{i\Omega}$ is plotted as function of $\frac{\sqrt{2}}{\pi\sqrt{\Omega}}\left(\frac{1}{L}+\frac{1}{W}\right)$, then for the real part the intersection on the ordinate axis will be one divided with the effusivity ($1/e_S = (\kappa_S c_S)^{-1/2}$) and the slope $-1/c_S$, while for the imaginary part the slope will be $1/c_S$ and it will point towards $(0,0)$ (when $\Omega \to \infty$). Thus from such a plot κ_S and c_S can be found. Further more, the plot can be used to evaluate where equation 12.4 breaks down, namely where deviations from straight lines is seen.

Note that when these edge effects become important and are taken into account not just the effusivity can be found (as is the case if the one–dimensional model is adequate), but the heat capacity and thermal conductivity can be found separately. At first glance this seems as an advantage, but depending on experimental uncertainties the separation of heat capacity and thermal conductivity may be subject to large errors. This is not surprising, since the separation of the two is based on equations (12.4 and 12.5) that take deviations from the one dimensional model into account. At high frequencies these deviations are small and the equations break down when the deviations becomes large (this will be shown for real measurements in chapter 16).

For the analysis of data measured with liquid it is interesting to look at $\tilde{Z}_{LS}/\tilde{Z}_S$. From equations 6.18 and 6.19 it follow that if the measurements with and without liquid are made under the same circumstances then:

$$\frac{\tilde{Z}_{LS}}{\tilde{Z}_S} = \frac{\tilde{V}_{3c,LS}}{\tilde{V}_{3c,S}} \equiv \tilde{V}_{3c,rel} \tag{12.7}$$

Using this and equations 12.4 and 12.5:[3]

$$V_{3c,rel} \approx \frac{1}{1+\sqrt{\tilde{\kappa}\tilde{c}}}\left(1-\frac{2}{\pi\sqrt{i\Omega}}\left(\frac{1}{W}+\frac{1}{L}\right)\left(F-\sqrt{\tilde{D}_S}\right)\right), \qquad (12.8)$$

$$\text{where } \tilde{\kappa} \equiv \frac{\tilde{\kappa}_L}{\tilde{\kappa}_S},\ \tilde{c} \equiv \frac{\tilde{c}_L}{\tilde{c}_S}$$

If κ_L can be found in the literature and κ_S and c_S are found as described, then equation 12.8 can be used to find $\tilde{c}_L$. Since c_L can not be isolated in equation 12.8 this must be done with a fitting routine.[4]

12.2 Data analysis: Integral

As mentioned the repeated evaluation of the double integral (equation 12.3) in a fitting routine might be very time consuming.

If the heater is square then $W = L$. Setting $1/2W$ equal to 1 (which just corresponds to measure length in units of $1/2W$ in stead of meters) equation 12.3 can be rewritten:

$$\tilde{Z}_{LS} \equiv \frac{1}{A}\frac{W}{2}\frac{1}{\tilde{\kappa}_S}\tilde{Z}_n = \frac{1}{2W\tilde{\kappa}_S}\tilde{Z}_n, \quad \text{where:} \qquad (12.9)$$

$$\tilde{Z}_n = \left(\frac{2}{\pi}\right)^2 \int_0^\infty \int_0^\infty \frac{\sin^2(u)\sin^2(v)\ dudv}{u^2v^2\left(\sqrt{u^2+v^2+\tilde{\xi}_S}+\sqrt{\tilde{\kappa}^2(u^2+v^2)+\tilde{\kappa}\tilde{c}\tilde{\xi}_S}\right)}, \qquad (12.10)$$

$$\tilde{\xi}_S \equiv \frac{i\Omega}{\tilde{\Omega}_S},$$

$$\tilde{\Omega}_S \equiv \frac{\tilde{\kappa}_S}{\tilde{c}_S(\frac{1}{2}W)^2} = \frac{4\tilde{\kappa}_S}{\tilde{c}_S A}, \quad \text{and (as above):} \quad \tilde{\kappa} \equiv \frac{\tilde{\kappa}_L}{\tilde{\kappa}_S},\ \tilde{c} \equiv \frac{\tilde{c}_L}{\tilde{c}_S}$$

$1/\tilde{\kappa}_S$ is taken outside the integral and reappears in equation 12.9 making Z_n without dimension. The factor $W/2$ converts back from measuring length in terms of $1/2W$ to meters.

[3] And using the expansion:

$$\frac{1+\varepsilon_1}{1+\varepsilon_2} \approx 1+\varepsilon_1-\varepsilon_2, \text{ for } \varepsilon_1, \varepsilon_2 \ll 1$$

[4] I have used Matlabs fminsearch routine.

Equation 12.10 can be rewritten in polar coordinates with:

$$r^2 = u^2 + v^2, \qquad \tan\theta = \frac{v}{u}$$
$$u = r\cos(\theta), \qquad v = r\sin(\theta),$$

and $dudv$ is given by the determinant of the Jacobian (e.g. [Chow, 2000, p. 29]):

$$dudv = \begin{vmatrix} \frac{\partial u}{\partial r} & \frac{\partial v}{\partial r} \\ \frac{\partial u}{\partial \theta} & \frac{\partial v}{\partial \theta} \end{vmatrix} drd\theta = \begin{vmatrix} \cos(\theta) & \sin(\theta) \\ -r\sin(\theta) & r\cos(\theta) \end{vmatrix} drd\theta = r\, drd\theta$$

and thus:

$$Z_n = \left(\frac{2}{\pi}\right)^2 \int_0^{\infty}\int_0^{\frac{\pi}{2}} \frac{\sin^2(r\cos\theta)\sin^2(r\sin\theta)\, d\theta dr}{r^3\cos^2(\theta)\sin^2(\theta)\left(\sqrt{r^2+\tilde{\xi}_S}+\sqrt{\tilde{\kappa}^2r^2+\tilde{\kappa}\tilde{c}\tilde{\xi}_S}\right)},$$

$$\Updownarrow$$

$$Z_n = \left(\frac{2}{\pi}\right) \int_0^{\infty} \frac{g(r)dr}{r^2\left(\sqrt{r^2+\tilde{\xi}_S}+\sqrt{\tilde{\kappa}^2r^2+\tilde{\kappa}\tilde{c}\tilde{\xi}_S}\right)}, \text{ where:} \tag{12.11}$$

$$g(r) \equiv \left(\frac{2}{\pi r}\right) \int_0^{\frac{\pi}{2}} \left(\frac{\sin(r\cos\theta)\sin(r\sin\theta)}{\cos(\theta)\sin(\theta)}\right)^2 d\theta \tag{12.12}$$

$g(r)$ can be solved numerical for a large array of r's once and for all. There after the evaluation of the double integral is reduced to solving a single integral (equation 12.11). This can be done numerical (on a computer) much faster than evaluating the double integral.

For the substrate alone equation 12.11 can be used with $\tilde{\kappa}_L = 0$. From such data $\tilde{\kappa}_S$ and $\tilde{c}_S$ can be found (details are given in chapter 16) and measurements with liquid can be analyzed in term of $\tilde{V}_{3c,rel}$ (c.f equation 12.7) using equation 12.11 to calculate $\tilde{Z}_{LS}$ and $\tilde{Z}_S$.

12.3 Numerical tools

Equations 12.2/12.4, 12.3/12.5, and 12.11 offers ways to interpret the data even when edge effects must be taken into account. But still these equations do not deal with the thermo–mechanical problem and they do not take the exact geometry of the setup into account, e.g. the glass cylinder containing the liquid and the electrodes are not dealt with.

It will probably not be possible to take all these things into account analytically. But, numerical tools exists, that can be used to do this. The program Femlab is such a tool and it can easily communicate with Matlab. I have not myself used this program, but Eva Uhre (a master student at the institute) and Tage Christensen have used this program (e.g. Tage has used the program to check equations 12.2 and 12.3). It seems that eventually it will be an advantage to use a program like this. It will then be possible to model the exact geometry of the setup, and also to take the thermo–mechanical problem into account, that is, use the full thermo–visco–elastic equations for the system. This is, though, beyond the scope of this work.

Part III

Fabrication of the heater

13 Electron beam evaporation chamber

The thin films that were used in the experiments described in this report were made in a electron beam evaporation chamber. The deal table and electron beam source are "Edwards six position electron beam source, $E09037000$, $E09086000$" driven by an "Edwards ebs power supply". In this chapter, the principles and design of the chamber will be described. In chapter 14, the exact procedure used to fabricate the films will be described.

The basic principle of the chamber is very simple. In the chamber there is a vacuum ($\approx 10^{-5} mbar$). A large potential difference ($\approx 4kV$) between a glowing filament and the metal to be evaporated drives electrons from the filament into the metal[1]. The metal is thereby heated and evaporates through a mask (with the desired film pattern) onto the substrate.

13.1 Inside the chamber

The basics of the chamber are shown on figure 13.1, the details of the filament surroundings on figure 13.2, and the details of the substrate and mask holder on figure 13.3.

The mask holder is the bottom copper part in figure 13.3. It is placed on the large round copper plate (with diameter $270mm$) in the chamber (see figure 13.1) and aligned by three small, cone–shaped feet that fit into holds in the large copper plate. This way the hole in the large copper plate is exactly below the hole in the mask holder. The $0.25mm$ thick brass masks fit exactly into the mask holder. The mask to the left (figure 13.3) is used first when the film material is deposited on the substrate, and the mask to the right is used for making the electrodes. The masks are made thin in order to avoid any shadow effects. On top of the mask is

[1] Of course, the filament is at electrical "-" compared to the metal, since electrons move from "-" to "+", though by definition a electrical current runs from "+" to "-".

placed the $40mm \times 40mm$ copper block. This block keeps the mask in place, and aligns the glass substrate that fit into the hole in the middle of the block. Behind the substrate is placed another copper block. This serves two purposes. Firstly, it leads some of the heat away from the substrate. Secondly, if it is not there, the substrate can be lifted or simply "blown" away by the beam of material hitting it.

The chamber must be opened in order to change the mask. Of course, it is possible to design a mask and substrate holder in such a way that the mask can be changed without opening the chamber (e.g. the mask could be moved by a electric motor, controlled from outside of the chamber).

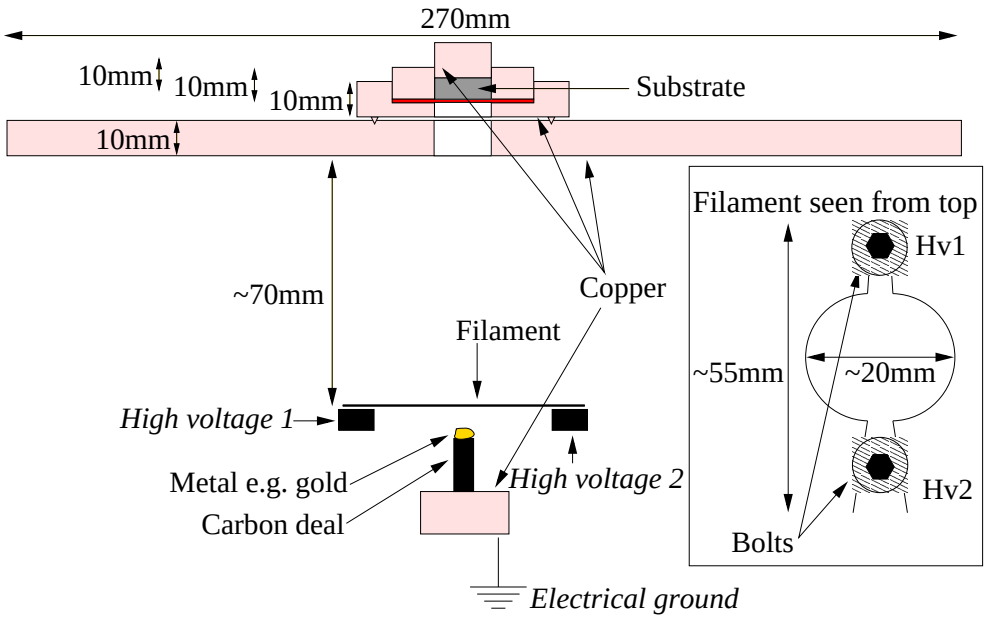

Figure 13.1 The principles of the electron beam evaporation chamber is simple. There is a voltage difference between the two ends of the filament labeled "*High voltage 1* (Hv1)" and "*High voltage 2* (Hv2)". This voltage difference drives a current through the filament, and makes the filament glow. But, still there is a much larger potential difference between the filament as a hole and the deal at electrical ground. Thus, electrons are driven from the filament into the metal on top of the deal. The metal is thereby heated, and evaporates through the hole in the large copper plate, through the pattern in the mask, just below the substrate, and onto the substrate. As can be seen in the insert to the right, the filament has a shape so that it does not block the evaporated metal on its way to the substrate. The filament surroundings is shown in more detail on figure 13.2.

The type of deal shown on figure 13.1 is used when metal is evaporated. The deal is shown in more detail on figure 13.4 (A and B). The deal is made of carbon and

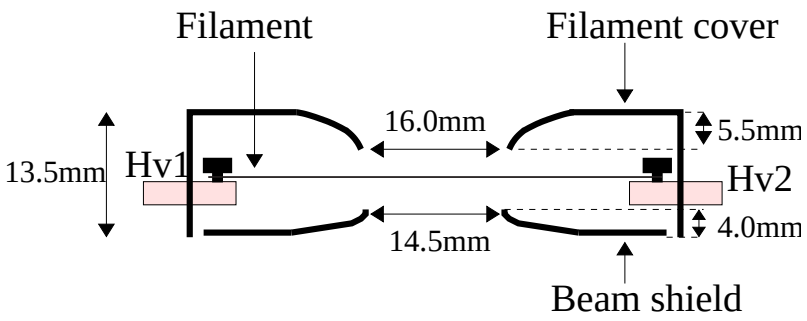

Figure 13.2 This figure shows how the filament cover and beam shield are placed above and below the filament (seen from the side). The outer diameter of the round filament cover is 53.0*mm*, and of the beam shield 50.0*mm*. The thickness of the filament cover material (some alloy) is 1*mm*, thus, the beam shield fixes the filament cover in position, and thereby ensures that it does not short–circuit the filament. The filament cover and beam shield are on the Hv1 potential. The filament is shown in more detail on figure 13.1.

is concave in the top where the metal source (i.e. the metal to be evaporated) is placed.

When the carbon films are made another type of deal is used. I have tried with several types of deals and shapes of the carbon source (that are to be deposited on the substrate). The two most successful types are shown on figure13.4 (C and D). The carbon is not really evaporated. It is more a process where the carbon is torn in small pieces. The electron beam “digs” a hole in the carbon source, and “ejects” the material away from the hole.

To begin with, I used a carbon source like the one shown on figure 13.4 (C) but flat at the top (instead of the cone). But it was difficult to predict where the electron beam would start “digging”. Sometimes the beam hit the carbon source on the side, and most of the carbon was “ejected” out horizontally. Therefore, the cone shaped tip was made, and as a result the beam almost always hits in the center of the tip (probably because the cone shaped tip focuses the electric field: the equipotential surfaces are closer to each other near the tip). The problem with this shape of the carbon source is that as the hole becomes deeper and deeper less and less material is ejected out of the hole per unit time. And so it may be necessary to use two or more of these carbon sources, in order to get the desired thickness of the carbon film. This problem is more or less solved with the type of source shown on figure13.4 (D). This source is so thin $(3.3mm)$ that in most cases the source simply becomes shorter as the beam ejects material from it. Thus, all that is needed is to move it closer to the filament during the process (this is easily done from outside the chamber). In some cases, the electron beam may leave one side of this carbon

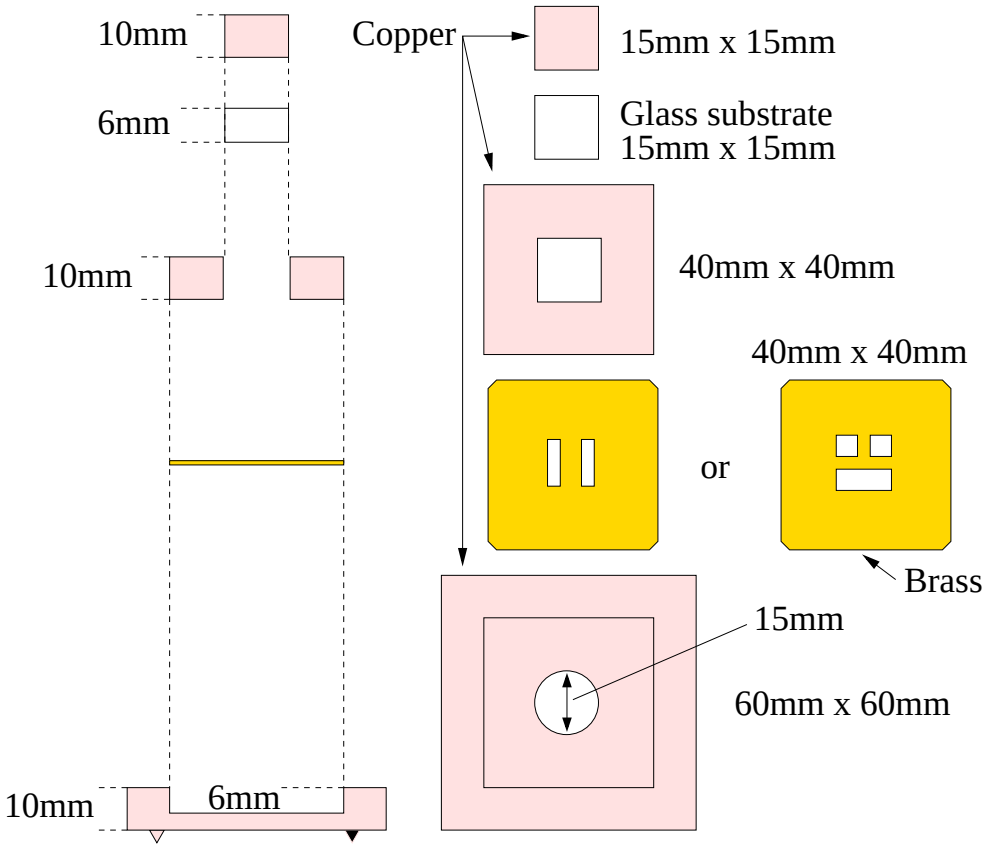

Figure 13.3 On the left side of this figure is shows a cross section of the different parts of the substrate and mask holder, as seen from the side. On the right each part is shown as seen from the top. The substrate and mask holder is designed so that everything fit tight together. This way the masks are always placed in the same position with respect to the substrate, which of course is important when the masks are changed.

source standing as a thin “wall” only “digging” away half of the source. In such a case, the carbon beam may be asymmetric, and in some instances almost non of the carbon hits the substrate, and in others the film is clearly made with a non uniform thickness. Probably a source with a smaller diameter (maybe 2.5*mm*) would solve this minor problem.

13.2 Outside the chamber

In this chamber, there is room for 6 deals on a table, that can be rotated from outside the chamber (see figure 13.5). Thus, changing material to be deposited on

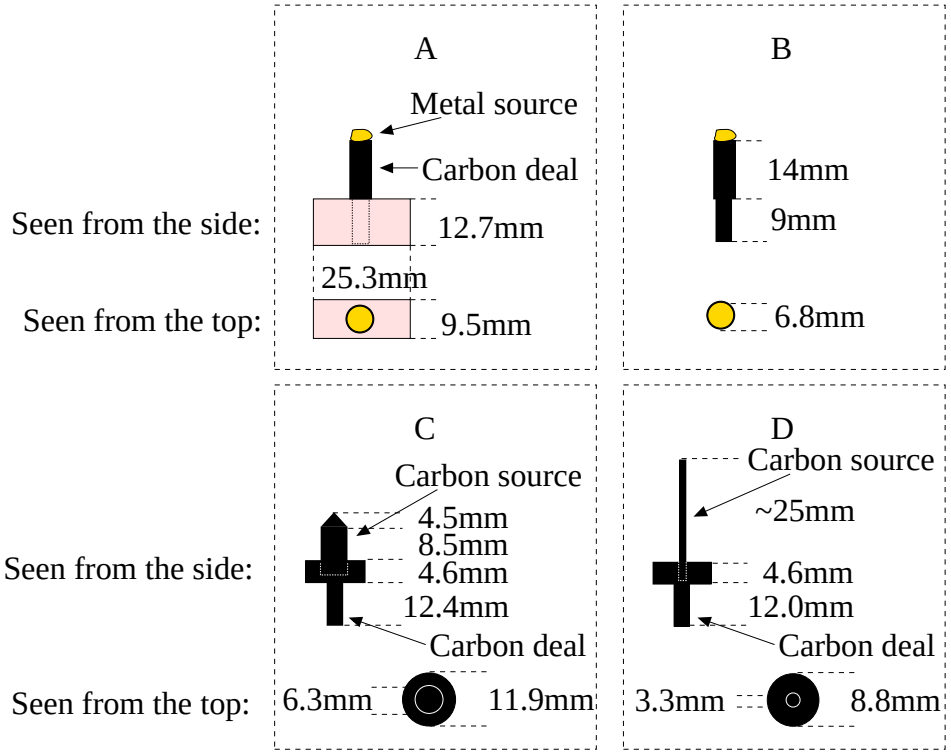

Figure 13.4 The different types of deals.

the substrate can be done without opening the chamber. The deal table can also be raised and lowered from outside the chamber, and thus, the distance between the deal and filament can be controlled.

Besides this only two other variables are controlled outside the chamber: the voltage across the filament, and the high–voltage between the filament and deal. The high–voltage is monitored by an analog voltmeter, and can be set by turning a nob to maximum $6kV$, but when the filament voltage is turned up and the filament starts to glow, the maximum high–voltage is about $5kV$. The filament voltage is controlled by turning another nob, but is not monitored. Instead the current of the electron beam is monitored by an analog ammeter.

The pressure is kept low in the chamber by a combination of a rotary pump and a diffusion pump. An Edwards Pirani and an Edwards Penning meter monitor the pressure at the rotary pump and in the chamber, respectively. The pressures given in this report are the ones read from these meters. The rotary pump takes the pressure down to just below $10^{-1}mbar$, and then, by turning a set of valves, the diffusion pump and rotary pump can be set in series (the diffusion pump closest

to the chamber), and the pressure can be pumped down to somewhere between $10^{-5}mbar$ and $10^{-6}mbar$. A cold finger, in the top of the chamber (see figure 13.5), can be filled with liquid N_2, and the pressure can usually come down to $10^{-6}mbar$ or a bit lower. During the fabrication of the films, the pressure may be significantly higher (usually between $10^{-3}mbar$ and $10^{-5}mbar$).

Everything in the chamber must be kept clean, and nothing should be touched by hand (gloves or clean tweezers must be used). If I need to use new copper parts or similar, I always first clean them carefully (e.g. with 2–propanol), and "bake" them in a vacuum oven at $\approx 350°C$, and $\approx 10^{-1}mbar$, for 24 hours or so, before putting them into the chamber. Else it will take too long before the pressure can be as low as desired. For example if just one small, not well cleaned, copper part is placed in the chamber, it may take several weeks before the pressure can be pumped down below $10^{-5}mbar$, and one touch by hand can lengthen this pump time with several days.

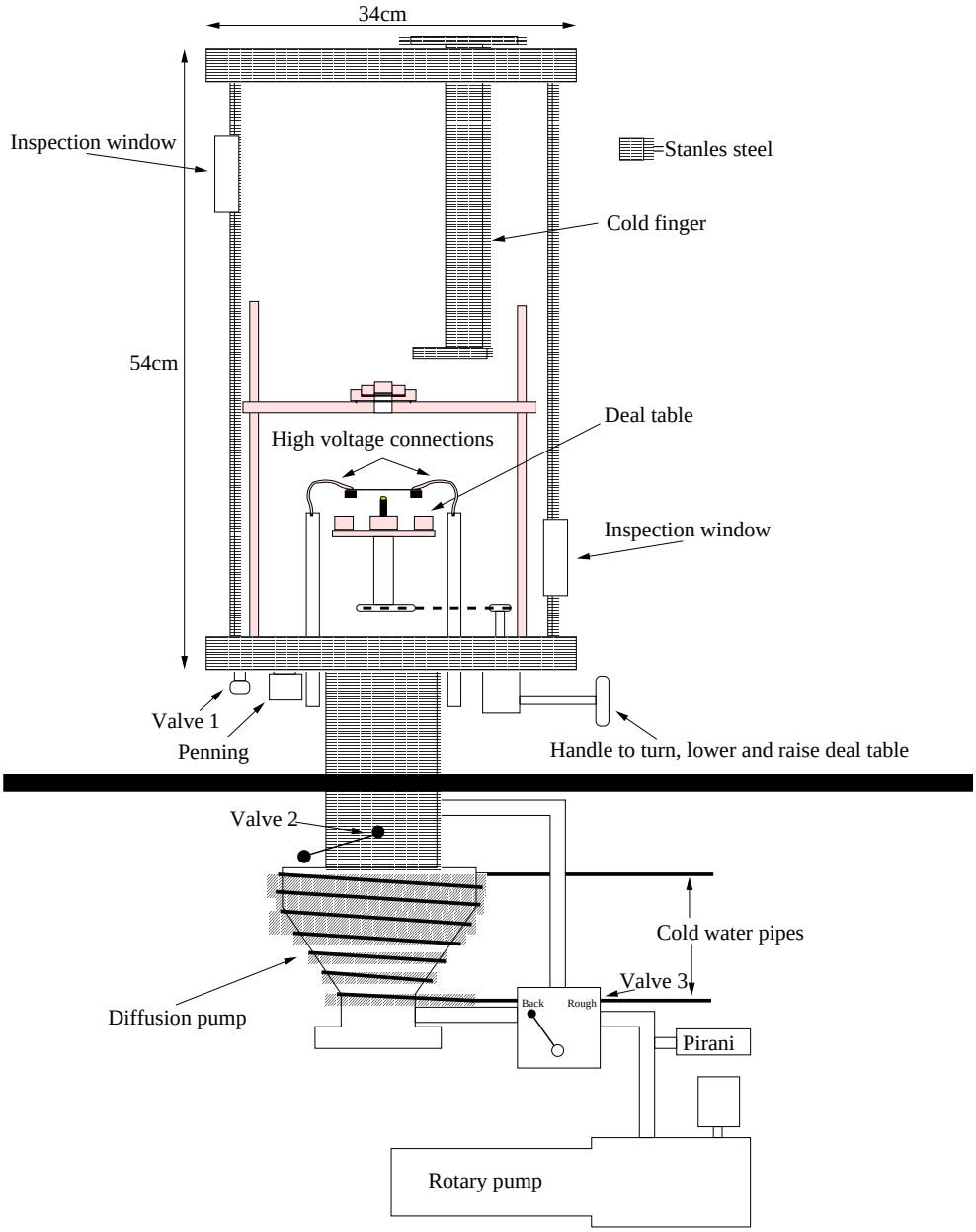

Figure 13.5 The electron beam evaporation chamber and pump system. Valve 1, in the bottom left side of the chamber (next to the penning), is used to let air into the chamber, when the chamber needs to be opened. Valve 2 open and closes the connection between the chamber and the diffusion pump. When valve 3 is in “back” position, the rotary pump pumps in the end of the diffusion pump, and when it is in “rough” position, it pumps directly on the chamber.

14 Fabrication of the thin films

This chapter describes the fabrication of the carbon thin films and gold electrodes. It is therefore primarily of interest to those who wish to fabricate the same types of films. The carbon films are deposited first and the gold electrodes afterwards.

14.1 Preparations

The distance between the carbon source and the substrate is important. During the depositing process, pieces of carbon of different sizes will be torn off the carbon source. But the larger pieces will not be able to travel so far upwards as the smaller ones. This can easily be seen by the naked eye looking at the process through the lower inspection window (see figure 13.5). If the distance between the carbon source and the substrate is made smaller, the larger pieces of carbon will hit the substrate and the film may become "rugged" or holed. If the distance becomes too large, non or only a small part of the carbon will hit the substrate. The distance I found to be optimal was $\approx 80mm$ between the filament and the substrate (see figure 13.1). The vertical distance between the filament and source is adjusted during the process (see below) but is probably less than $10mm$. These distances are also well suited for fabricating the gold electrodes.

Before fabricating the carbon films, the substrate must be cleaned. More or less advanced methods for this exists, but I have found the following simple method to be sufficient in most cases. In a few cases, though, where the carbon films are very thick (resistance below $150\Omega/\text{square}$), they have "curled off" when the heater has been cooled. This is probably due to a difference in expansion coefficient of the films and of the glass. Whether or not this problem can be solved by cleaning the substrate more efficiently, I do not know.

The cleaning procedure that I have used is to wash the substrate with detergent and rinse with plenty of distilled water. (Tap water can leave minerals on the substrate, and the tap water in Denmark in particular contains a lot of lime.) The substrate is then dried with clean compressed air. This is usually enough, but if the substrate does not look clean it is wiped with 2–propanol or similar and washed again.

The mask, substrate, deal and source are fitted in the right positions and the chamber is closed and evacuated. The evacuation of the chamber takes several hours (switching from the rotary pump alone to the diffusion pump in series with the rotary pump after $\approx 10min$). When the pressure is below $5 \times 10^{-6} mbar$ liquid N_2 is filled in the cold finger.

Before starting the actual film–making process, it is a good idea to turn on the filament for $\approx 1min$. This usually makes the pressure rise quite a lot (to around $10^{-4} mbar$). After this, it is necessary to wait a few minutes with the filament turned off until the pressure is low again. After this procedure, the filament can usually be turned on without such a large pressure increase; the filament (and its near surroundings) has been cleaned. If necessary, the cold finger is refilled and the actual film–making process can be started.

14.2 Fabrication procedure for the carbon films

Fabricating the carbon films is not always simple. For example, in some cases it is difficult to control the beam current: it is either high (e.g. $300mA$) or zero. Below I present the optimum and then describe what problems may arise and how they can usually be solved.

With the deal table in the lowest position, the high–voltage source is enabled and the voltage set to $4kV$. The filament is turned on and the voltage across the filament is slowly set to the maximum value. The high–voltage thereby drops to $\approx 3.5kV$. At this stage, there should be no beam current. The carbon source is then slowly raised (by raising the deal table) until the beam current is $45-50mA$. This beam current is maintained for some time (t_b) by continuously raising the source. If it is not raised, the beam current will drop as the beam shortens the carbon source. After about $8.5min$, some of the outside of the chamber starts to be so warm that it can hardly be touched by hand, and some of the inner parts must be much warmer. Therefore I never have the chamber running longer than that. If $t_b = 8.5min$ is not enough to reach the desired thickness or resistance of the film, I wait for about 1 hour and start again. If the goal is a film of around $100\Omega/\text{square}$, $t_b \approx 3 \times 8.5min$. This is summarized in figure 14.1.

As mentioned, it may not always be possible to keep the beam current at $45-50mA$. Sometimes it is either very high ($\approx 300mA$) or zero. For example, I have experienced that the beam current was zero, and when I raised the carbon source then suddenly it became $\approx 300mA$ for maybe $3s$, and then zero until I raised the source again (and so fourth). I think that when this happens, it is most likely because the geometry of the setup has changed. Usually the problem is that after

HV_{off}	$4kV$
V_f	Max.
HV_{on}	$\approx 3.5kV$
Beam current	$45-50mA$
t_b	$3\times 8.5min$

Figure 14.1 Possible values used when fabricating a carbon thin film of $\approx 100\Omega$/square. HV_{off} and HV_{on} is the value of the high–voltage with the filament turned off and on, respectively (HV_{on} is not adjusted, but just the value that HV_{off} drops to when the filament is turned on). V_f is the voltage across the filament, and t_b is the time the process is running.

the chamber has been used several times, material (e.g. carbon and gold) has been deposited on the beam shield and filament cover (see figure 13.2), and the hole is then smaller than is should be. If this is the case, it must be dismantled and cleaned.

In other cases I have had problems with getting any beam current at all (or it was only possible to get $30mA$ or lower). No matter how high the voltage, and how close the filament and carbon source was nothing happened. This probably have the same explanation as given above. But I have also noticed that sometimes an old filament works better than a new one. Therefore, I have tried to make the filament "old" fast. This can be done, but it is not always successful, and in some cases the filament is broken (thus, it is worth first to try and clean the filament cover and beam shield). What I have done is to let air into the chamber, and then use the rotary pump to lower the pressure to around $5\times 10^{-1}mbar$, just low enough so that the pressure controlled switch allows the filament to be turned on (for security reasons there is an automatic pressure controlled switch in the chamber, that ensures that the power cannot be turned on unless the pressure is $\approx 5\times 10^{-1}mbar$ or lower). Then I have turned on the filament at maximum for $\approx 10s$. After this procedure it is easy to see that material form the filament have been cast away and onto the filament cover and beam shield (and they may need cleaning).

Also, as mentioned in chapter 13, the chamber must be kept clean. If for some reason this is not the case, and the pressure is $10^{-5}mbar$ or higher before starting the process, the beam current may be totally uncontrollable.

Finally sometimes material short–circuits somewhere in the chamber. This can happen if, for example, a flake of material that has been deposited on the large copper plate in the chamber (with diameter $270mm$ see figure 13.1) falls off. If there is a short–circuit, it can bee seen from the fact that the ammeter shows a current as the high–voltage is turned on, even though the filament is not turned on. Usually the material just burns away, as the high–voltage is raised to a high enough value.

14.3 Fabrication procedure for gold electrodes

Fabricating the gold electrodes is more simple than fabricating the carbon heater. But of course, the need for cleaning the filament cover and beam shield, once in a while, apply here as well.

The procedure is a little different than when fabricating the carbon thin films. First, the deal is raised to a certain level, then the high–voltage is set, and the filament voltage is turned on and up until a certain beam current is obtained. This beam current is kept at the specified value during the evaporation process by continuously adjusting the voltage across the filament. The procedure that I have used as a standard for the electrodes is summarized in figure 14.2.

Deal level	$3\frac{3}{4}$ t.f.b.
HV_{off}	$5kV$
V_f	Adjusted
HV_{on}	$\approx 4.5kV$
Beam current	$45-50mA$
t_b	$5.5min$

Figure 14.2 The standard values used when fabricating the gold electrodes. Deal level is measured in “turns from bottom” (“t.f.b.”, see text). HV_{off} and HV_{on} is the value of the high–voltage with the filament turned off and on, respectively (HV_{on} is not adjusted, but just the value that HV_{off} drops to when the filament is turned on). V_f is the voltage across the filament and are adjusted to give the right beam current. t_b is the time the process is running. The electrodes have a resistance of less than 0.05Ω/square.

The deal level given in figure 14.2 is measured in “turns from bottom” (“t.f.b.”). This is to be understood as how many turns the nob that raises the deal table are turned from the lowest position. 1 turn raises the deal $\approx 3.2mm$. $3\frac{3}{4}$ t.f.b. corresponds to a vertical distance between the top of the deal and the filament of $\approx 4.0mm$.

The gold that I have used is $2.0mm$ thick wire with a purity of 99.5% (24 carat). To my experience, it is best to have the deal well filled with gold from the start of the evaporation. I bend the gold wire a few times, so that it fits on top of the deal (and maybe add the small chunk of gold, that is leftover from earlier evaporation). Before starting the actual evaporation, I melt the gold into one chunk. This is done by starting with the deal in the lowest position. Turning on the high–voltage to $5kV$. Slowly turning on the filament to maximum. Slowly raising the deal until the gold is melted (which is controlled by looking through the lower inspection window (see figure 13.5)).

14.4 Other metal films and techniques

Metal	Melting point $[K]$
Al	993
Cr	2160
In	430
Ni	1726
Pt	2042
Ag	1234
Au	1336

Figure 14.3 Melting point of selected metals at $1bar$ [Nordling and Österman, 1996, p. 28-29].

As mentioned in chapter 11, I have also made thin films of aluminum (Al), chromium (Cr), indium (In), nickel (Ni), platinum (Pt), and silver (Ag). The procedure for producing these films is the same as that of producing the gold electrodes described above, though the settings are different for different metals. For example gold and silver evaporate easier than chromium, since their melting points are significantly lower. The melting points of these metals are given in figure 14.3.

In figure 14.4 some possible settings are given for the different types of metals. Also, the resulting resistance of the thin films is given in the cases where I have measured this. The settings are not optimized in the same way as for the carbon and gold thin films, but can be taken as rough guidelines. For all the metals, except chromium, all the metal in the deal melts during the process. The chromium seems only to melt very locally, exactly where the electron beam hits.

14.5 Sputtering

Other techniques than using a electron beam evaporation chamber can be used to fabricate thin films, e.g. sputtering. The technique will not be described here, since it plays no role for the rest of this report. I just want to mention that I have tried fabricating thin films with a "Bal–Tec SDC 005 Cool Sputter Coater". The metal films can be sputtered, but I have not been able to fabricate carbon films of any significant thickness (I could not even make them thick enough to be electrically conducting). For the metal films this technique may have some advantages: it does not heat the substrate as much, and it is therefore possible to use substrates that cannot withstand high temperatures. Also it is possible to control the stress in the films by adjusting the pressure and the substrate to source (target) distance [Hudson and Somekh, 1992].

Metal	**Aluminum (Al)**
Deal level	$3\frac{3}{4}$ t.f.b.
HV_{off}	$6kV$
Beam current	$30mA$
t_b	$10s$
Resistance	$2\Omega/\text{square}$

Metal	**Chromium (Cr)**
Deal level	$3\frac{3}{4}$ t.f.b.
HV_{off}	$3kV$
Beam current	$20mA$
t_b	$17s$
Resistance	$8\Omega/\text{square}$

Metal	**Indium (In)**
Deal level	5 t.f.b.
HV_{off}	$3kV$
Beam current	$30mA$
t_b	$40s$
Comment	Pour attachment

Metal	**Platinum (Pt)**
Deal level	5 t.f.b.
HV_{off}	$6kV$
Beam current	$60-70mA$
t_b	$120s$
Resistance	$14\Omega/\text{square}$

Metal	**Silver (Ag)**
Deal level	4 t.f.b.
HV_{off}	$6kV$
Beam current	$70mA$
t_b	$17s$

Metal	**Chromium (Cr)**
Deal level	$3\frac{3}{4}$ t.f.b.
HV_{off}	$3kV$
Beam current	$20mA$
t_b	$7s$
Resistance	$20\Omega/\text{square}$

Metal	**Chromium (Cr)**
Deal level	$3\frac{3}{4}$ t.f.b.
HV_{off}	$3kV$
Beam current	$20mA$
t_b	$30s$
Resistance	$4\Omega/\text{square}$

Metal	**Nickel (Ni)**
Deal level	$4\frac{3}{4}$ t.f.b.
HV_{off}	$6kV$
Beam current	$25-30mA$
t_b	$12s$
Resistance	$14\Omega/\text{square}$

Metal	**Platinum (Pt)**
Deal level	$4\frac{3}{4}$ t.f.b.
HV_{off}	$6kV$
Beam current	$50-60mA$
t_b	$40s$
Resistance	$150\Omega/\text{square}$

Figure 14.4 Possible settings for the different types of metals. The resistance is at room temperature. In all cases is the filament voltage (V_f) adjusted to give the desired beam current.

Part IV

Measurements

15 Hardware

In this chapter a brief description of the hardware used in the experimental setup will be given.

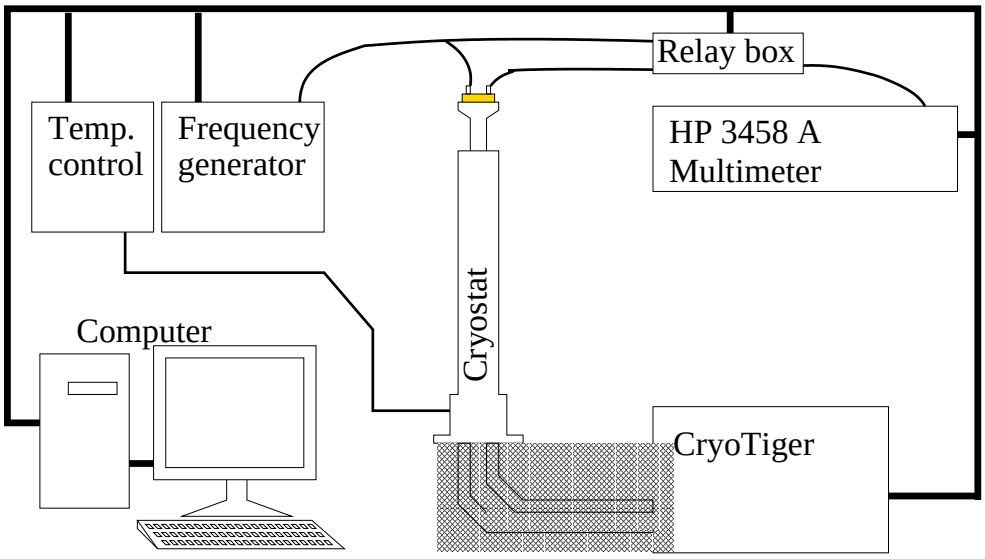

Figure 15.1 The technical setup consists of a home–build cryostate, cooled by a CryoTiger, a home–build temperature control, controlling the CryoTiger and the heating stage inside the cryostate, a home–build frequency generator, a home–build relay box, a HP 3458 A multimeter, and a computer controlling the measurements. The two connections between the cryostate and the CryoTiger box are the two gas tubes.

On figure 15.1 the technical setup is shown, and on figure 15.2 the electrical connections.

A CryoTiger from APD Cryogenetics INC cools the cryostate. The CryoTiger works basically like a refrigerator, thus, the cooling effect comes from the expansion of a gas[1]. The CryoTiger, and a heating stage inside the cryostate, are

[1]Information on the CryoTiger, could when this report was written, be found on http://www.apdcryogenics.com/.

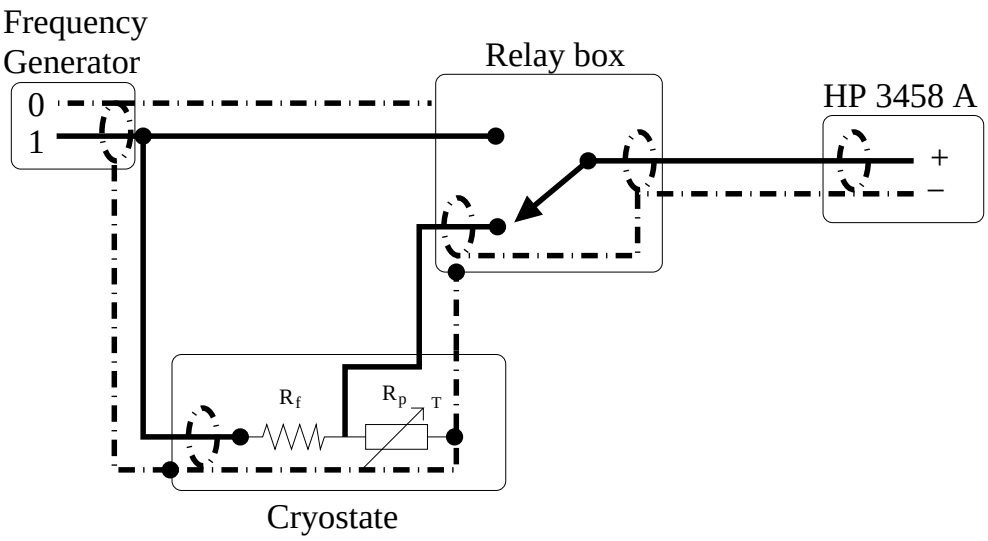

Figure 15.2 The electrical connections of the setup. The dotted lines are the outer concentric shield of the coaxial cables, and the solid lines are the inner core. The cryostate and relay box are shielded by connecting to the shield of the coaxial cables, as indicated by the "dots". In order to avoid having a loop, the shield of the coaxial cable from the generator to the relay box is not connected to the relay box.

controlled by the temperature control.

The frequency generator can generate frequencies in the interval $[1mHz; 1kHz]$ (16 discrete values per decade). The output voltage can be varied from $0-10V$ (256 discrete values), and the maximum power is $1W$. The frequency generator sends triggers to the HP 3458 A multimeter (now called Agilent Technologies 3458A multimeter), and had originally three modes: 512, 256 and 128, referring to the number of triggers send per period. Less than 2 weeks before turning in this report a new modified frequency generator was finished by the electronic workshop with modes 16, 32, 64, 128, 256 and 512. Unless explicitly noted mode 128 are used in the experiments reported here. The reason for this new development is twofold.

Firstly: the number of digits available in the multimeter depend on the sampling rate. At high rates digits are lost. Thus lowering the number of triggers per period increase the number of digits at high frequencies.

Secondly: the multimeter samples $50k$ (50000) times per second, and thus, the maximum frequency that can be used is $50ks^{-1}/\text{mode} \approx 98Hz$, $195Hz$, $391Hz$, $781Hz$, $1.6kHz$, $3.1kHz$ for the 512, 256, 128, 64, 32 and 16 mode respectively. This is the high frequency limits of the current setup, but it can be extended by letting the multimeter use sub–sampling. In sub–sampling the multimeter uses

more than one period for each measurement, and samples different part of the signal each period. With $50k$ samples per second, the time between the triggers is $20\mu s$, with sub–sampling this time can effectively be made 1000 times shorter [Aglient, 2000, p. 139-141][2].

The relay box is just a simple switch that sets the multimeter to measure V across the heater (inside the cryostate) or the input voltage U directly from the frequency generator. The setup is designed such that U is measured under the same conditions as V, that is the load on frequency generator is the same.

The computer sets the temperature control, frequency generator, and relay box. The computer also communicates with the multimeter, and controls when a measurement is made, and receives the measured data.

The temperature control, frequency generator, relay box, and cryostate (except of course the CryoTiger) are home made by the people at the institute workshop (IMFUFA, Roskilde University).

The software used on the computer is the rather old and somewhat outdated "Asyst". It works very well, but it takes a while to learn how to use it. Also, the computer is blocked while the measuring program runs, and the settings of the program cannot be changed after the program has been started. It would be convenient if it was possible to change settings, such as at what temperatures there shall be measured, after starting the measuring program. A switch to a modern program (probably Matlab) is on its way.

15.1 Making a frequency scan

The computer program that controls the measurements is made such that before measuring at the first frequency, in a frequency scan, it waits at least 4 periods (at the first frequency) before starting the scan. During a frequency scan it waits at least 3 periods after changing the frequency before measuring.

The different harmonics are found by Fast Fourier Transform of the measured input or output–voltage ($\mathrm{FFT}[U]$ or $\mathrm{FFT}[V]$). In mode 512 each frequency measurement is in principle a measurement of only one period. But above $1Hz$ ten such measurements are made (waiting at least 1 period between each), and the average is taken as the measured value. The setup and measuring program was originally designed to work in mode 512. As mentioned I have used mode 128 for the measurements presented here. Of course the programs could just have been

[2] When this report was written, a manual could be downloaded via Agilent Technologies homepage: http://we.home.agilent.com.

changed, such that the multimeter still just would measured one period, which would mean that a measurement would consist of 128 samples. Instead the multimeter still samples 512 times for each measurement, which means that 4 periods are measured instead of 1. Thus, below $1Hz$, each measurements is a measurement of 4 periods, and above, each measurement is a average of 10 such measurements (every one of the 10 being a measurement of 4 periods). V_n is thus no longer found as $\mathrm{FT}[V,n]$ but as $\mathrm{FT}[V,n\times 4]$ (and similar for U).

The Fast Fourier Transform (FFT) of the data is made in Asyst, but after this the data is exported to another computer, where the rest of the data treatment is made in Matlab.

15.2 Pros and cons

It is an advantage that the temperature control and the frequency generator run independently of the computer, e.g. the temperature is not changed unless the temperature control receives a message from the computer to do so. This means that all the settings (i.e. temperature, frequency and input–voltage) are maintained also if the computer is restarted or used for something else.

The CryoTiger cooled cryostat has obvious advantages over a nitrogen–cooled cryostate. It can in principle run forever, and no disturbances (mechanical/acoustic or thermal) are made while filling nitrogen. Occasionally, there have been problems with the CryoTiger. Probably this has been due to the formation of small ice crystals in the cold end (where the expansion of the gas takes place). Adding a filter that dries the gas (a Parker Liquid line Filter Dryer model 756S) has minimized these problems. The cold end has no mechanical parts and low vibration.

One disadvantages of the present setup is the program used in the computer (Asyst) but as mentioned a switch to another program is on its way.

The high frequency limit of the setup is $1kHz$. In order to go to higher frequencies than $1kHz$ a new frequency generator must be build. For the multimeter to go higher than $3.1kHz$ it must use sub–sampling. (If sub–sampling is also used at lower frequencies it is possible to samples more than 16 times per period. It is worth to test whether this is a advantage or not). It is desirable to be able to measure up to, at least, $10kHz$.

One other possibility would be to use a digital lock-in amplifier (such as the Stanford Research Systems SR830 DSP or SR850 DSP)[3] and a Wheatstone bridge, as

[3] Information on these could, when this report was written, be found at:
http://www.thinksrs.com/html/sr830.html and
http://www.thinksrs.com/html/sr850.html.

it is done in most of the experiments reported in the literature (e.g. [Menon, 1996, p. 5248]). Actually the Korean group uses a digital voltmeter for measurements below $1Hz$ and a lock-in above, e.g. [Moon et al., 1996, p. 479], [Jung et al., 1992, p. 479]. The Wheatstone bridge cancels or minimizes V_1. This will complicate the measurements a little, since the bridge needs to be balanced. In principle, though, the lock-in should be able to give good quality data, but unfortunately I have not had the opportunity to check this.

It is also possible cancel or minimize V_1 in the current setup using the (HP 3458 A) multimeter and a push–pull voltage supply. If this is done the multimeter can be set in the $1V$ range in stead of the $10V$ range, and this will give one more digit resolution in measuring the 3ω voltage component due to the heater. In order to let the multimeter measure a voltage difference relative to ground (and not a "floating" voltage difference as in a Wheatstone bridge) the frequency generator must have two channels giving signals with a relative phase shift of 180° (a push–pull voltage supply). The outputs must be connected to the two resistors (R_f and R_p) as described in figure 15.3 below.

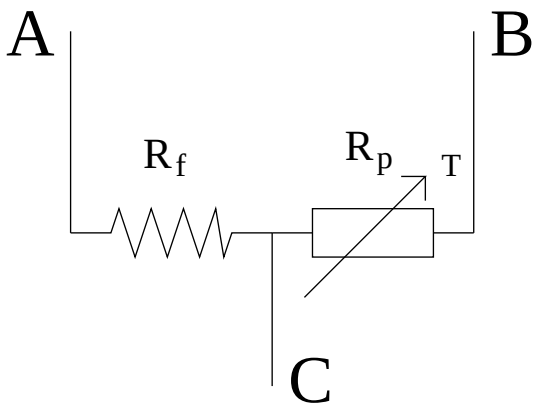

Figure 15.3 The two output channels (with a relative phase shift of 180°) from the frequency generator must be connected to *A* and *B*. The multimeter measures the voltage between *C* and ground. If $R_f = R_p$ and the two outputs are perfectly asymmetric the measured signal will be zero execpt from the higher harmonics that are produced (e.g. a 3ω signal from R_p).

If the setup is perfectly balanced (i.e. $R_f = R_p$ and the two input signals are perfectly asymmetric) the 1ω and 3ω component (and other harmonics) from the frequency generator will be eliminated (in the signal between *C* and ground, cf. figure 15.3), and only the harmonics due to the heater will be measured.

If the setup is not perfectly balanced these components will not be totally eliminated. This is not a problem as long as the voltage between *C* and ground is still

below $1V$, and the residual of the 3ω component from the frequency generator is negligible compared to the 3ω component due to the heater. If the former is not the case the multimeter can not work in the $1V$ range, and if the later is not the case the 3ω component from the frequency generator must be measured and in doing this the multimeter cannot work in the $1V$ range.

15.3 Temperature stability

The best way to check the temperature stability of the setup is to use the planar heater as the temperature censor. It has a high accuracy, and it measures the temperature exactly where it is most interesting and where it must be very stable. Besides the temperature stability, the time it takes the temperature to become stable after a change of the cryostate set temperature (T_S) and after a change of the input–voltage (U), must be known in order to find the needed waiting times: t_T; the time one must wait (before measuring) after changing T_S, and t_U; the time one must wait after changing U. Here, only the heater will be considered, but of course when measurements are made with liquid, these waiting times may become significantly longer depending on the relaxation time of the liquid.

Measuring once every minute (total$= 4095min \approx 68hours$) the following experiment has been performed:

$U_1[V]$	$T_S[K]$	Time [hours]
3.873	215	3
3.873	210	3
7.744	210	62.25

T_S is the set temperature of the cryostate. The experiment was started approximately 1.5 hour after changing T_S from $290K$ to $215K$.

The result of the experiment is shown on figure 15.4. To investigate these data more careful, two areas of the plot is shown enlarged on figure 15.5 (page 113). From the top plot in figure 15.5 it is seen that there is a long time drift of T_{pm} (T_k does of course not show this drift, since T_k is used in the temperature control). This drift is probably due to heat conduction through wires and the thin stainless steel cylinder, from the measuring cell to the top of the cryostate (see figure 9.1 page 55). There is a tendency that the same pattern is repeated every 24 hours, corresponding to the change of day and night temperature of the lab (the lab temperature is not controlled accurately). A frequency scan from $1mHz$ to $1kHz$ takes

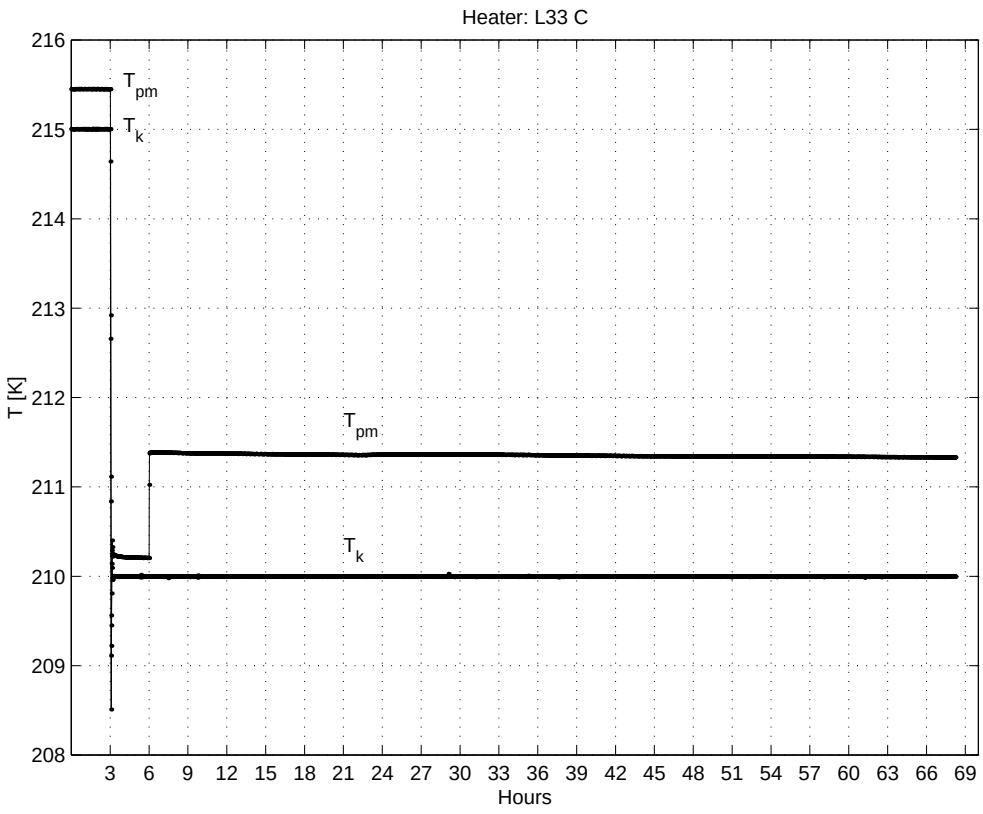

Figure 15.4 The top curve shows the temperature of the heater (T_{pm}), and the bottom curve the temperature of the cryostate T_k. The shift after 3 hours, is due to the change of T_S from $215K$ to $210K$. The shift in T_{pm} after 6 hours, is due to the change of U_1 from $3.873V$ to $7.744V$

about 11 hours, and a frequency scan from $10mHz$ to $1kHz$ takes about 2 hours (in mode 128, cf. page 106).

Also, from the top plot in figure 15.5, it is seen that a temperature stability of approximately $0.02K$ and $0.01K$ can be expected for the long and short scan, respectively. From the same plot, it is seen that the temperature of the heater is stable after only a few minutes, after changing U. Thus when measurements are made without liquid, t_U is only a few minutes. From the bottom plot in figure 15.5, it is seen that if the stability of the temperature must be $0.01K$ over a few hours, t_T is a little less than $1hour$.

The conclusion from these curves is that the temperature stability is $\approx 0.02K$ (over 11 hours), and that $t_{U,min} = 10min$, and $t_{T,min} = 1hour$, where subscript min indicates that this is the minimum waiting times. If measurements are made on

a liquid, with relaxation time τ, then there is a further requirement: $t_T, t_U > x\tau$, where x depend on the resolution of the experiment and must be found experimentally, but x is probably around 10. Thus, this is something one must be aware of when measurements are made at low temperatures, from around where $\tau > 100s$ (corresponding to a loss peak frequency of $10mHz$).

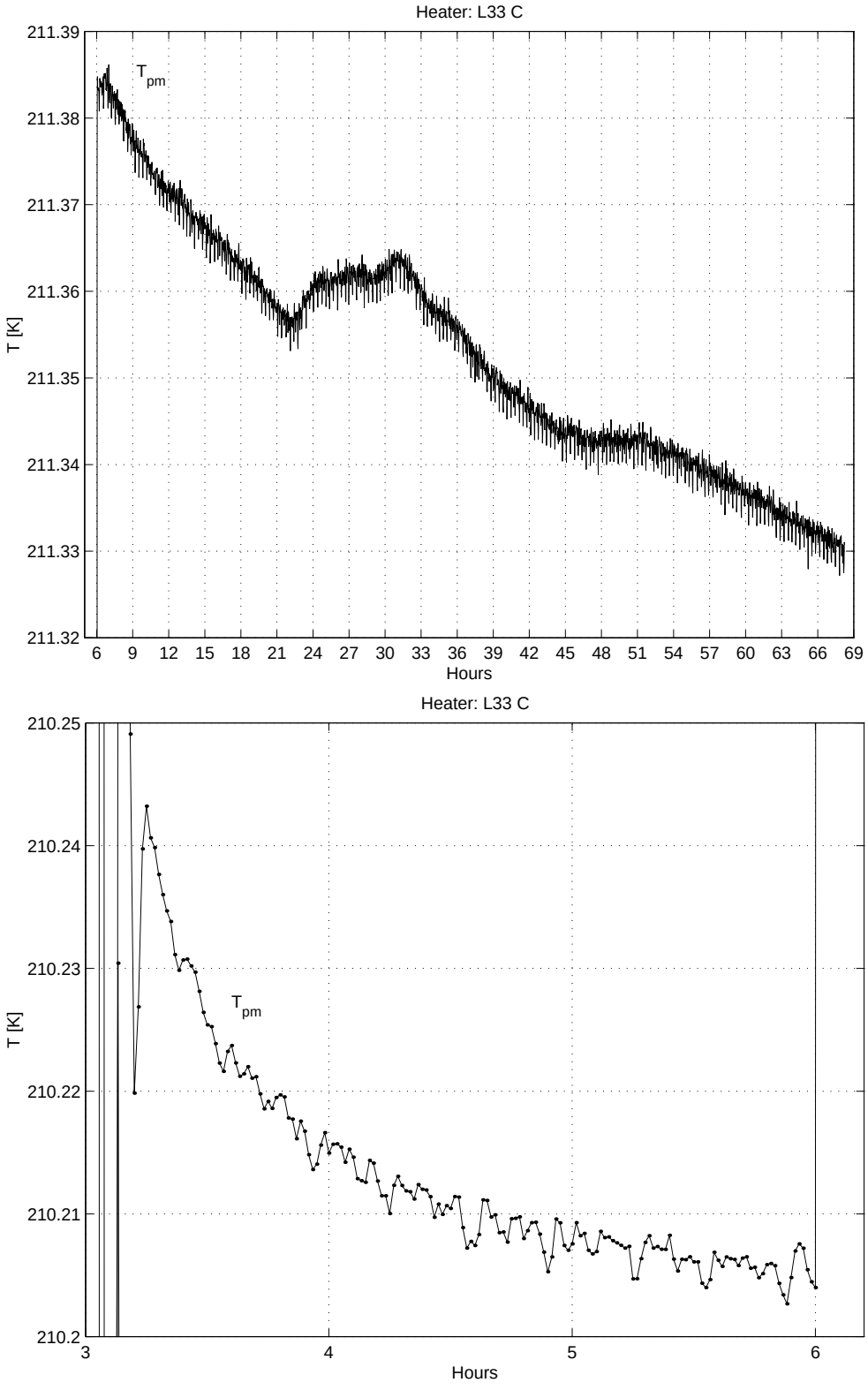

Figure 15.5 The top plot shows T_{pm} after the change of U_1 from $3.873V$ to $7.744V$ while the bottom plot shows T_{pm} after the change of T_S from $215K$ to $210K$.

16 Planar heater measurements

I would like to emphasize that no data points have been sorted away and no smoothing of the data have been performed, except if explicit stated or if the points lie outside the zoom level in the data plots (and besides taking the average of several measurements as described in section 15.1).

16.1 Calibration of the heater

In order to translate from the resistance (R_p) of the heater to the temperature (T_p) of the heater (and liquid), and in order to find α for the heater, a calibration procedure is needed: R_p must be found for different T_p. Since $T_k < T_p$ when $V > 0$ (as will be the case when R_p is measured), it is not possible directly to measure sets of R_p, T_p. Instead R_p must be measured for different values of V at each T_k, and a extrapolation to $V = 0$ (where $T_k = T_p$) must be made.

From equation 5.1 (page 21) it is seen that $\Delta T = T_p - T_k = Z_{T,DC} I_{Tm}$. For the nickel heater (Ni) equation 6.25 (page 33) must be used:

$$R_p = AT_p + B = A(T_k + \Delta T) + B = (R_p)_{T_k} + A\Delta T = (R_p)_{T_k} + AZ_{T,DC} I_{Tm},$$

where $(R_p)_{T_k}$ is R_p at $T_p = T_k$. Thus $(R_p)_{T_k}$ can be found in a plot of R_p as function of I_{Tm} extrapolating to $I_{tm} = 0$.

For the carbon heater (C) equation 6.22 (page 33) must be used:

$$R_p \approx (R_p)_{T_k} + \left(\frac{\partial R_p}{\partial T}\right)_{T_k} \Delta T = (R_p)_{T_k} \left(1 - \frac{T_0}{T_k^2}\Delta T\right) = (R_p)_{T_k} \left(1 - \frac{T_0}{T_k^2} Z_{T,DC} I_{Tm}\right)$$

Thus, as for the Ni heater, $(R_p)_{T_k}$ can be found in a plot of R_p as function of I_{Tm} extrapolating to $I_{tm} = 0$.

Examples of this is shown in figure 16.1. For both the Ni and C heater a straight line is fitted[1] to the data, and $(R_p)_{T_k}$ is found where the line crosses the ordinate axis. (In order to distinguish the different heaters they are given a name: e.g. the carbon heater on figure 16.1 is "T7 C", where "T" is short for "Thick glass substrate: $(6mm)$", and "C" is short for "Carbon".)

The extrapolated values for R_p are plotted as function of T_p for the Ni heater (equation 6.25), while $\ln R_p$ is plotted as function of $1/T_p$ for the carbon heater (equation 6.22). Examples of this is shown in figure 16.2. Again a straight line is fitted to the data. This fit gives A and B in equation 6.25 for the Ni heater, and T_0 and $\ln R_0$ in equation 6.22 for the C heater.

Equation 6.27 and equation 6.23 show:

$$\begin{aligned} \alpha_{Ni} &= 1/(T_p + B/A), \quad \text{for the } Ni \text{ heater} \\ \alpha_C &= -T_0/T_p^2, \quad \text{for the } C \text{ heater} \end{aligned}$$

In figure 16.3 α_{Ni} and α_C is plotted as function of T_p.

[1] I use Matlabs least–square "polyfit" routine.

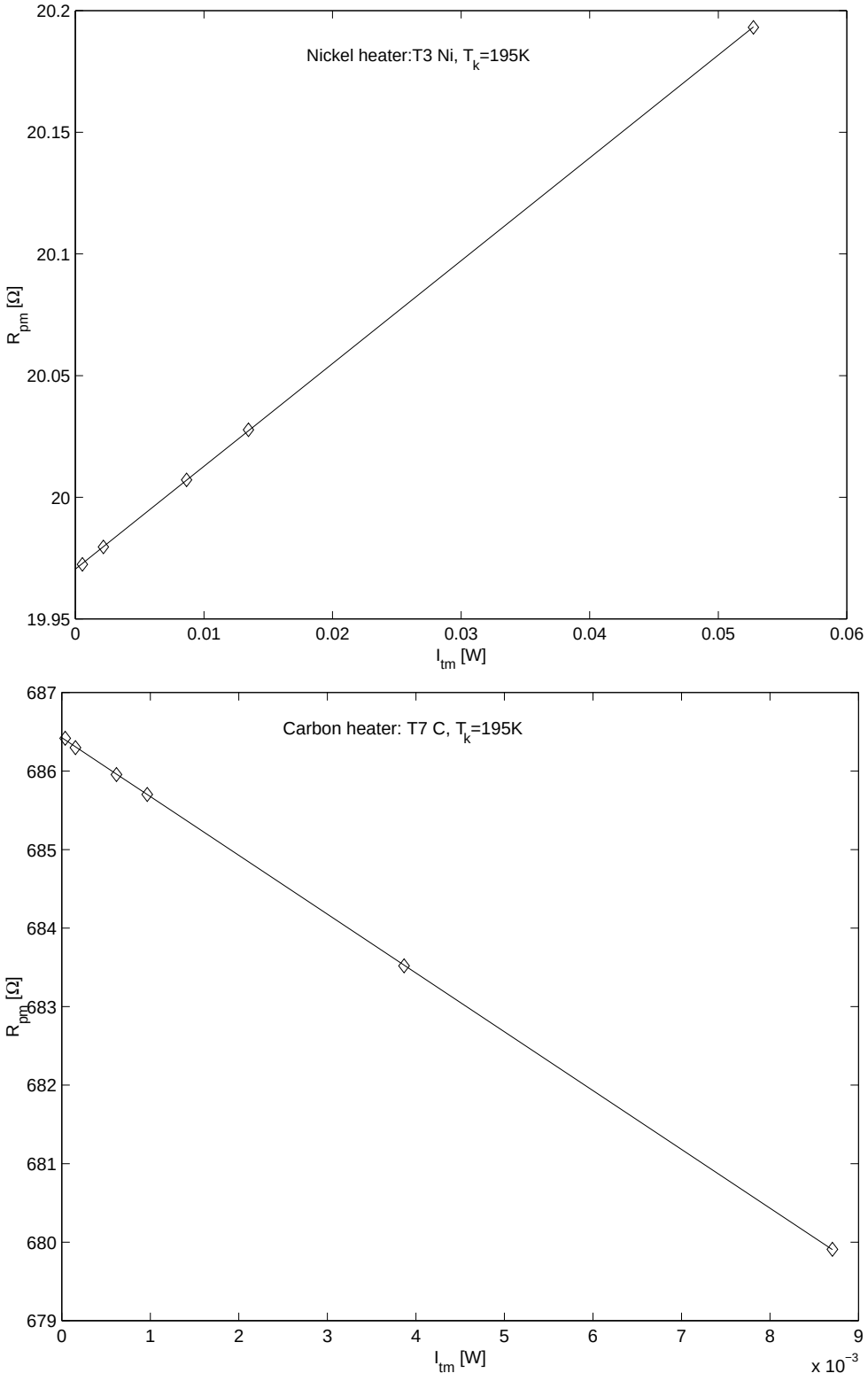

Figure 16.1 The top plot shows R_{pm} as function of I_{Tm} for the "T3 Ni" nickel heater. The lower plot shows R_{pm} as function of I_{Tm} for the "T7 C" carbon heater.

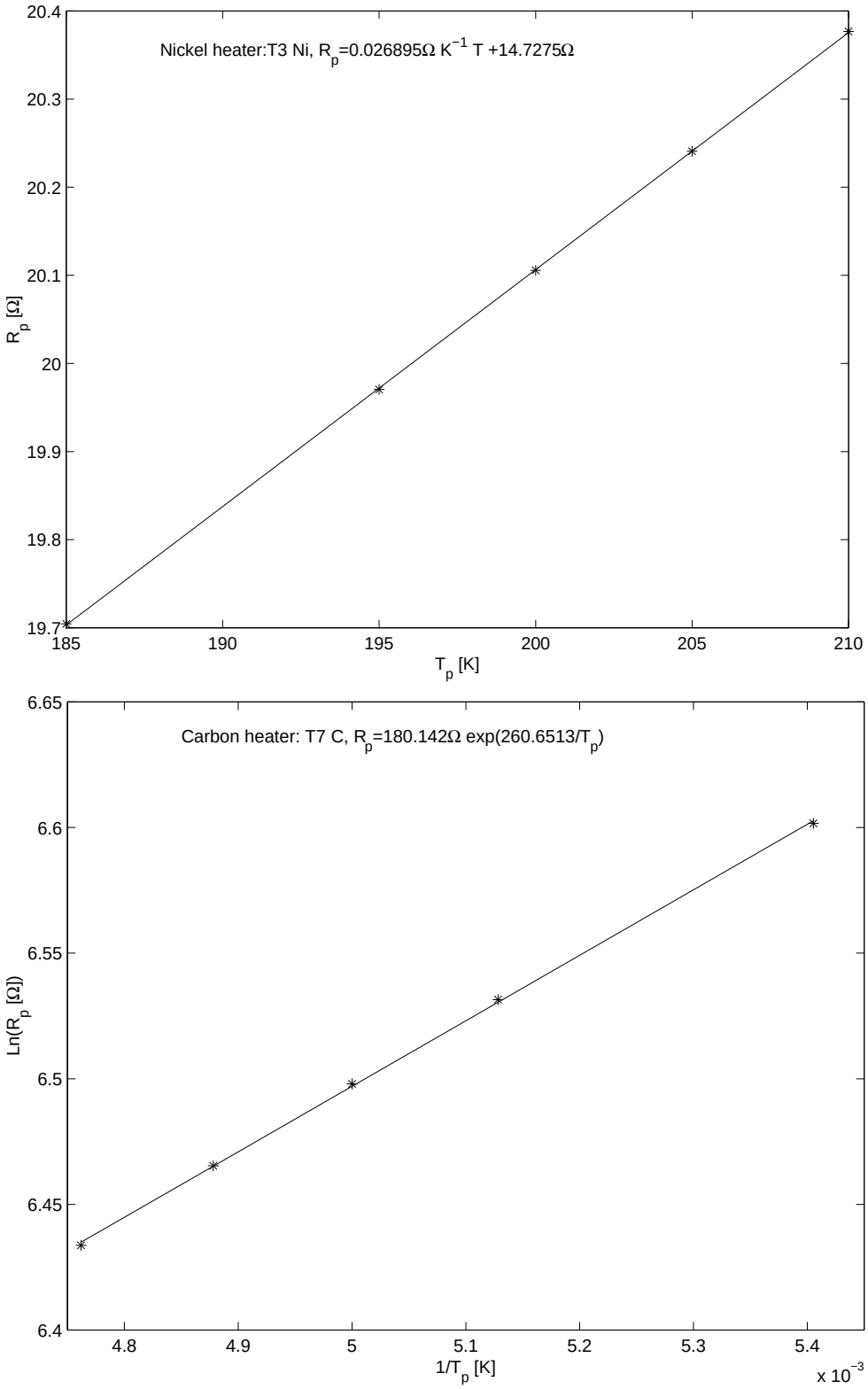

Figure 16.2 The top plot shows R_p as function of T_p for the "T3 Ni" nickel heater. The lower plot shows $\ln R_p$ as function of $1/T_p$ for the "T7 C" carbon heater. The fitted lines gives $R_p(T_p)$.

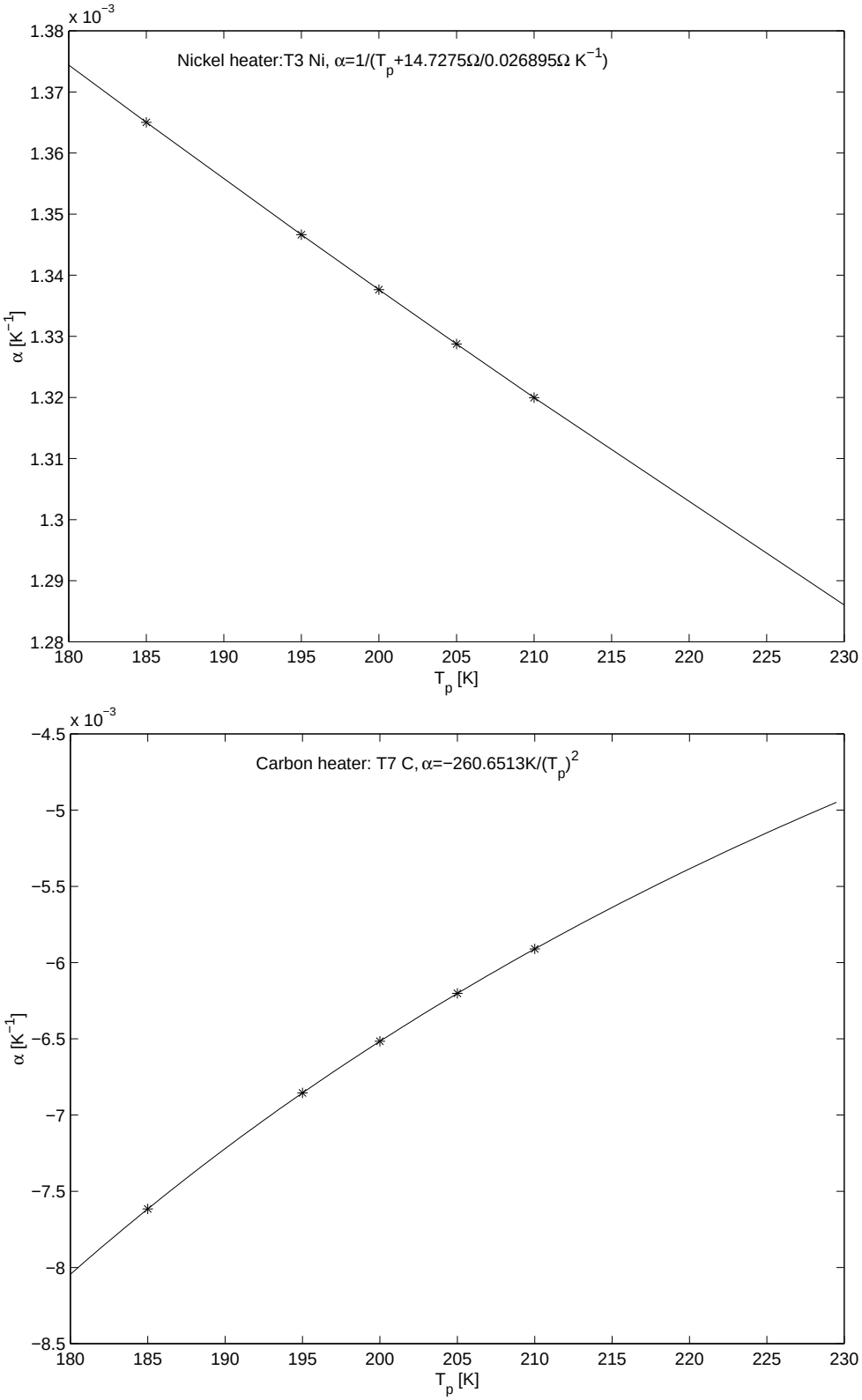

Figure 16.3 The top and bottom plot shows α_{Ni} for "T3 Ni", and α_C for "T7 C", respectively, as function of T_p. The stars mark the temperatures used to measure α.

16.2 Data analysis: Phase

In the following the equations (12.2, 12.3 and 12.11) that fully take the edge effects into account will be referred to as "integral" equations. The equations (equations 12.4 and 12.5) that are approximations of these will be referred to as "approximate".

If the one–dimensional model is valid the expression $1/\tilde{Z} = \tilde{Y} = \sqrt{i\Omega\tilde{\kappa}\tilde{c}}$ can be used (equation 7.5). From this expression it is seen that if $\tilde{\kappa}$ and $\tilde{c}$ are frequency independent then the phase (χ) of $\tilde{Z}$ (see equation 5.4 page 22) is $-\pi/4$ or -45° (since $\sqrt{i} = e^{i\pi/4}$). Since the one–dimensional model will be valid for high frequencies it is expected that χ must approach -45° as $2f \to \infty$.

The phase of $\tilde{Z}_S$ (measured without liquid) is shown in figure 16.4. As expected the phase seems to approach -45° at high frequencies. The deviations from -45° at low frequencies are due to the edge effects. (Note that I plot the data as function of $2f = \Omega/(2\pi) = \omega/\pi$. This choice is made in order to ease the comparison to literature data, where this choice is the most common one.)

In figure 16.4 there are two sets of solid lines: the upper and lower (at low frequencies). Though it is not seen on this figure there are in fact five lines in each set corresponding to different values of κ_S and c_S. The reason for this is explained in section 16.3. The (lower) solid lines that fit the data well over the whole frequency range are calculations using equation 12.11 (integral). The (upper) solid lines that deviate from the data at low frequencies are calculations using equation 12.4 (approximation).

It is clearly seen that the one–dimensional model is insufficient to analyze these data since the phase deviates significantly from -45°. The approximate equation (equation 12.4) fits the data well at high frequencies (above $2f \approx 5Hz$) but fail at low. The integral equation (equation 12.11) fits the data well over the whole frequency range though the phase (of the data) seems to be a little two high at the highest frequencies.

From figure 16.4 it is obvious that the integral equations must be used in order to describe the data well. In section 16.3 the measured data is analyzed using the integral equations (equation 12.11). To illustrate the importance of taking the edge effect into account the data is analyzed using the approximate expressions (equations 12.4 and 12.5) in section 16.4 and the one–dimensional model in section 16.5.

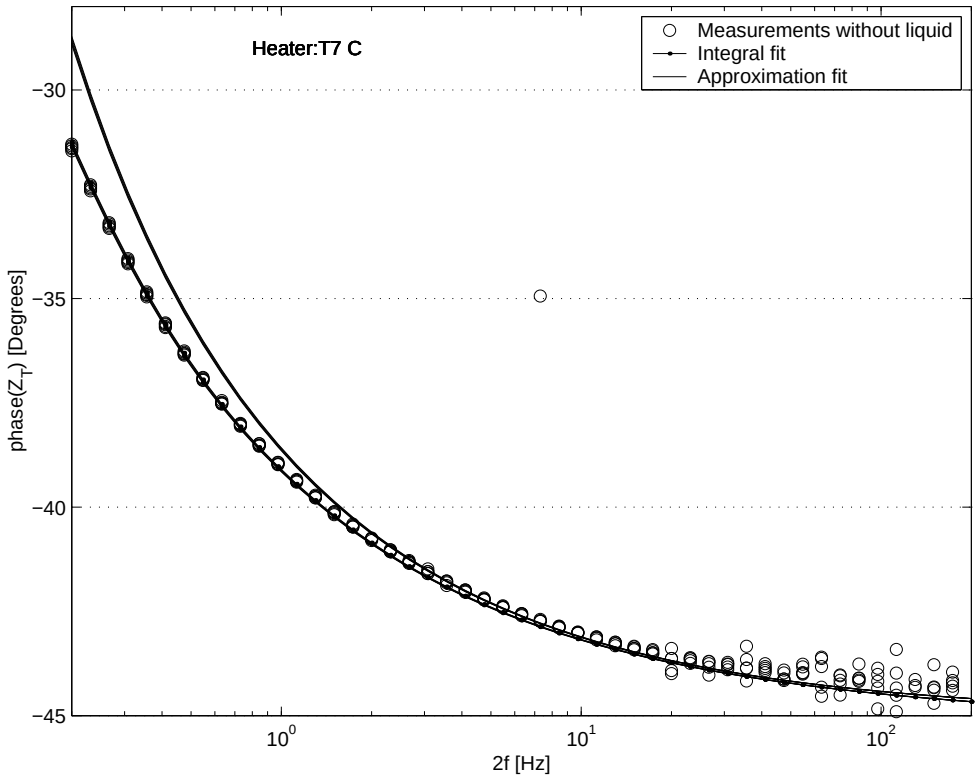

Figure 16.4 The phase of the thermal impedance as function of $2f$. All 5 measured temperatures are shown ($U_1 = 9.9V$). There are two sets of solid lines: the upper and lower (at low frequencies). Though it is not seen on this figure there are in fact five lines in each set (see section 16.3 for details). The (lower) solid lines that fit the data well over the whole frequency range are calculations using equation 12.11 (integral). The (upper) solid lines that deviate from the data at low frequencies are calculations using equation 12.4 (approximation).

16.3 Data analysis: integral

Figure 16.5 show a Cole–Cole plot (a plot of the imaginary part as function of the real part) of the effusivity function for the substrate $\tilde{E}_S$ defined as:

$$\tilde{E}_S \equiv \frac{1}{\tilde{Z}_S A\sqrt{i\Omega}}$$

It is given the name effusivity function since it is equal to the effusivity if the one–dimensional model is correct.

Fits using the integral equation (equation 12.11) is also shown in figure 16.5.

Though not perfect, the fits are quite good. The thermal parameters κ_S and c_S are determined from these fits and plotted in figure 16.6. As mentioned in the previous section there are in fact five curves plotted on top of each other in each set of solid lines in figure 16.4. These five curves correspond the the five values of κ_S and c_S determined from figure 16.5. The variations of these parameters are such that it is not possible to distinguish the five curves in figure 16.4.

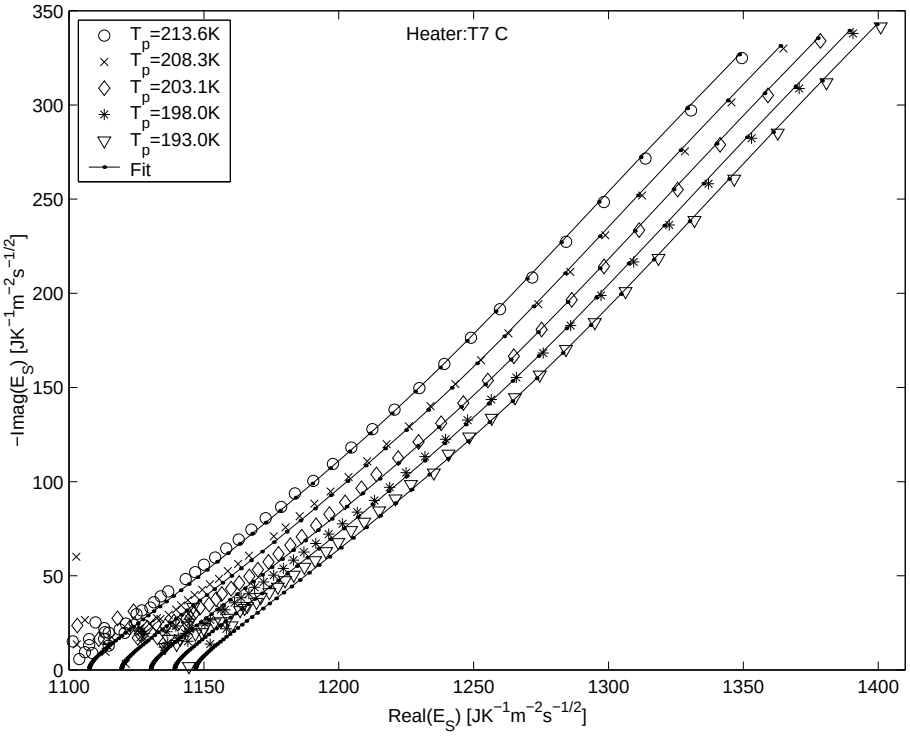

Figure 16.5 Cole–Cole plot of the effusivity function ($\tilde{E_S}$) at the five measured temperatures (measurements without liquid). The solid lines are fits using the integral equation 12.11. The thermal parameters κ_S and c_S are determined from these fits. ($U_1 = 9.9V$).

16.3.1 Measurements on glycerol

Besides the thermal parameters of the substrate found as described above also the thermal conductivity of glycerol ($\kappa_{Glycerol}$) is needed in order to extract the heat capacity of glycerol. $\kappa_{Glycerol}$ is by Sandberg et al. [1977] measured to $0.29WK^{-1}m^{-1}$ in the temperature interval $[130K; 300K]$ [Sandberg et al., 1977, p. 475] and the value $0.285WK^{-1}m^{-1}$ at $292K$ is given in [Nordling and Österman,

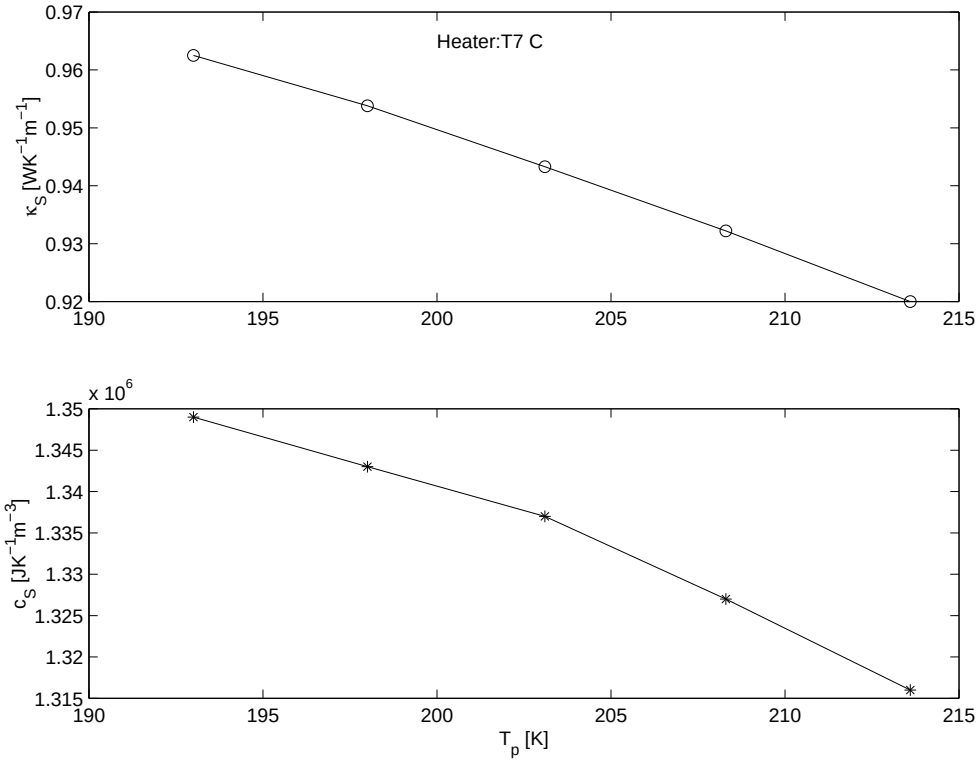

Figure 16.6 κ_S and c_S determined from the fits shown in figure 16.5 as function of temperature (T_p).

1996, p. 37]. Now I use the value $\kappa_{Glycerol} = 0.29 WK^{-1}m^{-1}$. Later I will show how the extracted heat capacity is influenced by this choice.

The heat capacity of glycerol is extracted form the data in a point by point inversion algorithm. From equation 6.17 and equation 6.19:

$$Z_{rel} \equiv \frac{\tilde{Z}_{T,S}}{\tilde{Z}_{T,LS}} = \frac{\tilde{V}_{3c,S}}{\tilde{V}_{3c,LS}} = \frac{\tilde{Y}_{LS}}{\tilde{Y}_S} \tag{16.1}$$

For each point Z_{rel} is calculated using equation 12.11 and fitted to the measured Z_{rel} (the real and imaginary part of $c_{Glycerol}$ is the fit parameters)[2].

The extracted heat capacity of glycerol is shown in figure 16.7.

[2]The integral in equation 12.12 is solved using matlabs "quadL" routine. The integral in equation 12.11 is then solved using a "home written" Simpson integration (e.g. [Chow, 2000, p. 469]) routine in matlab. (On my computer the inversion of the complete data set takes about 3 minutes. If the double integral (equation 12.3) were used the inversion procedure would probably take several days, possible more.)

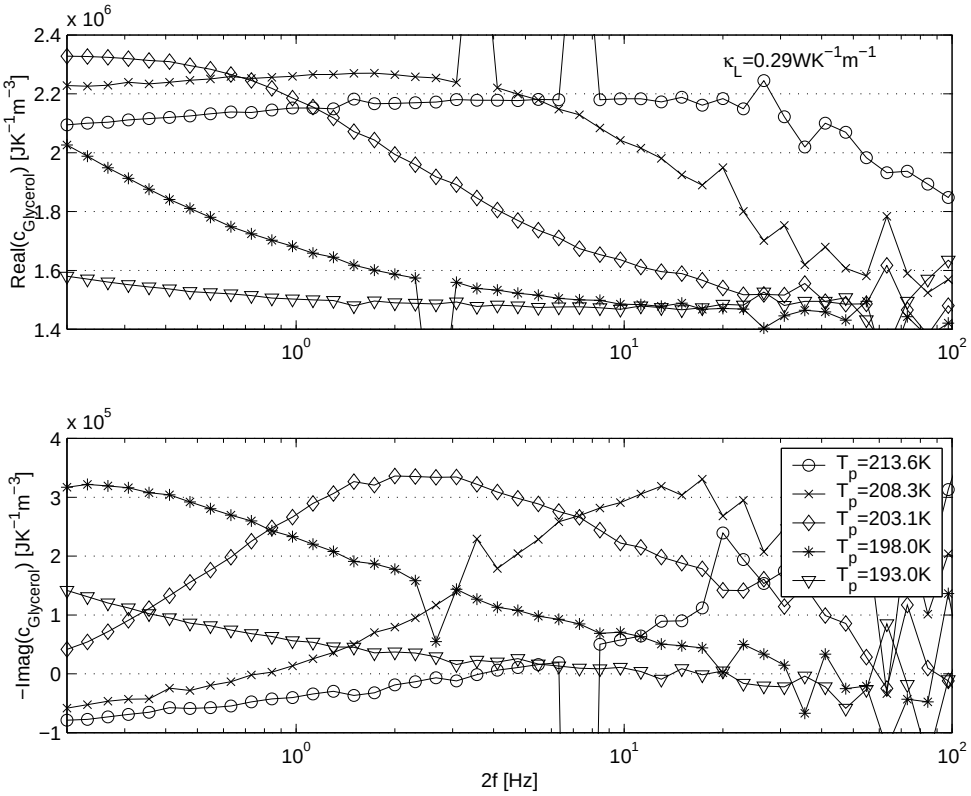

Figure 16.7 The extracted heat capacity of glycerol ($U_1 = 9.9V$). The value $\kappa_{Glycerol} = 0.29WK^{-1}m^{-1}$ has been used. (The cryostate temperatures was: $210.0K$, $205.0K$, $200.0K$, $195.0K$, $190.0K$).

The extracted heat capacity in figure 16.7 does not look entirely correct. E.g. for $T_p = 208.3K$ the real part bend downwards at low frequencies and the imaginary part becomes negative. This might have to do with the chosen value $\kappa_{Glycerol} = 0.29WK^{-1}m^{-1}$. To illustrate this also the heat capacity is extracted using $\kappa_{Glycerol} = 0.25WK^{-1}m^{-1}$ and $\kappa_{Glycerol} = 0.35WK^{-1}m^{-1}$. The results are shown on figure 16.8 and figure 16.9 respectively. It is seen that the value $\kappa_{Glycerol} = 0.25WK^{-1}m^{-1}$ seems to give a better result and the value $\kappa_{Glycerol} = 0.35WK^{-1}m^{-1}$ a worse one. Obviously it would been interesting to actually know the value for the liquid I have measured – it might be temperature dependent as well, unfortunately I do not have that information.

In order to compare these measurements with the ones reported by Birge and Nagel [1985] / Birge [1986] consider the following (they report data for $e^2_{Glycerol}$

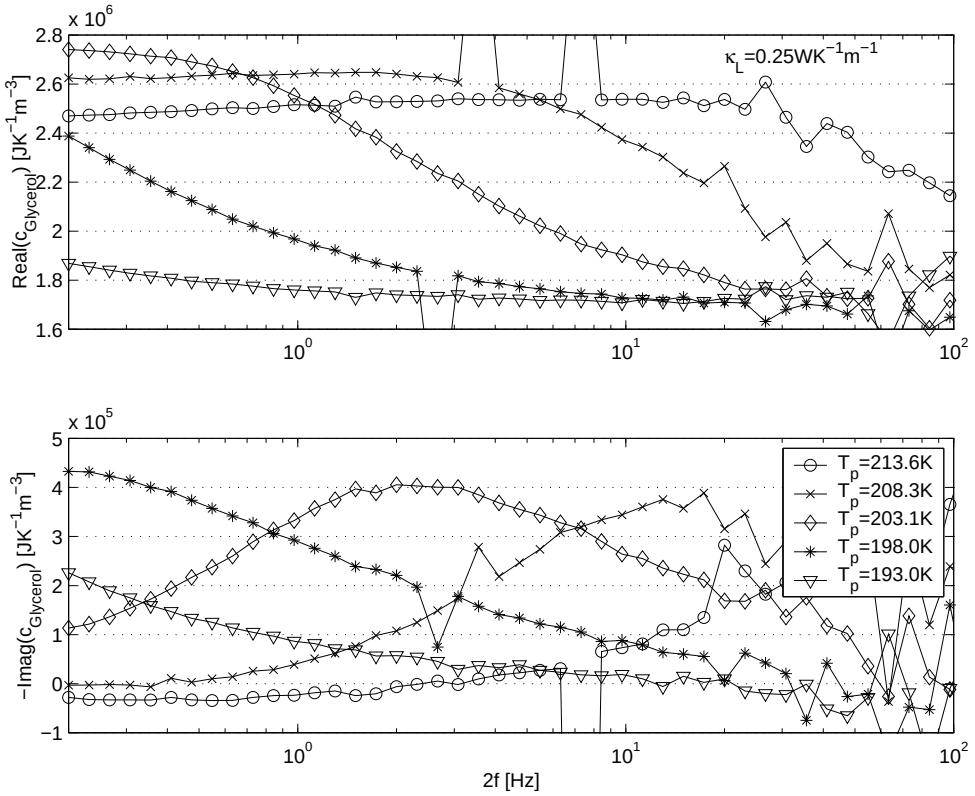

Figure 16.8 The extracted heat capacity of glycerol ($U_1 = 9.9V$). The value $\kappa_{Glycerol} = 0.25WK^{-1}m^{-1}$ has been used.

and I divide their data with $\kappa_{Glycerol} = 0.29WK^{-1}m^{-1}$). They find[3],[4]:

$$\begin{aligned} c_\infty &\approx 1.45 \times 10^6 JK^{-1}m^{-3} \\ c_0 &\approx 2.93 \times 10^6 JK^{-1}m^{-3} \\ c''_{max} &\approx 4.83 \times 10^5 JK^{-1}m^{-3} \\ f_p(203.9K) &\approx 2Hz \quad \text{(on a 2f axis)} \\ \frac{c''_{max}}{\Delta c} &\approx 0.35, \end{aligned}$$

where c_∞ and c_0 is the heat capacity in the limits $2f \to \infty$ and $2f \to 0$, respectively,

[3]In these original measurements by Birge et al. no corrections were made for the edge effects. But since their heater is much larger ($6mm \times 20mm$) than the one I have used ($3mm \times 3mm$) the edge effects in their measurements is not as large. This is shown in more detail in section 16.5.

[4]Note that the scale on the figure in [Birge and Nagel, 1985, p. 2675] must be multiplied by ≈ 1.5 according to [Birge, 1986, p. 1635].

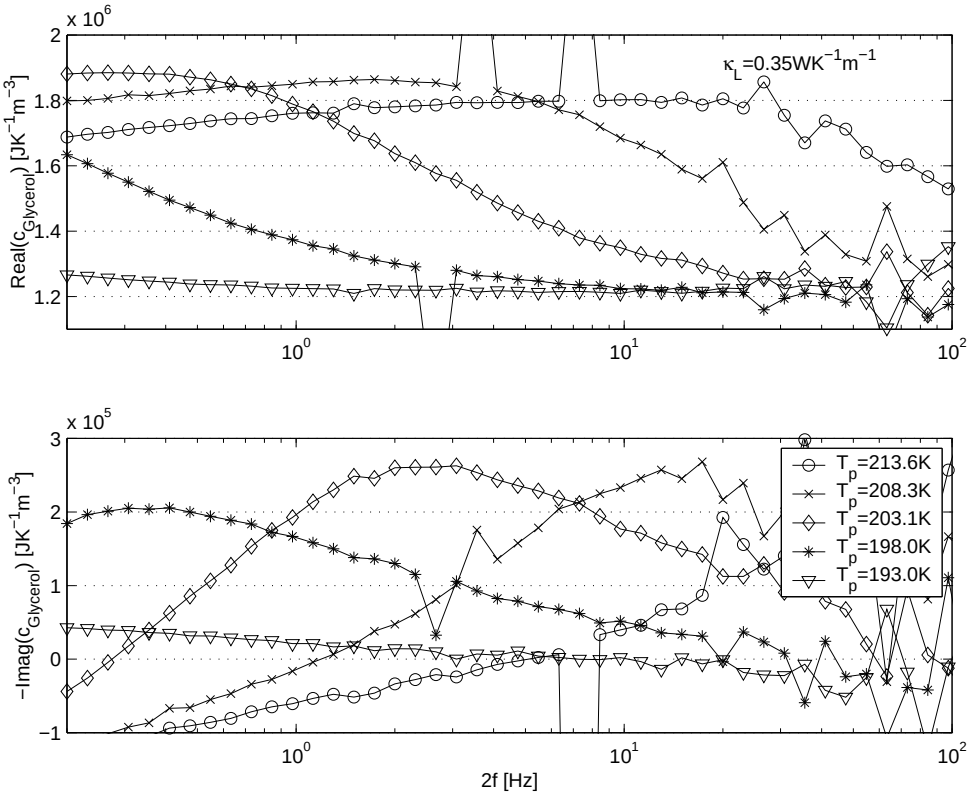

Figure 16.9 The extracted heat capacity of glycerol ($U_1 = 9.9V$). The value $\kappa_{Glycerol} = 0.35WK^{-1}m^{-1}$ has been used.

c''_{max} and f_p are the maximum value of the imaginary part of $c_{Glycerol}$ and the corresponding frequency (loss peak frequency, on a $2f$ axis) and $\Delta c \equiv c_0 - c_\infty$.

Comparing this with figure 16.7 it is seen that there is agreement on the loss peak frequency but not on the absolute values of $c_{Glycerol}$. Also I find $c''_{max}/\Delta c \approx 0.4$ which is a little higher than the value they find. Another way of comparing the data is to look at them in a Cole–Cole plot.

If time–temperature–superposition (TTS) is fulfilled it means that the shape of the curves does not change with temperature (e.g. [Olsen et al., 2000], [Olsen et al., 2001]). Therefore, if TTS is fulfilled the curve composed of data for the different temperatures in a Cole–Cole plot, will represent the shape of the relaxation spectrum at all the temperatures.

The normalized heat capacity c_N is defined as [Christensen, 1985, p. 636]:

$$c_N \equiv \frac{c(2f,T) - c_\infty(T)}{\Delta c}, \qquad \Delta c = c_0(T) - c_\infty(T),$$

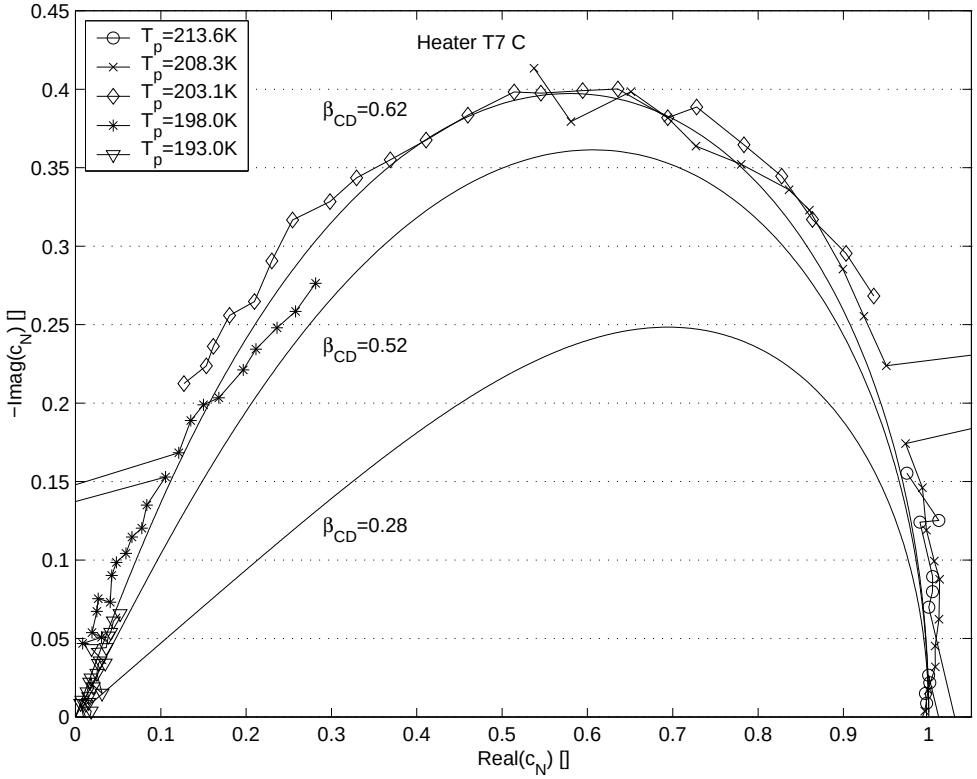

Figure 16.10 Cole–Cole plot of the extracted heat capacity of glycerol (with $U_1 = 9.9V$). The tree solid curves are the Cole–Davidson function with $\beta_{CD} = 0.62$ (top curve), $\beta_{CD} = 0.52$, and $\beta_{CD} = 0.28$ (lower curve). $c_0 \times 10^{-6} = 2.18, 2.26, 2.30, 2.40, 2.50 JK^{-1}m^{-3}$ at $T_p = 213.6, 208.3, 203.1, 198.0, 193.0K$ respectively and $c_\infty = 1.46 \times 10^6 JK^{-1}m^{-3}$. The data extracted with $\kappa_{Glycerol} = 0.29WK^{-1}m^{-1}$ has been used. This curve does not change significantly if the data extracted with $\kappa_{Glycerol} = 0.25WK^{-1}m^{-1}$ or $\kappa_{Glycerol} = 0.35WK^{-1}m^{-1}$ is used only the values of c_0 and c_∞ are changed.

Figure 16.10 shows a Cole–Cole plot of (c_N) (the same data as figure 16.7). Only data in the frequency range $[0.7; 17.3]Hz$ has been used. The tree solid curves are the Cole–Davidson function with $\beta_{CD} = 0.62$ (top curve), $\beta_{CD} = 0.52$, and $\beta_{CD} = 0.28$ (lower curve), given by:

$$c_{CD} \equiv \frac{c_\infty + \Delta c}{\left(1 + i\left(\frac{f}{f_p}\right)\right)^{\beta_{CD}}},$$

(the value of f_p plays no role for the curves in this plot (figure 16.10)).

The Cole–Davidson function with $\beta_{CD} = 0.62$ fit the data in figure 16.10. The accuracy of the data are not that high but at least $\beta_{CD} = 0.62 \pm 0.02$ judged from

figure 16.10. This finding is not in agreement with the value $\beta_{CD} = 0.51 \pm 0.03$ [Birge, 1986, p. 1637]. The data are in disagreement with the value $\beta_{CD} = 0.28$ which corresponds closely to the data measured by Christensen [1985] (Christensen [1989]).

16.4 Data analysis: approximation

From figure 16.4 it is clear that the approximate equations (equations 12.4 and 12.5) do not accurately describe the data. In this section I will show the result of analyzing the data with these equations despite this fact.

κ_S and c_S can be found from measurements without liquid as described in section 12.1. The results of such measurements are shown in figure 16.11. Straight lines are fitted to the data at high frequencies (to the left). The two solid vertical lines show the fit–range (the data–range used for the fit). The highest frequencies are not used, since they are very noisy, and the lower frequencies are not used, since they deviate from the straight line as a consequence of the breakdown of equation 12.6. For each of the temperatures $T_p = 214.4K$ and $T_p = 209.1K$ (and for both the real and imaginary part) one noisy point in the fit–range have not been used for the fit (it is easy to see the points in the figure). The vertical dot–and–dash–lines mark where $2f = 100Hz, 10Hz, 1Hz$ (high frequencies to the left).

In figure 16.11 is $1/e_S$ found where the real part intersects the ordinate axis, and $-1/c_S$ and $1/c_S$ is the slope of the fitted lines for the real and imaginary part, respectively (as described in section 12.1). The fitted values for e_S and c_s are shown in figure 16.12. One problem with this analysis is that the found values are dependent on the chosen fit range (which just show that the used equation does not describe the data well). E.g. the result of using a much narrower fit range (5 points only in the interval $[26;48]Hz$) is shown on figure 16.13. This "improves" the result in the sense that there is closer agreement between the values (of c_S) found from the real and imaginary part but, also the "noise" on the points are larger.

The values found from figure 16.13 are (e_S and κ_S is listed in order of decreasing temperature):

$$\begin{aligned} e_S &\approx 1135.4,\ 1127.8,\ 1119.2,\ 1109.8,\ 1098.0 \quad JK^{-1}m^{-2}s^{-1/2} \\ c_S &\approx 1.2810^6 \quad JK^{-1}m^{-3} \\ \Updownarrow & \\ \kappa_S &\approx 0.94,\ 0.96,\ 0.98,\ 0.99,\ 1.01 \quad WK^{-1}m^{-1} \end{aligned}$$

(For c_S the average is taken of the value found from the real and imaginary part.) These value are not in total agreement with the values found using the "integral" analysis c.f. figure 16.6.

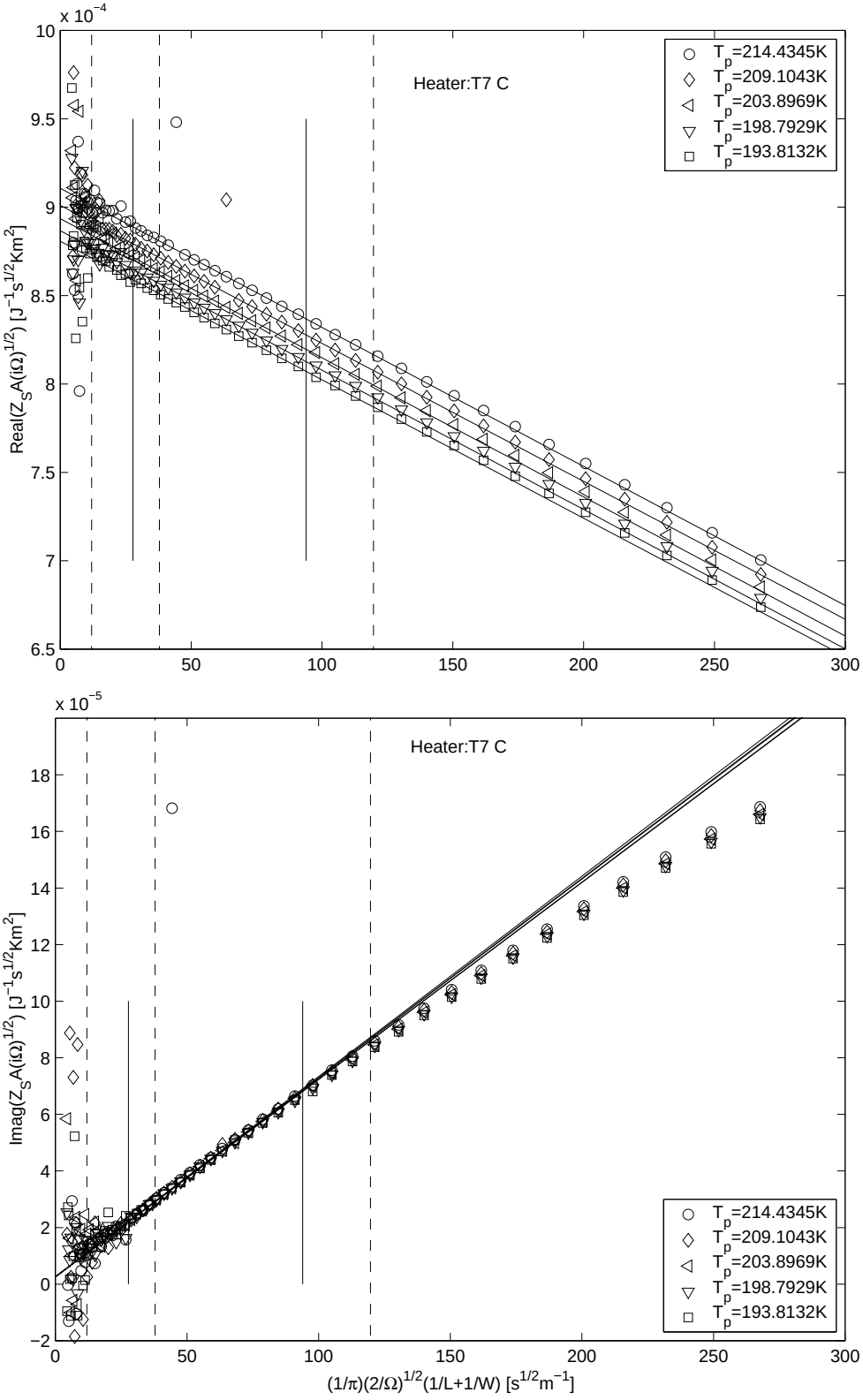

Figure 16.11 $\tilde{Z}_S A\sqrt{i\Omega}$ as function of $\frac{1}{\pi\sqrt{2\Omega}}\left(\frac{2}{L}+\frac{2}{W}\right)$ ($W = L = 3mm$ cf. figure 9.1) .

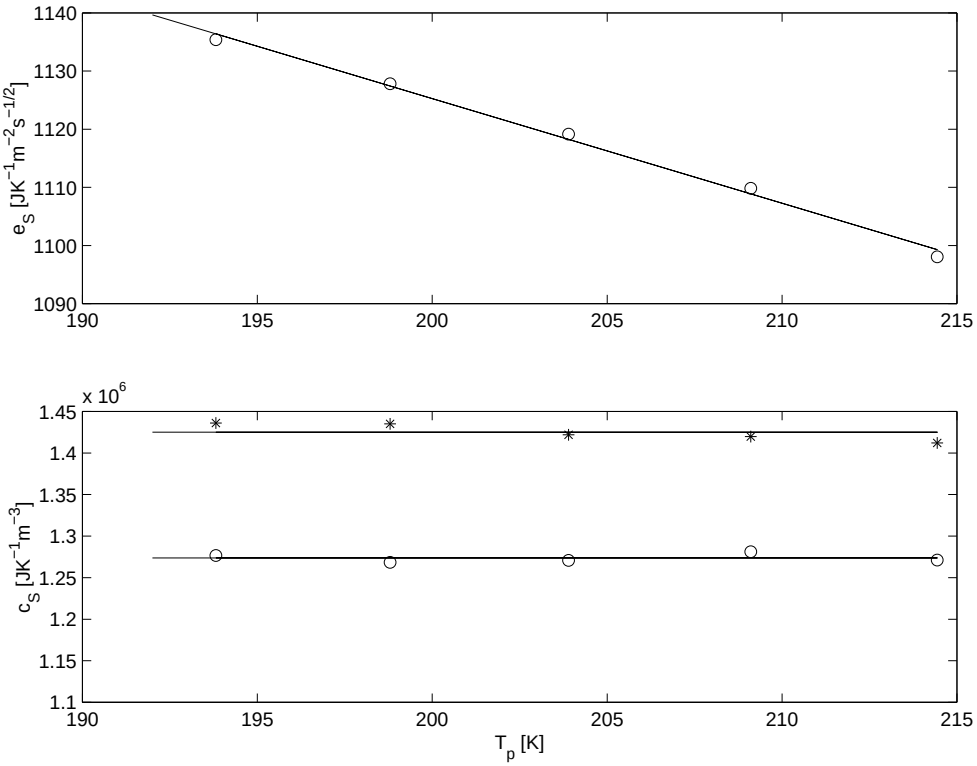

Figure 16.12 The top plot show the extrapolated values for e_S found in figure 16.11. The bottom plot show the found values for c_S, where the circles and stars represent the values found using the real and imaginary part, respectively. The straight lines are best fit to the points (assuming c_S constant).

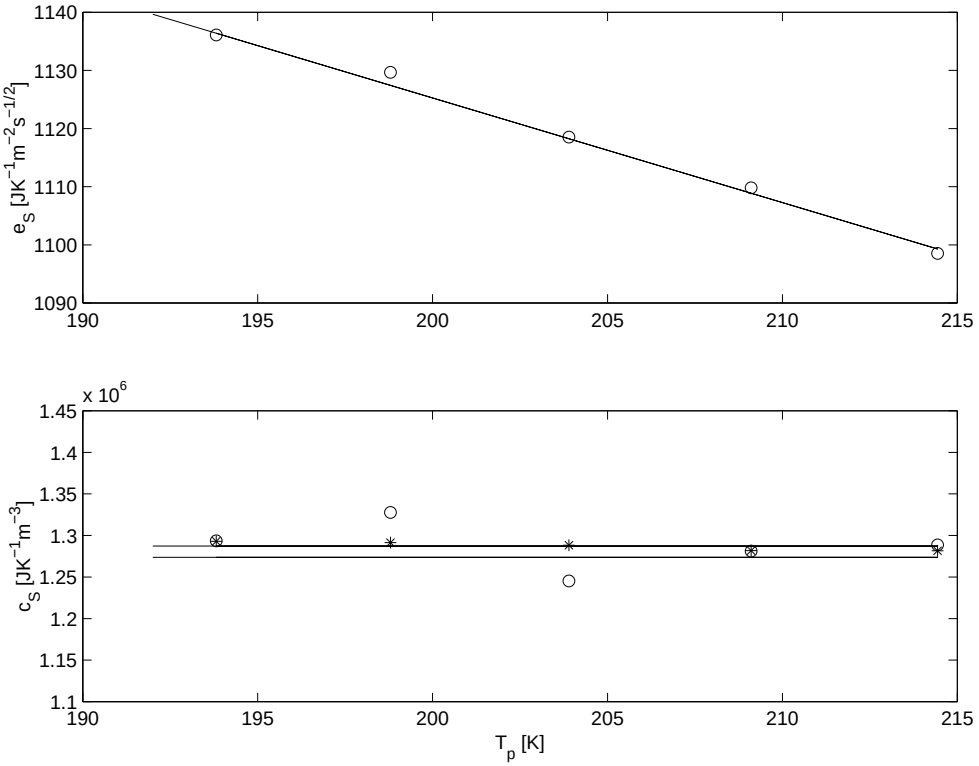

Figure 16.13 As in figure 16.12 the top plot show the extrapolated values for e_S and the bottom plot show the found values for c_S, where the circles and stars represent the values found using the real and imaginary part, respectively. The fit range used is narrower (5 points only in the interval $[26;48]Hz$) than the one used in figure 16.12.

Using the above values for κ_S and c_S (page 129) and $\kappa_{Glycerol} = 0.29WK^{-1}m^{-1}$ the data has been inverted[5] using the same point by point inversion strategy as described in section 16.3 (see page 123) but with the use of equation 12.8 in stead of equation 12.11. The result is shown on figure 16.14.

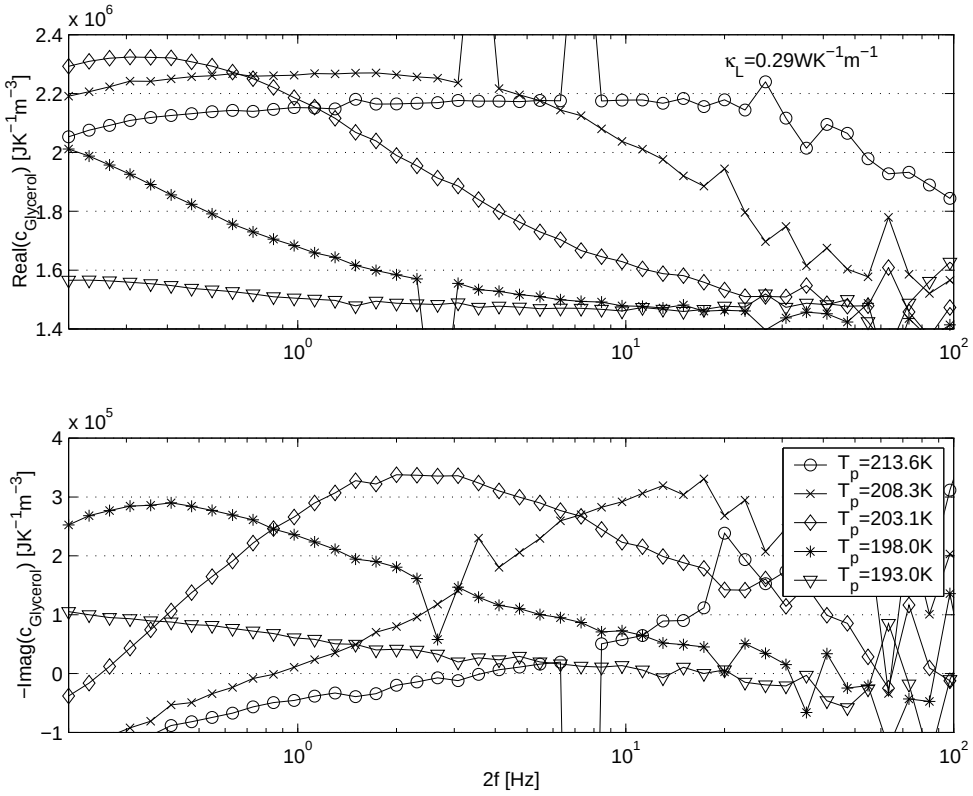

Figure 16.14 The extracted heat capacity of glycerol (with $U_1 = 9.9V$) using the "approximate" equation. The value $\kappa_{Glycerol} = 0.29WK^{-1}m^{-1}$ has been used. Comparing this with figure 16.7 it is clear that the "integral" equation does a better job, as expected.

Also the inversion has been done using $\kappa_{Glycerol} = 0.25WK^{-1}m^{-1}$. The result is shown on figure 16.15. From the comparison of figure 16.14 and 16.7 and figure 16.15 and 16.8 it is clear that the "integral" equation does a better job than the "approximate" equation (this shows up clearly at low frequencies as expected).

[5] On my computer the inversion of the complete data set takes about 20 seconds.

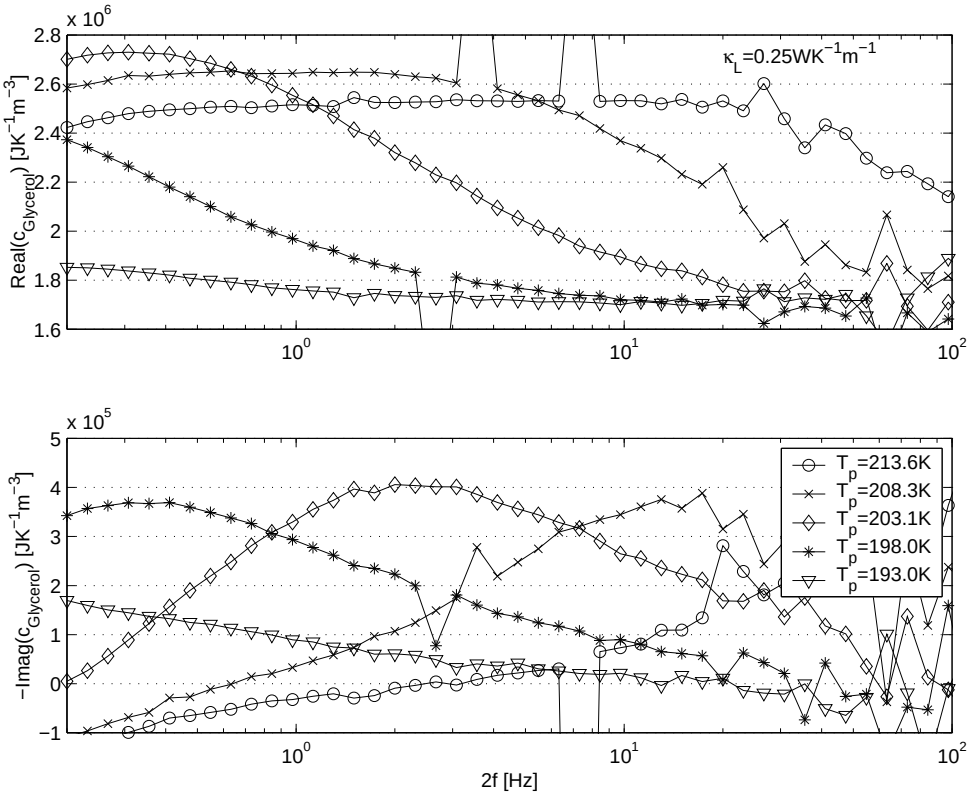

Figure 16.15 The extracted heat capacity of glycerol (with $U_1 = 9.9V$) using the "approximate" equation. The value $\kappa_{Glycerol} = 0.25WK^{-1}m^{-1}$ has been used. Comparing this with figure 16.8 it is clear that the "integral" equation does a better job, as expected.

16.5 One–dimensional model

In order to visualize the importance of correcting for the edge effect the data can be treated assuming the one–dimensional model. Here three approaches to this is discussed.

Using equation 7.22 (page 45) for $\tilde{Y}_{LS}$ in equation 16.1:

$$\tilde{Y}_L = \tilde{Y}_S \left(\frac{\tilde{V}_{3c,S}}{\tilde{V}_{3c,LS}} - 1 \right) \tag{16.2}$$

If the one–dimensional model is adequate then $\tilde{Y}_S$ and $\tilde{Y}_L$ is given by:

$$\tilde{Y}_x = A\sqrt{i\Omega\kappa_x\tilde{c}_x} \tag{16.3}$$

(c.f. equation 7.5 page 38).

If $\tilde{Y}_S$ is given it can be used in equation 16.2 together with the measured data for $\tilde{V}_{3c,S}$ and $\tilde{V}_{3c,LS}$. If the thereby obtained $\tilde{Y}_L$ is put into equation 16.3 together with a table value for κ_L, then a value for $\tilde{c}_L$ can be obtained.

Now there are two approaches to $\tilde{Y}_S$:

1. It is expected that $e_S = \sqrt{\kappa_S c_S}$ is frequency independent and thus it is natural to use a constant value for this and calculate $\tilde{Y}_S$ from equation 16.3. The constant value can be found in the high frequency limit, where the edge effect is insignificant, or it can be found as in section 16.3 or section 16.4 (though the later requires knowledge of the equations that take the edge effect into account). This will be referred to as the "constant value method 1" (CVM1).

2. Another possibility is use $\tilde{Y}_S = 1/\tilde{Z}_S$ where $\tilde{Z}_S$ is the measured thermal impedance for the substrate alone. This will of course give a wrong value for $\tilde{Y}_S$ at low frequencies where the edge effect is significant. This will be referred to as the "variable value method" (VVM).

The third method (CVM2) is to use a constant value for $e_S = \sqrt{\kappa_S c_S}$ and calculate $\tilde{Y}_S$ from equation 16.3 (as in the CVM1) and use $\tilde{Y}_L = \tilde{Y}_{LS} - \tilde{Y}_S$ (equation 7.22) to calculate $\tilde{Y}_L$ (instead of equation 16.2 as is done in CVM1) and finally use equation 16.3 to calculate $\tilde{c}_L$ from $\tilde{Y}_L$. This will be referred to as the "constant value method 2" (CVM2).

In order to study what should be expected from using the CVM1, CVM2 or VVM a set of artificial data can be produced using equation 12.11. The result of using this equations with $W = L = 3mm$, $\kappa_S = 0.9WK^{-1}m^{-1}$, $c_S = 1.3 \times 10^6 JK^{-1}m^{-3}$, $\kappa_L = 0.29WK^{-1}m^{-1}$ ($\kappa_L = 0WK^{-1}m^{-1}$ for data without liquid) and $c_L = 2.2 \times 10^6 JK^{-1}m^{-3}$ is shown in figure 16.16 (equation 16.3 and equation 12.11 is used to calculate $\tilde{Y}_S$ in the CVM and VVM, respectively). It is seen that a bending downwards (of the real and imaginary part) at low frequencies should be expected for the CVM1 while a bending upwards is to be expected for the CVM2 and VVM.

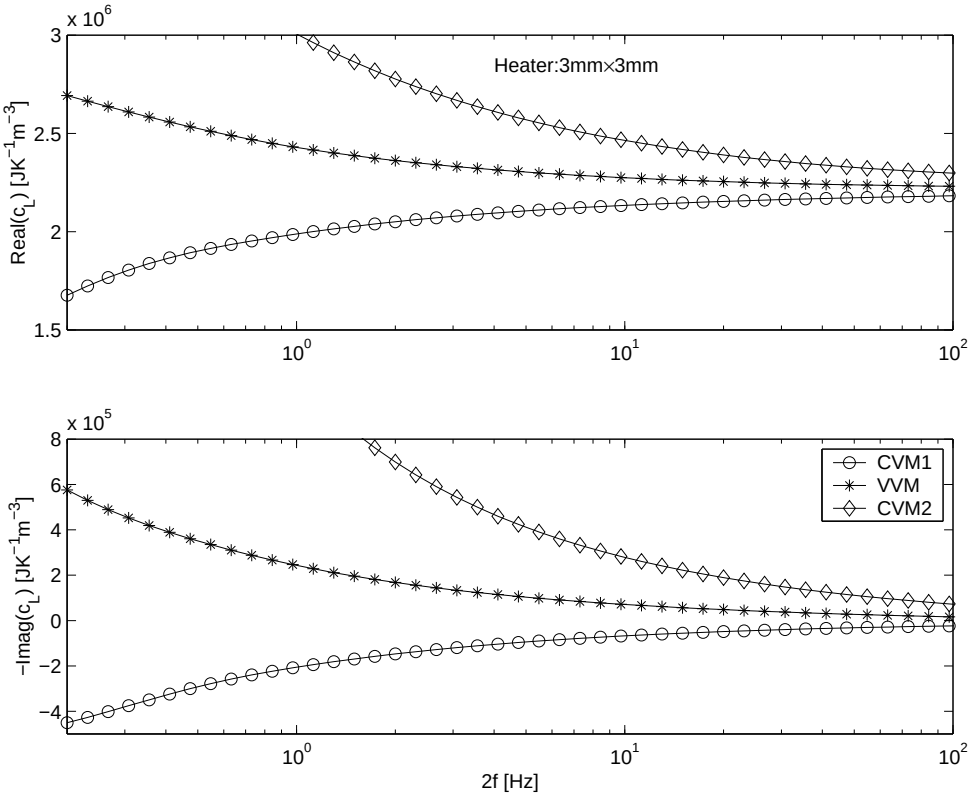

Figure 16.16 In this figure the following values are used: $\kappa_S = 0.9WK^{-1}m^{-1}$, $c_S = 1.3 \times 10^6 JK^{-1}m^{-3}$, $\kappa_L = 0.29WK^{-1}m^{-1}$, and $c_L = 2.2 \times 10^6 JK^{-1}m^{-3}$.

With the values used in figure 16.16 the CVM1 and VVM gives equally good (or poor) results while the CVM2 gives a worse result. But, if instead the thermal parameters for the substrate were closer to those of the liquid this will not be so. To illustrate this the same type of plot is shown again in figure 16.17 but with $W = L = 3mm$, $\kappa_S = 0.3WK^{-1}m^{-1}$, $c_S = 2.0 \times 10^6 JK^{-1}m^{-3}$, $\kappa_L = 0.29WK^{-1}m^{-1}$ ($\kappa_L = 0WK^{-1}m^{-1}$ for data without liquid), and $c_L = 2.2 \times 10^6 JK^{-1}m^{-3}$. In this case the CVM1 clearly gives the best result.

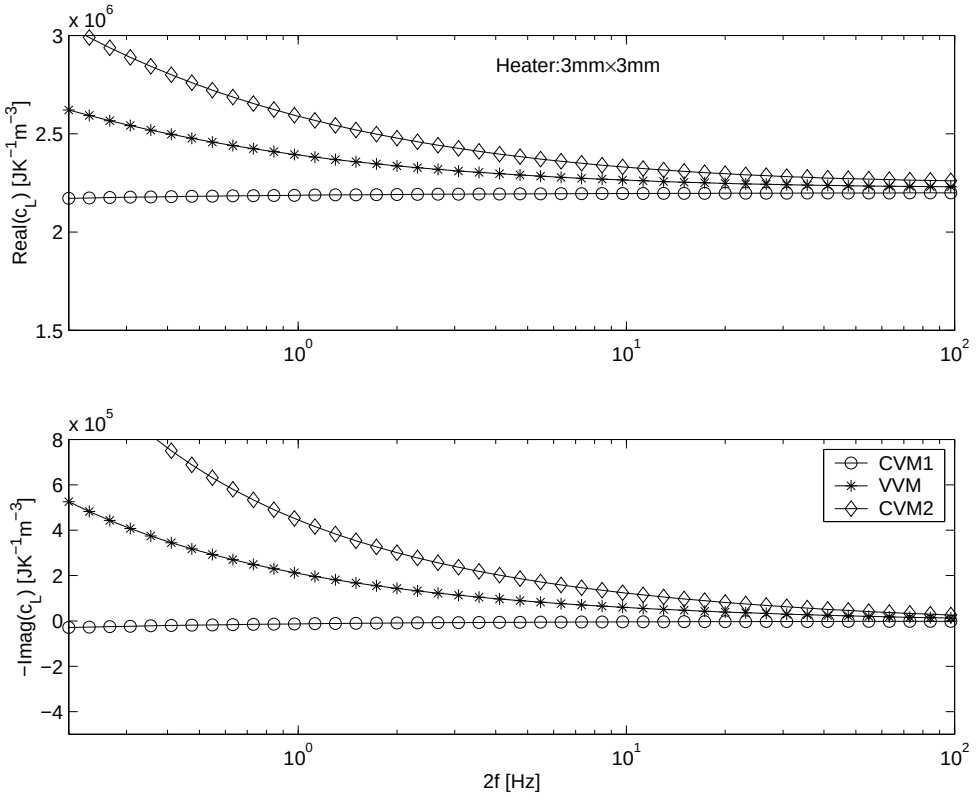

Figure 16.17 In this figure the following values are used: $W = L = 3mm$, $\kappa_S = 0.3WK^{-1}m^{-1}$, $c_S = 2.0 \times 10^6 JK^{-1}m^{-3}$, $\kappa_L = 0.29WK^{-1}m^{-1}$, and $c_L = 2.2 \times 10^6 JK^{-1}m^{-3}$.

With the same type of plot the expected contribution from the edge effect in the original measurements by Birge and Nagel (Birge and Nagel [1985] / Birge [1986]) can be estimated. They do not state what the thermal parameters of their substrate was but, in a later article Birge et al. writes $\kappa_S \approx 1 WK^{-1}m^{-1}$ and $c_S \approx 10^6 JK^{-1}m^{-3}$ [Birge et al., 1997, p. 55]. The shortest dimensions of their heater were $\approx 6mm$ [Birge and Nagel, 1987, p. 1466] (for the lowest frequencies). Thus to illustrate the edge effect the same type of plot is shown again in figure 16.18 but with $W = 6mm$, $L = 6mm$, $\kappa_S = 0.9 WK^{-1}m^{-1}$, $c_S = 1.3 \times 10^6 JK^{-1}m^{-3}$, $\kappa_L = 0.29 WK^{-1}m^{-1}$ ($\kappa_L = 0 WK^{-1}m^{-1}$ for data without liquid), and $c_L = 2.2 \times 10^6 JK^{-1}m^{-3}$.

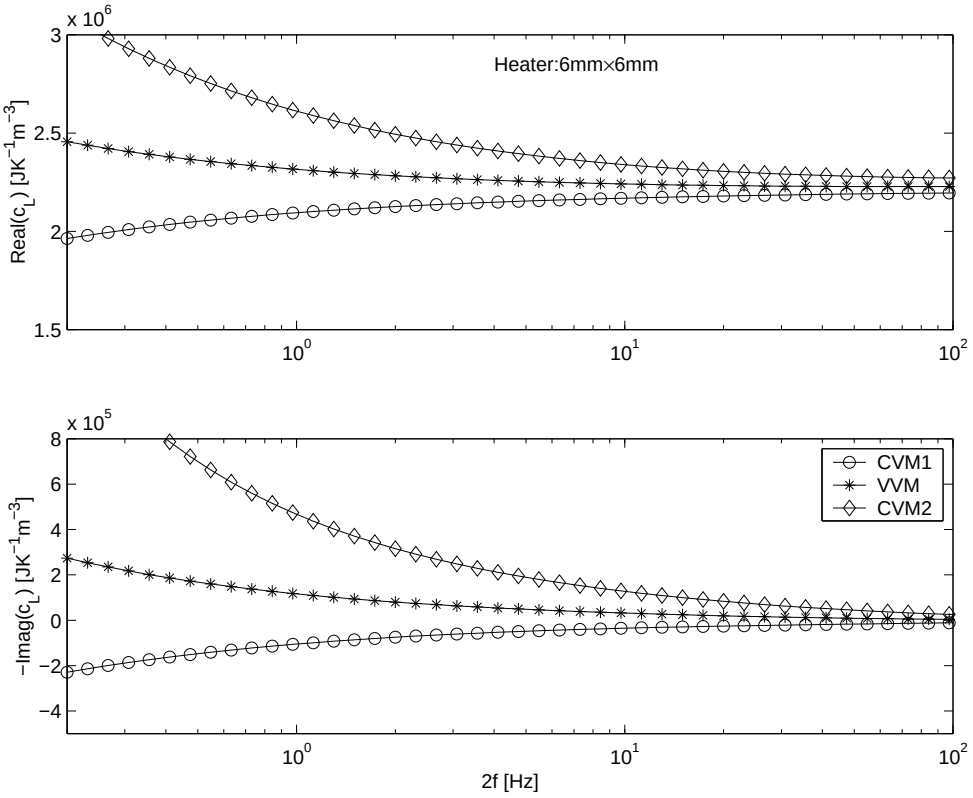

Figure 16.18 In this figure the following values are used: $W = 6mm$, $L = 6mm$, $\kappa_S = 0.9 WK^{-1}m^{-1}$, $c_S = 1.3 \times 10^6 JK^{-1}m^{-3}$, $\kappa_L = 0.29 WK^{-1}m^{-1}$, and $c_L = 2.2 \times 10^6 JK^{-1}m^{-3}$.

Not surprisingly the edge effect is smaller for the $6mm \times 6mm$ heater in figure 16.18 than for the smaller heater ($3mm \times 3mm$) in figure 16.16. In fact the edge effect shown in figure 16.18 is so small that it will be hard to detect with the noise level of the Birge et al. data. This is the reason the correction for the edge effect

was not as critical for their measurements. Still, it may be possible that (at least part of) the deviations between my data and theirs are due to this lack of edge effect correction.

Both the CVM1, VVM and the CVM2 have been used on the data also treated in the previous sections. The results are shown on figure 16.19, 16.20 and 16.21 respectively. As expected a bending downwards (of the real and imaginary part) at low frequencies is seen for the CVM1 while a bending upwards is seen for the VVM and CVM2. As expected the CVM2 gives the poorest result.

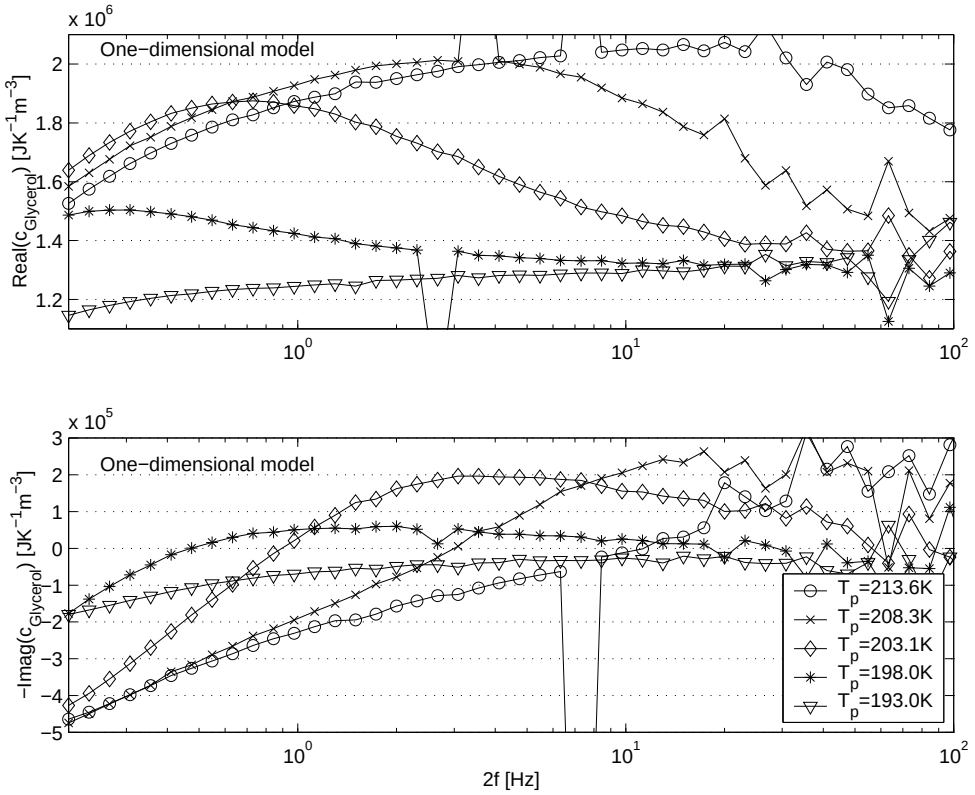

Figure 16.19 The extracted heat capacity of glycerol (with $U_1 = 9.9V$) using the CVM1.

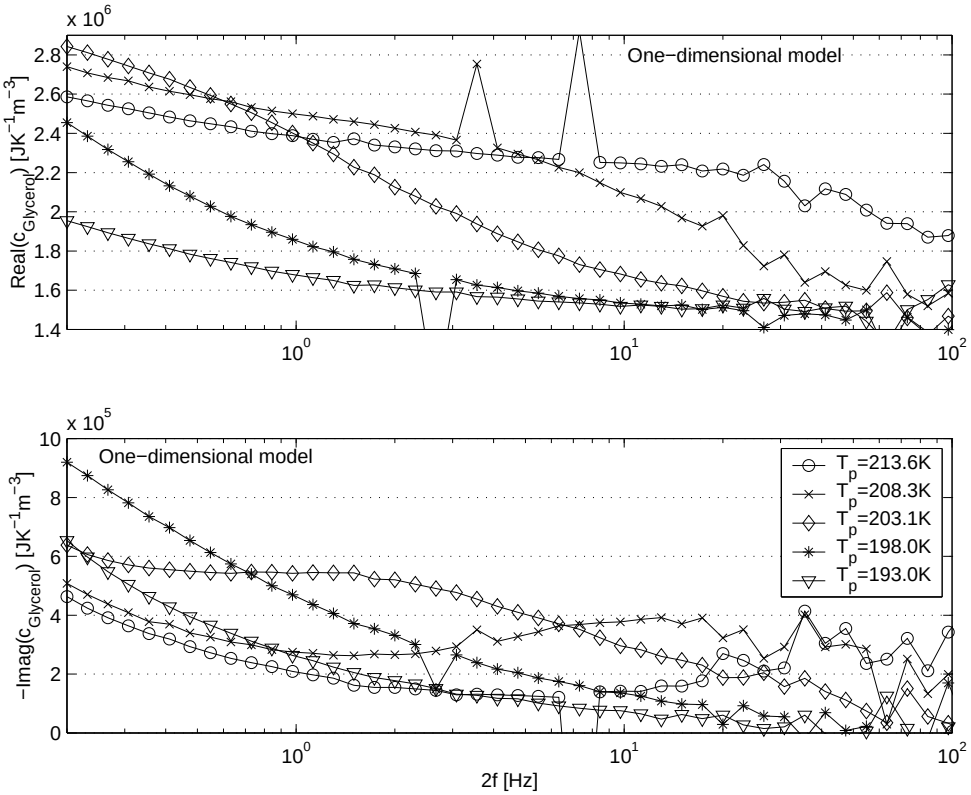

Figure 16.20 The extracted heat capacity of glycerol (with $U_1 = 9.9V$) using the VVM.

As can been seen from the comparison of figures 16.7, 16.19 and 16.20 the edge effect becomes more and more important as the frequency is lowered (as expected). It looks as if the one–dimensional model starts to become adequate above $2f \approx 50Hz$. The diffusion lengths is at this frequency: $L_{D,L} \approx 0.02mm$ and $L_{D,S} \approx 0.05mm$ for glycerol and substrate, respectively, corresponding to $\approx 1/100$ of W.

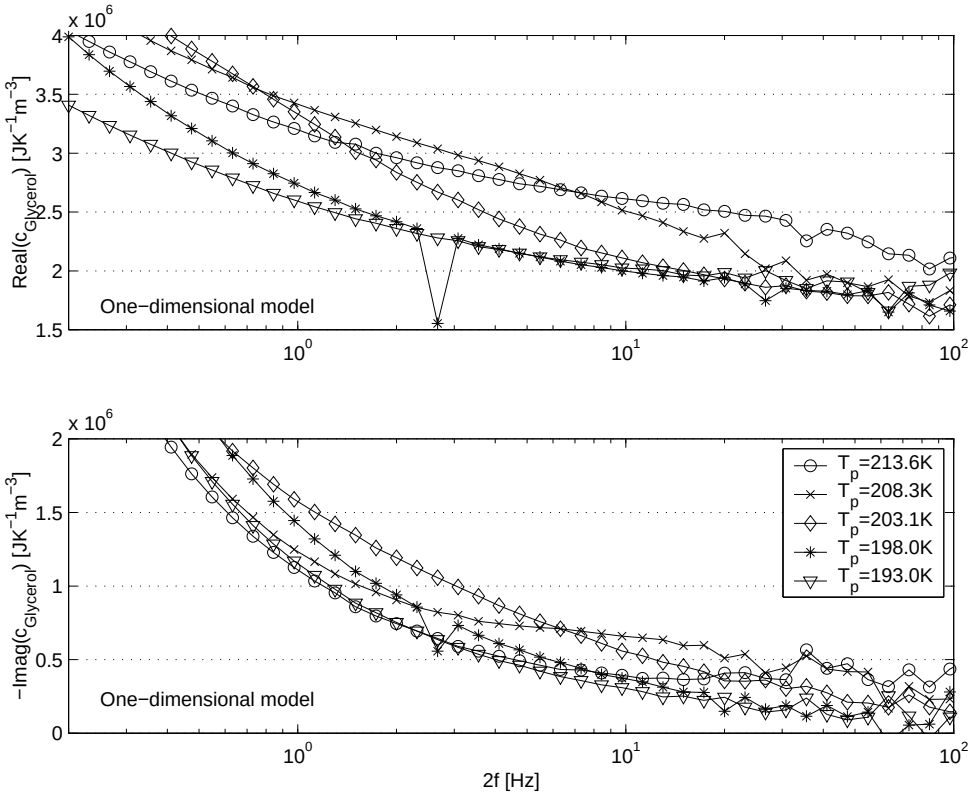

Figure 16.21 The extracted heat capacity of glycerol (with $U_1 = 9.9V$) using the CVM2.

16.6 Linearity

The input–voltage was set to $U_1 = 9.9V$ (the maximum) in the measurements discussed in the previous sections. The same measurements was performed with $U_1 = 7.8V$ and $U_1 = 3.9V$. The resulting temperature amplitudes (T_A) for the three cases is shown in figure 16.22 (T_A is calculated using equation 5.4).

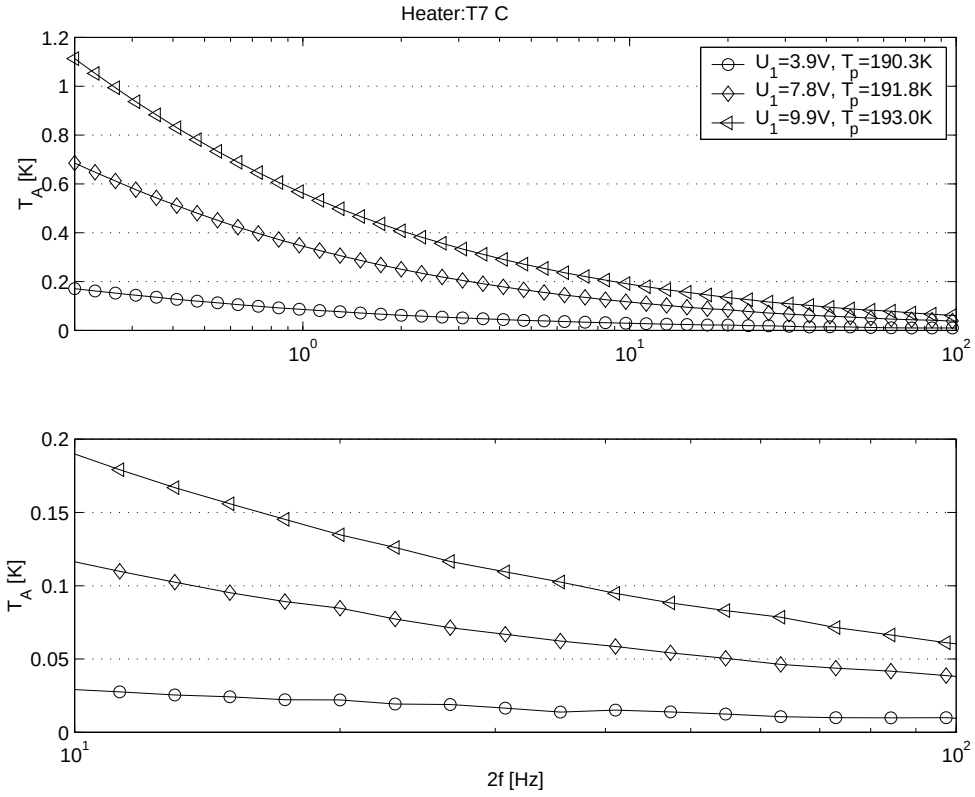

Figure 16.22 The temperature amplitude as function of $2f$ shown for the lowest measured temperature ($T_k = 190.0K$) ($T7C$ with glycerol). T_A is a little lower for the higher temperatures. It is the same curves that are shown in the top and bottom plot. Given $R_f = 469.7\Omega$ and the calibration of the heater (figure 16.2) I_{Tm} is calculated (equation 6.7): $I_{Tm} = 0.004W, 0.017W, 0.028W$ for the three different U_1.

T_A is $\approx 1.1K$ at the lowest measured frequency and $\approx 0.6K$ at $2f = 1Hz$ for the highest input–voltage. The figure clearly shows one of the dilemmas of this technique: the temperature amplitude must be low in order to stay in the linear regime, but in order to make it sufficiently high at high frequencies, it becomes very high at low frequencies. Of course, the problem can be solved by choosing the input–voltage different for different frequency ranges. But, since the input–voltage also

determines the temperature DC offset this requires an appropriate change of the cryostate temperature in order to measure at the same T_p at all frequencies. I have not had time to try such an approach.

In order to judge whether or not T_A is too high for $U_1 = 9.9V$ I have also plotted the extracted heat capacity for the two lower input–voltages. This is shown in figure 16.23 for $U_1 = 7.8V$ and in figure 16.24 for $U_1 = 3.9V$.

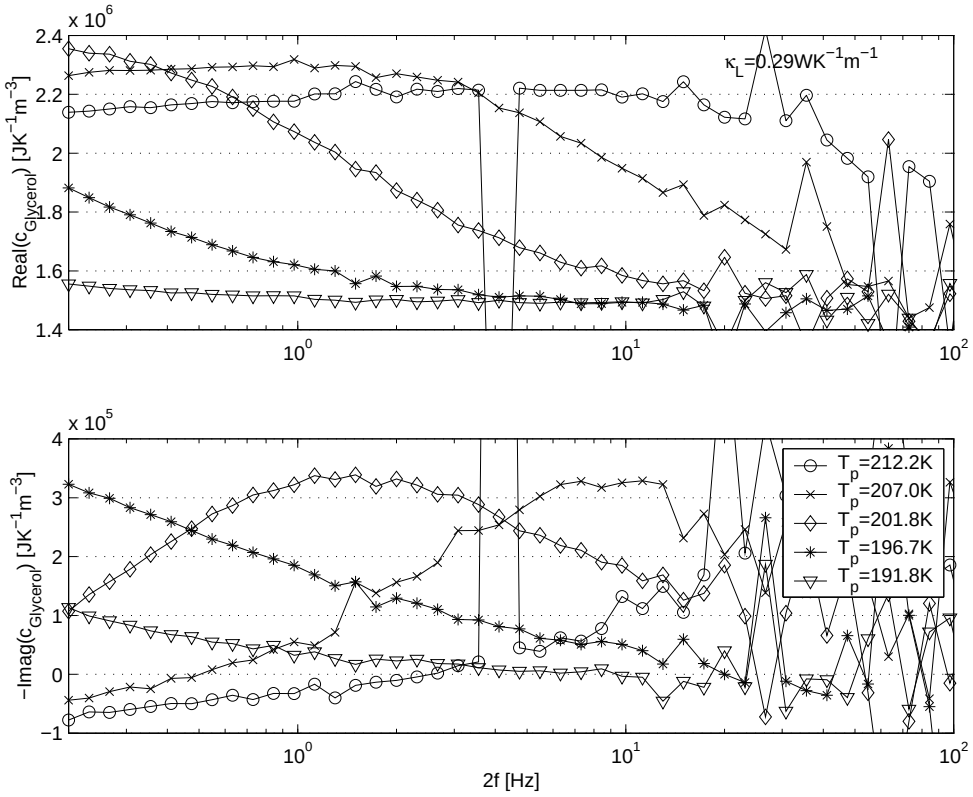

Figure 16.23 The extracted heat capacity of glycerol with $U_1 = 7.8V$.

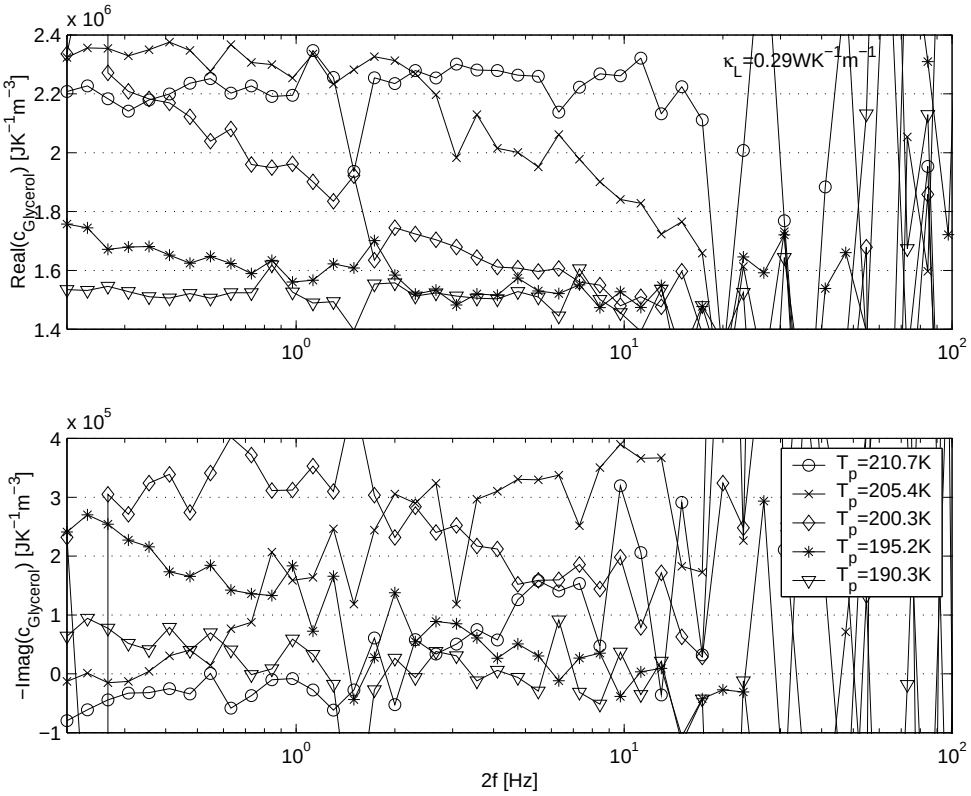

Figure 16.24 The extracted heat capacity of glycerol with $U_1 = 3.9V$.

The data in figure 16.24 are extremely noisy, but still the glass transition can be seen. The data in figure 16.23 are much better. Judging from these plots it seems as if the temperature amplitude for $U_1 = 9.9V$ (figure 16.7) is not too high (with the experimental uncertainty in the current setup), since no significant change in the extracted quantity is seen with the change of T_A.

16.7 Comparison between Ni and C heater

Measurements have been performed using the $T3Ni$ heater (for which calibration curves are shown in section 16.1). Due to the lack of time, measurements have only been performed at one cryostate temperature: $T_k = 200.0K$. The resulting temperature amplitude is shown in figure 16.25.

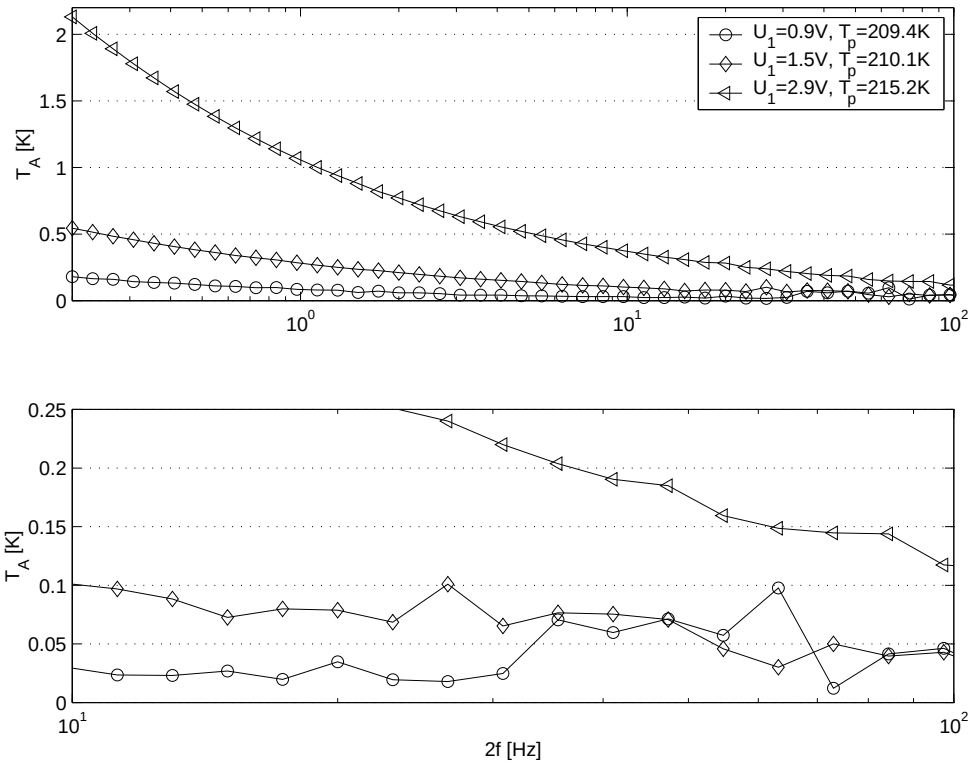

Figure 16.25 The temperature amplitude as function of $2f$ shown for the $T3Ni$ heater with glycerol ($T_k = 200.0K$). It is the same curves that are shown in the top and bottom plot. Given $R_f = 20.2\Omega$ and the calibration of the heater (figure 16.2) I_{Tm} is calculated (equation 6.7): $I_{Tm} = 0.005W, 0.012W, 0.045W$ for the three different U_1.

From the comparison of figures 16.22 and 16.25 it is seen that the carbon heater give a better resolution than the nickel heater. In order to make the comparison easier $V_{3c,rel}$ (cf. equation 12.7) has been calculated for the $T3Ni$ measurements with $U_1 = 1.5V, 2.9V$ (and $I_{Tm} = 0.012W, 0.045W$) and for the $T7C$ measurements with $U_1 = 3.9V, 7.8V$ (and $I_{Tm} = 0.004W, 0.017W$). The result is shown in figures 16.26 and 16.27.

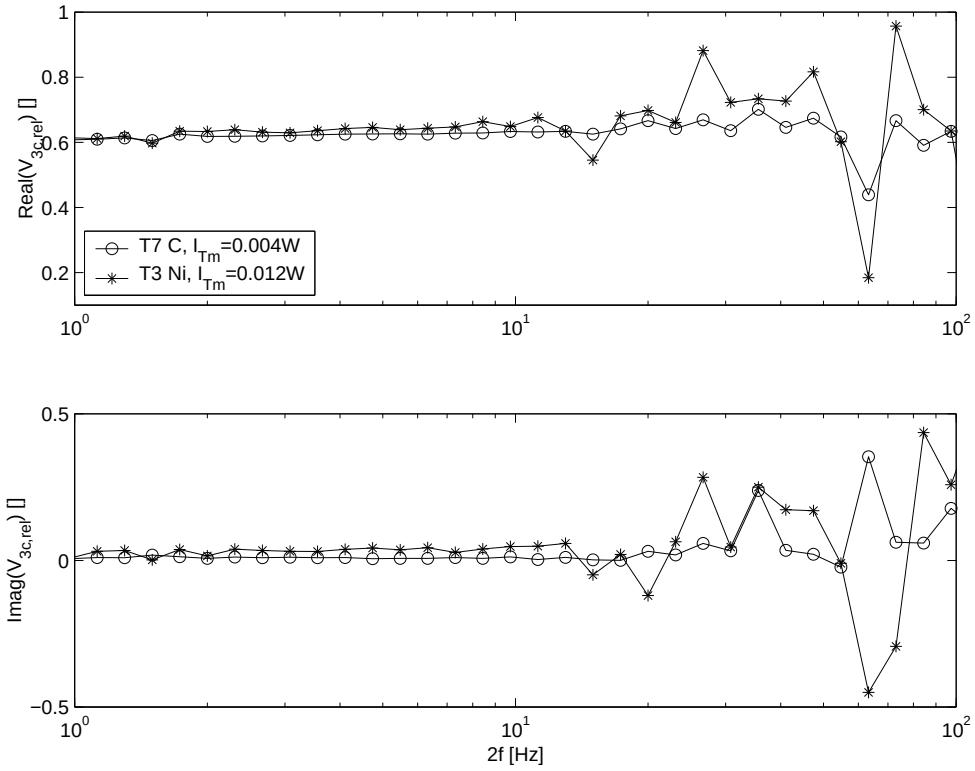

Figure 16.26 $V_{3c,rel}$ for the $T3Ni$ measurements with $U_1 = 1.5V$ (and $I_{Tm} = 0.012W$) and for the $T7C$ measurements with $U_1 = 3.9V$ (and $I_{Tm} = 0.004W$).

In figures 16.26 and 16.27 the noise level is a little higher for the $T3Ni$ heater than for the $T7C$ heater. I_{Tm} is approximately 3 times higher for the $T3Ni$ heater than for the $T7C$ heater and thus the carbon heater performs better than the nickel heater (with the same temperature amplitude the quality of the data obtained with the carbon heater is better than those obtained with the nickel heater).

This is not surprising, remembering that $|\alpha_C|$ is around 5 times that of α_{Ni} (at $T_p \approx 210K$), cf. figure 16.3. Further, the relative influence of resistances in the rest of the setup (e.g. in wires and contacts) influences the measurement of the resistance of $T7C$ ($\approx 700\Omega$) much less than the measurement of the much smaller resistance of $T3Ni$ ($\approx 20\Omega$).

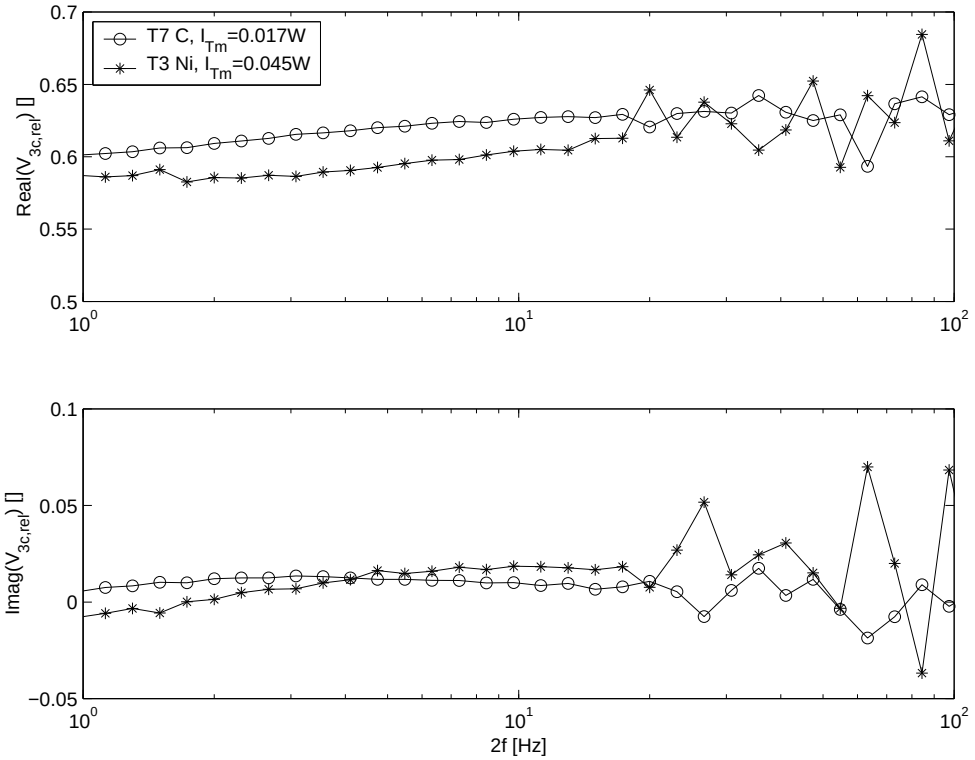

Figure 16.27 $V_{3c,rel}$ for the $T3Ni$ measurements with $U_1 = 2.9V$ (and $I_{Tm} = 0.045W$) and for the $T7C$ measurements with $U_1 = 7.8V$ (and $I_{Tm} = 0.017W$).

Part V

Wrapping up

17 Summary

▷ Planar heater and 3ω detection technique

This report is based on using a electrical conducting thin film as a planar heater and temperature censor simultaneously. The thin film is on a glass substrate, and measurements are made with and without liquid on the other side of the heater. In such a configuration a thermal impedance can be measured using the 3ω detection technique (cf. chapters 5 and 6).

▷ Frequency dependent heat capacity

A frequency dependence of the heat capacity can be found in highly viscous liquids such as a super-cooled liquid near the glass transition (cf. chapter 3). It is the goal to extract the frequency dependent heat capacity (or at least some quantity proportional to this, i.e. the effusivity) from the measured thermal impedance.

▷ Modeling

The relation between the measured thermal impedance and the properties of the liquid and substrate depend on the exact experimental configuration (cf. chapters 7 and 12 and section 10.1).

In the simplest case a one–dimensional heat diffusion model can be assumed, and the relation between the thermal impedance and the effusivity is simple (equation 7.5).

The one–dimensional diffusion model only hold as long as the thermal diffusion length is much shorter than the width of the heater ($L_D \ll W$). If this is not the case, edge effects will be present and must be taken into account. The equations describing these effects has been worked out by Tage Christensen (cf. chapter 12).

▷ Thermo–mechanical problem

No matter whether edge effects play a role or not, it may not be c_p that is actually measured in the experiment. The liquid expands (and contracts) while heated (and cooled), and the induced stress relax on the same time scale as the heat capacity. This thermo–mechanical problem has only been described and dealt with superficially in this report. Still, one important experimental development addressing this problem has been presented: it is important to get rid of the DC heat through the substrate and not through the liquid (cf. section 10.1). This is ensured in the measuring cell used in the measurements presented in this report, by gluing the glass substrate onto a copper backing, and making sure that the copper is in good thermal contact with the temperature bath (cryostate) (cf. chapters 9 and 10).

▷ New improved heaters

New developments regarding the fabrication of the heaters has been presented. It has been shown that carbon heaters have advantages over nickel heaters: higher resistance and higher (absolute value) temperature coefficient (cf. chapter 11). A fabrication procedure for these films have been described (cf. chapter 14), and it has been shown that more accurate measurements can be made with the carbon heaters compared to nickel heaters (cf. section 16.7). Also, a procedure for soldering wires onto the gold electrodes, using indium based solder, have been described (cf. section 11.4).

▷ Heat capacity measurements on glycerol

Finally, measurements of the frequency dependent heat capacity of super–cooled glycerol have been presented (cf. chapter 16). The frequency range of these measurements is only ≈ 2 decades. The data are in closer agreement with the data published by Birge and Nagel [1985] / Birge [1986] than with the measurements by Christensen [1985] (Christensen [1989]).

18 Conclusion

Carbon thin films can be used in a planar heater experiment employing the 3ω detection technique. Nickel heaters are most commonly used, but the carbon heaters (that I have made) have two advantages over nickel heaters: higher resistance and higher temperature coefficient (absolute value). This improves the accuracy of the measurements.

A one–dimensional diffusion model can be used if the diffusion length is much longer than the width of the heater ($L_D \ll W$). If this is not the case edge effects must be considered. The common way of taking these edge effects into account ignores the problem of boundary mismatch and are not entirely correct (as discussed on page 79). Equations that take these edge effects into account without a boundary mismatch are given in chapter 12.

It is important to get rid of the DC heat through the substrate rather than through the liquid. When the thermo–mechanical problem is taken into account this turns out to be important, in order to measure a well defined quantity. This can be ensured by placing the glass substrate on a copper backing that is held at constant temperature.

I have presented measurements of the frequency dependent heat capacity of glycerol. Comparison of the data with the data published by Birge and Nagel [1985] / Birge [1986] show that the loss peak frequencies agree but not the absolute values. The shape of the curves have been evaluated from the Cole–Cole plot of the C_N. For the Cole–Davidson functional form I find a $\beta_{CD} = 0.62 \pm 0.02$. Birge et al. find that $\beta_{CD} = 0.51 \pm 0.03$[Birge, 1986, p. 1637].

19 Outlook

Several things that ought to be looked into in more detail in the future have already been mentioned throughout this report. Here, these will be summarized and a few other ideas presented.

- The thermo–mechanical problem should be taken into account. This can probably be done using a numerical tool, e.g. Femlab, to extract the thermal parameters from the data.
- It is worth looking for a material with a higher temperature coefficient than carbon. On possibility might be a high resistive semiconductor. A sandwich geometry with electrodes on each side of a planar semiconductor (see figure 19.1) could be a possibility. If this can be realized as a round (disk) heater it will make the modeling in Femlab easier.

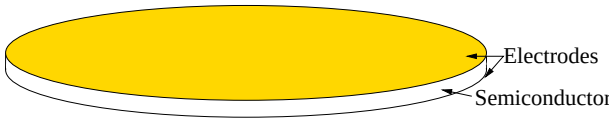

Figure 19.1 A sandwich structure with electrodes on each side of a semiconductor disk.

- The homogeneity of the thin films should be checked. This can probably be done by using IR photography.
- The frequency range of the current setup needs to be extended. Several possibilities exists, and it would be interesting to compare the different methods. In order to go up in frequency: use less than 128 samples per period, let the multimeter use sub–sampling, or use a digital lock-in amplifier and a Wheatstone bridge. In order to go down in frequency: use thicker glass substrates, or use Femlab in the data treatment.

- Also it would be worth trying to use a push–pull type power supply with the digital voltmeter. This would allow the multimeter to work in the $1V$ range instead of the $10V$ range and thus make it possible to measure a voltage that is 10 times less than what is possible in the current setup.

A Appendix: Using two heaters

The temperature–independent resistor R_f (see figure 6.1) can be replaced by another heater (with the same properties as the first heater, i.e. the same temperature coefficient and resistance). This situation will be considered in this appendix. The heater replacing R_f will be called R_1, and the other heater R_2 (V are measured across R_2). All the other quantities related to these heaters are also labeled with the subscript 1 or 2, i.e.: R_{pm1}, R_{pm2}, α_1, α_2, $\tilde{Z}_{T1}$, $\tilde{Z}_{T2}$, $\tilde{I}_{TA1}$, $\tilde{I}_{TA2}$, and ΔT_1, ΔT_2.

To make the expressions simple, in this appendix no higher harmonics of the input–voltage (U) are considered (but of course they can be included if necessary):

$$U = \tfrac{1}{2}\left(\tilde{U}_1 e^{i\omega t} + \tilde{U}_1^* e^{-i\omega t}\right) \tag{A.1}$$

The current though R_1 and R_2 is the same:

$$\frac{V}{R_2} = \frac{U}{R_1 + R_2} \Leftrightarrow \frac{V}{U} = \frac{R_2}{R_1 + R_2}, \tag{A.2}$$

and for small variations of their resistance:

$$R_j(t) = R_{pmj} + \Delta R_j \approx R_{pmj}(1 + \alpha_j \Delta T_j) \equiv R_{pmj} + dR_j, \text{ for } j = 1,2 \tag{A.3}$$

Combining equation A.2 and equation A.3:

$$\begin{aligned} \frac{V}{U} &\approx \frac{R_{pm2} + dR_2}{R_{pm1} + dR_1 + R_{pm2} + dR_2} = \frac{R_{pm2} + dR_2}{R_{pm1} + R_{pm2}} \frac{1}{1 + \left(\frac{dR_1 + dR_2}{R_{pm1} + R_{pm2}}\right)} \\ &\approx \frac{R_{pm2}}{R_{pm1} + R_{pm2}} \left(1 - \frac{R_{pm1}(\alpha_1 \Delta T_1 - \alpha_2 \Delta T_2)}{R_{pm1} + R_{pm2}}\right), \end{aligned} \tag{A.4}$$

neglecting 2^{nd} order terms in ΔT_j.

Corresponding to equation 6.12:

$$\Delta T_j = \tfrac{1}{2}\left(\tilde{Z}_{Tj} \tilde{I}_{TAj} e^{i2\omega t} + \tilde{Z}_{Tj}^* \tilde{I}_{TAj}^* e^{-i2\omega t}\right), \text{ for } j = 1,2$$

Inserting this into equation A.4 and using the expression for U (equation A.1):

$$V = \tfrac{1}{2}\left(\tilde{U}_1 e^{i\omega t} + \tilde{U}_1^* e^{-i\omega t}\right)\frac{R_{pm2}}{R_{pm1}+R_{pm2}}$$
$$\left(1 - \frac{\alpha_1 \tfrac{1}{2}\left(\tilde{Z}_{T1}\tilde{I}_{TA1}e^{i2\omega t} + \tilde{Z}_{T1}^*\tilde{I}_{TA1}^* e^{-i2\omega t}\right) - \alpha_2 \tfrac{1}{2}\left(\tilde{Z}_{T2}\tilde{I}_{TA2}e^{i2\omega t} + \tilde{Z}_{T2}^*\tilde{I}_{TA2}^* e^{-i2\omega t}\right)}{1+\frac{R_{pm2}}{R_{pm1}}}\right)$$
$$= \tfrac{1}{2}\left(\tilde{U}_1 e^{i\omega t} + \tilde{U}_1^* e^{-i\omega t}\right)\frac{R_{pm2}}{R_{pm1}+R_{pm2}} - \frac{R_{pm2}}{2(R_{pm1}+R_{pm2})\left(1+\frac{R_{pm2}}{R_{pm1}}\right)}$$
$$\left\{\alpha_1 \tfrac{1}{2}\left(\tilde{Z}_{T1}\tilde{I}_{TA1}\tilde{U}_1 e^{i3\omega t} + \tilde{Z}_{T1}^*\tilde{I}_{TA1}^*\tilde{U}_1 e^{-i\omega t} + \tilde{Z}_{T1}\tilde{I}_{TA1}\tilde{U}_1^* e^{i\omega t} + \tilde{Z}_{T1}^*\tilde{I}_{TA1}^*\tilde{U}_1^* e^{-i3\omega t}\right)\right.$$
$$\left.-\alpha_2 \tfrac{1}{2}\left(\tilde{Z}_{T2}\tilde{I}_{TA2}\tilde{U}_1 e^{i3\omega t} + \tilde{Z}_{T2}^*\tilde{I}_{TA2}^*\tilde{U}_1 e^{-i\omega t} + \tilde{Z}_{T2}\tilde{I}_{TA2}\tilde{U}_1^* e^{i\omega t} + \tilde{Z}_{T2}^*\tilde{I}_{TA2}^*\tilde{U}_1^* e^{-i3\omega t}\right)\right\}$$

The third harmonic can then be written as (using the same notation as on page 29):

$$V_{3\omega} = -\frac{R_{pm2}}{2(R_{pm1}+R_{pm2})\left(1+\frac{R_{pm2}}{R_{pm1}}\right)}\left\{\alpha_1 \tfrac{1}{2}\left(\tilde{Z}_{T1}\tilde{I}_{TA1}\tilde{U}_1 e^{i3\omega t} + \tilde{Z}_{T1}^*\tilde{I}_{TA1}^*\tilde{U}_1^* e^{-i3\omega t}\right)\right.$$
$$\left.-\alpha_2 \tfrac{1}{2}\left(\tilde{Z}_{T2}\tilde{I}_{TA2}\tilde{U}_1 e^{i3\omega t} + \tilde{Z}_{T2}^*\tilde{I}_{TA2}^*\tilde{U}_1^* e^{-i3\omega t}\right)\right\}$$
$$\Downarrow$$
$$\mathrm{FT}[V,3] = -\frac{R_{pm2}}{2(R_{pm1}+R_{pm2})\left(1+\frac{R_{pm2}}{R_{pm1}}\right)}\left\{\alpha_1 \tilde{Z}_{T1}^*\tilde{I}_{TA1}^*\tilde{U}_1^* - \alpha_2 \tilde{Z}_{T2}^*\tilde{I}_{TA2}^*\tilde{U}_1^*\right\}$$

Now, if $R_{pm1} = R_{pm2}$, and $\alpha_1 = \alpha_2 \equiv \alpha$, then $\tilde{I}_{TA1}^* = \tilde{I}_{TA2}^* \equiv \tilde{I}_{TA}^*$, and:

$$\mathrm{FT}[V,3] = -\frac{\alpha \tilde{I}_{TA}^*\tilde{U}_1^*}{8}\left\{\tilde{Z}_{T1}^* - \tilde{Z}_{T2}^*\right\}$$

From this it is seen that, if $\tilde{Z}_{T1} = \tilde{Z}_{T2}$, then $\mathrm{FT}[V,3] = 0$.

Bibliography

Aglient [2000]. Aglient technologies 3458a multimeter user's guide. When this report was written it could be downloaded via Agilent Technologies homepage: http://we.home.agilent.com.

Arfken, G. [1985]. *Mathematical Methods for Physicists*, third edn, Academic Press, Inc.

Atake, T., Abe, R., Honda, K., Kawaji, H., Johnsen, H.-B. and Stølen, S. [2000A]. Heat capacities of glassy and crystalline $GeSe_2$, *Journal of Physics and Chemistry of Solids* **61**: 1373–1377.

Atake, T., Kawaji, H., Tojo, T., Kawasaki, K., Ootsuka, Y., Katou, M. and Koga, Y. [2000B]. Heat capacities of isomeric 2-butoxyethanols from 13 to 300k: Fusion and glass transition, *The Chemical Society of Japan* **73**(9): 1987–1991.

AWS [1978]. *Soldering Manual*, second edn, American Welding Society, INC., 2501 N.W. 7th Street, Miami, Florida 33125. ISBN: 0-87171-151-6.

Bae, D. J., Koo, T. Y., Lee, K. B. and Jeong, Y. H. [1994]. Dynamic specific heat of KH2PO4 near the curie point, *Ferroelectrics* **159**: 91–96.

Bae, D. J., Lee, K. B., Jeong, Y. H., Lee, S. M. and Kwun, S. I. [1993]. Thermal conductivity measurements of insulating single crystals, *Journal of the Korean Physical Society* **26**(2): 137–141.

Behrens, C. F., Christensen, T. E. and Uhre, E. [n.d.]. To be published.

Beiner, M., Kahle, S., Hempel, E., Schröter, K. and Donth, E. [1998]. Crossover region of dynamic glass transition in poly(*n*-hexyl methacrylate) by heat capacity spectroscopy, *Macromolecules* **31**(25): 8973–8980.

Beiner, M., Korus, J., Lockwenz, H., Schröter, K. and Donth, E. [1996]. Heat capacity spectroscopy compared to other linear response methods at the dynamic glass transition in ploy(vinyl acetate), *Macromolecules* **29**(15): 5183–5189.

Beiser, R. B. [1954]. A technique of soldering to thin metal films, *The Review of Scientific Instruments* **25**(2): 180–183.

Bentefour, E. H. [2002]. *Photothermal Spectroscopy of Thermophysical Properties of Glass-Forming Loquids*, PhD thesis, Katholieke Universiteit Leuven.

Bentefour, E. H., Chirtoc, M., Glorieux, C. and Thoen, J. [2001]. étude thermophysique dans la région de dispersion des liquides vitreux par la technique photopyroélectrique (PPE), *Congrès français de Thermique* p. ??

Birge, N. O. [1986]. Specific-heat spectroscopy of glycerol and propylene glycol near the glass transition, *Physical Review B* **34**(3): 1631–1642.

Birge, N. O., Dixon, P. K. and Menon, N. [1997]. Specific heat spectroscopy: Orgins, status and applications of the 3ω method, *Thermochimica Acta* **304/305**: 51–66.

Birge, N. O. and Nagel, S. R. [1985]. Specific-heat spectroscopy of the glass transition, *Physical Review Letter* **54**(25): 2674–2677.

Birge, N. O. and Nagel, S. R. [1987]. Wide-frequency specific heat spectrometer, *Review of Scientific Instruments* **58**(8): 1464–1470.

Brawer, S. [1985]. *Relaxation in Viscous Liquids and Glasses – Review of Phenomenology, Molecular Dynamics Simulations, and Theoretical Treatment*, The American Ceramic Society, Inc., Columbus, Ohio.

Büchner, B. and Korpium, P. [1987]. Frequency-dependent specific heat near the glass transition measured with the photoacoustic effect, *Applied Physics B* **43**(1): 29–33.

Caerels, J., Glorieux, C. and Thoen, J. [1998]. Absolute values of specific heat capacity and thermal conductivity of liquids from different modes of operation of a simple photopyroelectric setup, *Review of Scientific Instruments* **69**(6): 2452–2458.

Cahill, D. G. [1990]. Thermal conductivity measurement from 30 to 750k: The 3ω method, *Review of Scientific Instruments* **61**(2): 802–808.

Carslaw, H. S. and Jaeger, J. C. [1959]. *Conduction of Heat in Solids*, second edn, Oxford University Press.

Chirtoc, M., Bentefour, E. H., Glorieux, C. and Thoen, J. [2001]. Development of the front–detection photopyroelectric (FPPE) configuration for thermophysical study of glass–forming liquids, *Thermochimica Acta* **377**: 105–112.

Chirtoc, M. and MihăIlescu, G. [1989]. Theory of the photopyroelectric method for investigation of optical and thermal materials properties, *Physical Review B* **40**(14): 9606–9617.

Chow, T. L. [2000]. *Mathematical Methods for Physicists. A Concise Introduction*, Cambridge University Press.

Christensen, T. [1985]. The frequency dependence of the specific heat at the glass transition, *Journal de Physique* **Colloque C8**(12): 635–637.

Christensen, T. E. [1989]. *En metode til bestemmelse af den frekvensafhængige varmefylde af en underafkølet væske ved glasoergangen*, TEKSTER fra IMF-UFA nr. 184, Roskilde University, Denmark. (In Danish).

Christensen, T. and Olsen, N. B. [1997]. How to compare the frequency dependent adiabatic compressibility with other thermoviscoelastic responce functions at the glass transition, *Progress of Theoretical Physics Supplement* **(No. 126)**: 273–276.

Corbino, V. O. M. [1911]. Periodische widerstandsänderungen von metallfäden, *Physik Zeitschrift* **XII**: 292–295.

D. Gerlich, B. Abeles, A. R. E. M. [1965]. High-temperature specific heats of ge, si, and ge-si alloys, *Journal of Applied Physics* **36**(1): 76–79.

Debenedetti, P. G. [1996]. *Metastable Liquids – Concepts and Principles*, Princeton University Press, 41 William Street, Princeton, New Jersey 08540.

Dixon, P. K. [1990]. Specific-heat spectroscopy and dielectric susceptibility measurements of salol at the glass transition, *Physical Review B* **42**(13): 8179–8186.

Dixon, P. K. and Nagel, S. R. [1988]. Frequency-dependent specific heat and thermal conductivity at the glass transition in *o*-terphenyl mixtures, *Physical Review Letters* **61**(3): 341–344.

Donth, E., Beiner, M., Reissig, S., Korus, J., Garwe, F., Vieweg, S., Kahle, S., Hempel, E. and Schröter, K. [1996]. Fine structure of the main transition in amorphous polymers: Entanglement spacing and characteristic length of the glass transition. discussion of examples, *Macromolecules* **29**(20): 6589–6600.

Dădârlat, D., Chirtoc, M., Nemaţu, C., Cândea, R. M. and Bicanic, D. [1990]. Inverse photopyroelectric detection method, *Physica status solidi (a)* **121**: K231–K234.

Fujimori, H., Adachi, Y. and Oguni, M. [1992]. Temperature-jump method for characterization of structural flucturations and irreversible relaxation processes in liquids and glasses, *Physical Review B* **46**(22): 14 501– 14 505.

Fujimori, H. and Oguni, M. [1993]. Construction of an adiabatic calorimeter at low temperatures and glass transition of crystaline 2-bromothiophene, *Journal of Physics and Chemistry of Solids* **54**(2): 271–280.

Fujimori, H. and Oguni, M. [1994]. Non-exponentiality of the enthalpy relaxation under constant-temperature conditions in the time domain in supercooled liquids and glasses, *Journal of Non-Crystaline Solids* **172-174**: 601–607.

Gmelin, E. [1997]. Classical temperature-modulated calorimetry: A review, *Thermochimica Acta* **304/305**: 1–26.

Harrison, G. [1976]. *The Dynamic Properties of Supercooled Liquids*, Academic Press, Inc., London.

Holland, L. R. [1963]. Physical properties of titanium. III. the specific heat, *Journal of Applied Physics* **34**(8): 2350–2357.

Holland, L. R. and Smith, R. C. [1966]. Analysis of temperature fluctuations in ac heated fliaments, *Journal of Applied Physics* **37**(12): 4528–4536.

Hudson, C. and Somekh, R. E. [1992]. Stresses in uhv planar magnetron sputtered films, *Materials Research Society Symposium Procedings* **239**: 145–150.

Inada, T., Kawaji, H., Atake, T. and Saito, Y. [1990]. Construction of a heat capacity spectrometer and aplication to some molecular glass forming substances, *Thermichimica Acta* **163**: 219–224.

Indium [n.d.]. Research solder kit information, Indium Corporation of America, 1676 Lincoln Avenue, PO Box 269, Utica, NY, USA 13503-0269, www.indium.com. Form No. 97699 RO.

Jeong, Y.-H. [1997]. Progress in experimental techniques for dynamic calorimetry, *Thermochimica Acta* **304/305**: 67–98.

Jeong, Y. H., Bae, D. J., Kwon, T. W. and Moon, I. K. [1991]. Dynamic specific heat near the curie point of gd, *Journal of Applied Physics* **70**(10): 6166–6168.

Jeong, Y. H. and Moon, I. K. [1995]. Ergodic-nonergodic glass transition and enthalpy relaxation of a supercooled liquid $[ca(no_3)_2]_{0.4}(kno_3)_{0.6}$, *Physical Review B* **52**(9): 6381–6385.

Jonsson, U. G. and Andersson, O. [1998]. Investigations of the low– and high–frequency responce of 3ω–sensors used in dynamic heat capacity measurements, *Measurement Science and Technology* **9**: 1873–1885.

Jonsson, U. G., Andersson, O. and Fransson, Å. [2000]. Investigations of the temperature gradients affecting the temperature scale of a 3ω–heat capacity spectrometer, *Thermochimica Acta* **347**: 45–51.

Jung, D. H., Kwon, T. W., Bae, D. J., Moon, I. K. and Jeong, Y. H. [1992]. Fully automated dynamic calorimeter, *Measurement Science and Technology* **3**: 475–481.

Jung, D. H., Moon, I. K. and Jeong, Y. H. [1999]. The principle and aplications of dynamic calorimetry, *Journal of the Korean Physical Society* **35**: S1359–S1363.

Kobashi, K., Kyômen, T. and Oguni, M. [1998]. Construction of an adiabatic calorimeter in the temperature range between 13 and 505 k, and thermodynamic study of 1-chloroadamantane, *Journal of Physics and Chemistry of Solids* **59**(5): 667–677.

Korus, J., Beiner, M., Busse, K., Kahle, S., Unger, R. and Donth, E. [1997A]. Heat capacity spectroscopy at the glass transition in polymers, *Thermochimica Acta* **304/305**: 99–110.

Korus, J., Hempel, E., Beiner, M., Kahle, S. and Donth, E. [1997B]. Temperature dependence of α glass transition cooperativity, *Acta Polymer* **48**: 369–378.

Mailly, F., Giani, A., Bonnot, R., Temple-Boyer, P., Pascal-Delannoy, F., Foucaran, A. and Boyer, A. [2001]. Anemometer with hot platinum thin film, *Sensors and Actuators* **A 94**: 32–38.

Menon, N. [1996]. Dynamic specific heat of a supercooled liquid, *Journal of Chemical Physics* **105**(12): 5246–5257.

Minakov, A. A., Adamovsky, S. A. and Schick, C. [2001]. Simultaneous measurements of complex heat capacity and complex thermal conductivity by two-channel AC calorimeter, *Thermochimica Acta* **377**: 173–182.

Moon, I. K., Jeong, Y. H. and Furukawa, T. [2001]. Enthalpy and dielectric relaxation in the glass transition region of polypropylene glycol, *Thermochimica Acta* **377**: 97–104.

Moon, I. K., Jeong, Y. H. and Kwun, S. I. [1996]. The 3ω technique for measuring dynamic specific heat and thermal conductivity of a liquid or solid, *Review of Scientific Instruments* **67**(1): 29–35.

Nordling, C. and Österman, J. [1996]. *Physics Handbook for Science and Engineering*, fifth edn, Studentlitteratur, Lund, http://www.studli.se/.

Olsen, N. B., Christensen, T. and Dyre, J. [2001]. Time-temperature superposition in viscous liquids, *Physical Review Letters* **86**(7): 1271–1274.

Olsen, N. B., Christensen, T. and Dyre, J. C. [2000]. Time-temperature superposition in viscous liquids, *arXiv:cond-mat/0006165 (Web address: http://xxx.lanl.gov)* pp. 1–4.

Rosenthal, L. A. [1961]. Thermal response of bridgewires used in electroexplosive devices, *The Review of Scientific Instruments* **32**(9): 1033–1036.

Sandberg, O., Andersson, P. and Bäckström, G. [1977]. Heat capacity and thermal conductivity from pulsed wire probe measurements under pressure, *Journal of Physics E: Scientific Instruments* **10**: 474–477.

Spiegel, M. R. [1995]. *Shaum's Outline Series: Mathematical Handbook of Formulars and Tables*, McGraw-Hill, INC. 34th Printing.

Suga, H. and Matsuo, T. [1989]. Adiabatic calorimeter as a ultra-low frequency spectrometer, *Pure and Applied Chemistry* **61**(6): 1123–1132.

Thoen, J. and Glorieux, C. [1997]. Photoacoustic and photopyroelectric approach to calorimetric studies, *Thermochimica Acta* **304/305**: 137–150.

Wu, L., Dixon, P. K., Nagel, S. R., Williams, B. D. and Carini, J. P. [1991]. Relaxation spectroscopies of viscous liquids, *Journal of Non-Crystaline Solids* **131-133**: 32–36.